VOLUME XXXVIII-2017

MATHEMATICA MONTISNIGRI

MATHEMATICA MONTISNIGRI

VOLUME XXXVIII-2017

The journal Mathematica Montisnigri is published by the Society of mathematicians and physicists of Montenegro and Department of Mathematics of The University of Montenegro.

At the front page there is a detail from the first known text in astronomy-mathematics that appeared in Montenegro. It was published in the book Psaltir in 1495. Psaltir was printed on September 22, 1495 in the printing shop of Djurdje Crnojević which was the first printing shop of South Slavs. In the book six, volume 23, Djurdje Crnojević, the sovereign of Montenegro, adapted the Tables of Jovan Damaskin and wrote the Paschalia with lunar calendar. He worked out a series of rules regarding the counting of days of Easter celebrations. Djurdje's Paschalia Tables can be found in numerous written and printed books of later period.

The journal *Mathematica Montisnigri* publishes original scientific works from all fields of mathematics and mathemat ical modelling which comprise new and significant results with complete proofs, which are of interest for a larger mathematical community. It also contains expository articles. The journal does not publish works of polemical or methodological interest, as well as works that have been offered for publishing in other journals. The journal publishes papers in English, Russian, French and German. It is usually issued thrice a year.

Instructions to the authors:

Authors should submit the Manuscript electronically at the address:

zarkop@ac.me,
borkov@ac.me,
orgcom@LPpM3.ru.

The paper should be prepared in MS Word by the instructions, which can be found at the web page: **lppm3.ru/en/pub/manusc** .

The file has to be translated into Portable Document Format (PDF) before submission to the Editorial board of the journal.

The papers should have a precise and informative title. 2010 Mathematics Subject Classification and Key words and Phrases should be included at the bottom of first page of the paper.

Theorems, other statements and formulae must be clearly marked, separating the results of the authors from the already known results. The list of references has to be enclosed in alphabetical or chronological order at the end of the paper as well as the affiliation of the author.

Subscription for one volume is 40 USA dollars for institutions and 20 USA dollars for individuals.

For subscriptions and exchange please refer to the above address.

Computer processing of the press Olga Koroleva, Moscow, Russia.
Print: AP Print, Podgorica, Montenegro.

CIP – Каталогизација у публикацији
Централна народна библиотека, Цетиње, 51(05)

MATHEMATICA Montisnigri = Математика Црне Горе/ главни и одговорни уредник Жарко Павићевић. - Књ. 1 (1993) - Подгорица (Џорџа Вашингтона бб) : Друштво математичара и физичара Црне Горе: Природно – математички факултет Универзитета Црне Горе, 1993 – (Подгорица: АП Принт). - 30 cm

Три пута годишње. – Текст на руском и енг. језику.

ISSN 0345-2238 – Mathematica Montisnigri
COBISS.CG-ID 150244359

MATHEMATICA MONTISNIGRI
Vol XXXVIII (2017) 5-99

CONTENTS

Mathematics

Romeo Meštrović and Miomir Andjić. Certain congruences for harmonic numbers..... 5

Mathematical Modeling

A.V. Kolesnichenko, M. Ya. Marov. Stochastic-thermodynamic modeling of the developed structured turbulence…… 12

O.N. Koroleva, V.I. Mazhukin, A.V. Mazhukin. Calculation of silicon band gap by means of Fermi-Dirac integrals ……..……..…… 49

A. Alexeev, A. Bondarev. On exact solution enclosure on ensemble of numerical simulations…….. 63

A.A. Samokhin, V.I.Mazhukin, A.V. Shapranov, M.M. Demin, A.E. Zubko. Molecular dynamics modeling of nanosecond laser ablation: transcritical regime…….. 78

V. Egorova, M. Zhukovskiy. Handling of the radiative electron emission modeling results by use of the neural networks……. 89

CERTAIN CONGRUENCES FOR HARMONIC NUMBERS

ROMEO MEŠTROVIĆ[1] AND MIOMIR ANDJIĆ[2]

[1]Maritime Faculty Kotor, University of Montenegro
85330 Kotor, Montenegro
e-mail: romeo@ac.me

[2]Faculty for Information Technology, University "Mediterranean"
81000 Podgorica, Montenegro
e-mail: miomir.andjic@unimediteran.net

Summary. For given positive integers *n* and *m*, the harmonic numbers of order *m* are those rational numbers $H_{n,m}$ defined as

$$H_{n,m}=\sum_{k=1}^{n}\frac{1}{k^m}.$$

If m=1, then $H_n := H_{n,1}=\sum_{k=1}^{n}1/k$ is the *n*th harmonic number. In [12] Z.W. Sun obtained basic congruences modulo a prime $p > 3$ for several sums involving harmonic numbers. Further generalizations and extensions of these congruences have been obtained by R. Tauraso in [16], by Z.W. Sun and L.L. Zhao in [14] and by R. Me_strovi_c in [6] and [7]. In this paper we prove that for each prime $p > 3$ and all integers $m = 0, 1,\ldots,p-2$ there holds

$$\sum_{k=m}^{p-1}\binom{k}{m}H_k\equiv\frac{(-1)^m}{m+1}\left(1-pH_{m+1}+\frac{p^2}{2}\left(H_{m+1}^2-H_{m+1,2}\right)\right)\qquad\left(\mathrm{mod}\ p^3\right)$$

As an application, we determine the mod p^3 congruences for the sums $\sum_{k=1}^{p-1}k^rH_k$ with r = 0, 1, 2, 3 and a prime $p > 3$.

1 INTRODUCTION

Given positive integers *n* and *m*, the *harmonic numbers of order m* are those rational numbers $H_{n,m}$ defined as

$$H_{n,m}=\sum_{k=1}^{n}\frac{1}{k^m}.$$

For simplicity, we will denote by

$$H_n := H_{n,1}=\sum_{k=1}^{n}\frac{1}{k}$$

2010 Mathematics Subject Classification: Primary 11A07; Secondary 05A10, 05A19, 11B65, 11B68.
Key words and Phrases: harmonic number, harmonic numbers of order m, congruence modulo a prime (prime power), Wolstenholme's theorem.

the nth *harmonic number* (in addition, we define $H_0 = 0$).

Harmonic numbers play important roles in mathematics. Throughout this paper, for a prime p and two reduced rational numbers a/b and c/d such that b and d are not divisible by p, we write $a/b \equiv c/d (\mathrm{mod}\, p^s)$ (with $s \in \mathbb{N}$) to mean that $ad - bc$ is divisible by p^s.

In 2012 Z.W. Sun [12] investigated their arithmetic properties and obtained various basic congruences modulo a prime $p > 3$ for several sums involving harmonic numbers. In particular, Sun established the congruences $\sum_{k=1}^{p-1}(H_k)^r \,(\mathrm{mod}\, p^{4-r})$ for $r = 1, 2, 3$. Further generalizations and extensions of these congruences have been obtained by R. Tauraso in [16], by Z.W. Sun and L.L. Zhao [14] and by R. Meštrović in [6] and [7]. Furthermore, Z.W. Sun [13] initiated and studied congruences involving both harmonic and Lucas sequences (especially, including Fibonacci numbers or Lucas numbers). Moreover, some congruences involving multiple harmonic sums were established in [9], [18] and [19].

Recall that Bernoulli numbers $B_0, B_1, B_2, \ldots$ are recursively given by

$$B_0 = 1 \quad \text{and} \quad \sum_{k=0}^{n} \binom{n+1}{k} B_k = 0 \ (n = 1, 2, 3, \ldots).$$

It is easy to find the values $B_0 = 1$, $B_1 = -\frac{1}{2}$, $B_2 = \frac{1}{6}$, $B_4 = -\frac{1}{30}$, and $B_n = 0$ for odd $n \geq 3$. Furthermore, $(-1)^{n-1}B_{2n} > 0$ for all $n \geq 1$. These and many other properties can be found, for instance, in [3]. Recently, the first author of this paper in [6, Theorem 1.1] established the following six congruences involving harmonic numbers contained in the following result.

Theorem 1.1 ([6, Theorem 1.1]). *Let $p > 5$ be a prime, and let $q_p(2) = (2^{p-1} - 1)/p$ be the Fermat quotient of p to base 2. Then*

$$\sum_{k=1}^{p-1} \frac{2^k H_k}{k} \equiv -q_p(2)^2 + \frac{2}{3}pq_p(2)^3 + \frac{p}{12}B_{p-3} \pmod{p^2}, \tag{1}$$

$$\sum_{k=1}^{p-1} \frac{2^k H_k}{k^2} \equiv -\frac{1}{3}q_p(2)^3 + \frac{23}{24}B_{p-3} \pmod{p}, \tag{2}$$

$$\sum_{k=1}^{p-1} \frac{H_k}{k^2 \cdot 2^k} \equiv \frac{5}{8}B_{p-3} \pmod{p}, \tag{3}$$

$$\sum_{k=1}^{p-1} \frac{2^k H_k^2}{k} \equiv -\frac{1}{3}q_p(2)^3 + \frac{11}{24}B_{p-3} \pmod{p}, \tag{4}$$

$$\sum_{k=1}^{p-1} \frac{H_k^2}{k \cdot 2^k} \equiv \frac{7}{8}B_{p-3} \pmod{p} \tag{5}$$

and

$$\sum_{k=1}^{p-1} \frac{2^k H_{k,2}}{k} \equiv -\frac{1}{3}q_p(2)^3 - \frac{25}{24}B_{p-3} \pmod{p}. \tag{6}$$

In this paper we prove the following result.

Theorem 1.2. *Let $p > 3$ be a prime. Then for each $m = 0, 1, \ldots, p-2$ there holds*

$$\sum_{k=m}^{p-1} \binom{k}{m} H_k \equiv \frac{(-1)^m}{m+1} \left(1 - pH_{m+1} + \frac{p^2}{2}(H_{m+1}^2 - H_{m+1,2})\right) \pmod{p^3}. \tag{7}$$

The particular cases of Theorem 1.2 yield the following result.

Corollary 1.3. *Let $p > 3$ be a prime. Then*

$$\sum_{k=1}^{p-1} H_k \equiv 1 - p \pmod{p^3}, \tag{8}$$

$$\sum_{k=1}^{p-1} kH_k \equiv -\frac{p^2 - 3p + 2}{4} \pmod{p^3}, \tag{9}$$

$$\sum_{k=1}^{p-1} k^2 H_k \equiv \frac{15p^2 - 17p + 6}{36} \pmod{p^3}, \tag{10}$$

and

$$\sum_{k=1}^{p-1} k^3 H_k \equiv -\frac{21p^2 - 10p}{48} \pmod{p^3}, \tag{11}$$

Reducing the modulus in congruences (8), (9), (10) and (11) of Corollary 1.3, immediately gives the following two corollaries.

Corollary 1.4. *Let $p > 3$ be a prime. Then*

$$\sum_{k=1}^{p-1} H_k \equiv 1 - p \pmod{p^2}, \tag{12}$$

$$\sum_{k=1}^{p-1} kH_k \equiv \frac{3p - 2}{4}, \pmod{p^2}, \tag{13}$$

$$\sum_{k=1}^{p-1} k^2 H_k \equiv -\frac{17p - 6}{36} \pmod{p^2}, \tag{14}$$

and

$$\sum_{k=1}^{p-1} k^3 H_k \equiv \frac{5p}{24} \pmod{p^2}. \tag{15}$$

Corollary 1.5. *Let $p > 3$ be a prime. Then*

$$\sum_{k=1}^{p-1} H_k \equiv 1 \pmod{p}, \tag{16}$$

$$\sum_{k=1}^{p-1} kH_k \equiv -\frac{1}{2} \pmod{p}, \tag{17}$$

$$\sum_{k=1}^{p-1} k^2 H_k \equiv \frac{1}{6} \pmod{p}, \tag{18}$$

and

$$\sum_{k=1}^{p-1} k^3 H_k \equiv 0 \pmod{p}. \tag{19}$$

Remark 1.5. Notice that the congruences (8) and (9) are proved by Z.W. Sun in [12, p. 419 and p. 417].

2 PROOF OF THEOREM 1.2 AND COROLLARY 1.3

For the proof of Theorem 1.2 we will need the following three auxiliary results.

Lemma 2.1 (see the identity (6.70) in [1]; also [11, p. 2]). *If m and n are nonnegative integers such that $m \leq n$, then*

$$\sum_{k=m}^{n} \binom{k}{m} H_k = \binom{n+1}{m+1} \left(H_{n+1} - \frac{1}{m+1} \right). \tag{20}$$

The following result is well known as Wolstenholme's theorem established in 1862 by J. Wolstenholme [17].

Lemma 2.2 (see [17]; also [2], [5] and [10]). *If $p > 3$ is a prime, then*

$$H_{p-1} \equiv 0 \pmod{p^2}. \tag{21}$$

The following result is well known and elementary.

Lemma 2.3 (see, e.g., [12, Lemma 2.1 (2.2)]). *If $p \geq 3$ is a prime, then*

$$\binom{p-1}{k} \equiv (-1)^k \left(1 - pH_k + \frac{p^2}{2}(H_k^2 - H_{k,2}) \right) \pmod{p^3}, \tag{22}$$

for each $k = 0, 1, \ldots, p-1$.

Proof of Theorem 1.2. Taking $n = p-1$ into the identity (20) of Lemma 2.1 and using the identities $\binom{p}{m+1} = \frac{p}{m+1}\binom{p-1}{m}$ and $\binom{p}{m+1} - \binom{p-1}{m} = \binom{p-1}{m+1}$, we find that

$$\begin{aligned}
\sum_{k=m}^{p-1}\binom{k}{m}H_k &= \binom{p}{m+1}\left(H_p - \frac{1}{m+1}\right)\\
&= \binom{p}{m+1}\left(H_{p-1} + \frac{1}{p} - \frac{1}{m+1}\right)\\
&= \binom{p}{m+1}H_{p-1} + \frac{1}{p}\binom{p}{m+1} - \frac{1}{m+1}\binom{p}{m+1} \qquad (23)\\
&= \binom{p}{m+1}H_{p-1} + \frac{1}{m+1}\binom{p-1}{m} - \frac{1}{m+1}\binom{p}{m+1}\\
&= \binom{p}{m+1}H_{p-1} - \frac{1}{m+1}\left(\binom{p}{m+1} - \binom{p-1}{m}\right)\\
&= \frac{p}{m+1}\binom{p-1}{m}H_{p-1} - \frac{1}{m+1}\binom{p-1}{m+1}.
\end{aligned}$$

Using the congruence (21) of Lemma 2.2 and the assumption $0 \le m \le p-2$, we obtain

$$\frac{p}{m+1}\binom{p-1}{m}H_{p-1} \equiv 0 \pmod{p^3}. \qquad (24)$$

Furthermore, by the congruence (22) of Lemma 2.3, we have

$$-\binom{p-1}{m+1} \equiv (-1)^m\left(1 - pH_{m+1} + \frac{p^2}{2}(H_{m+1}^2 - H_{m+1,2})\right) \pmod{p^3}. \qquad (25)$$

Applying the congruences (24) and (25) to the right hand side of the identity (23), we immediately get

$$\sum_{k=m}^{p-1}\binom{k}{m}H_k \equiv \frac{(-1)^m}{m+1}\left(1 - pH_{m+1} + \frac{p^2}{2}(H_{m+1}^2 - H_{m+1,2})\right) \pmod{p^3}. \qquad (26)$$

The congruence (26) is actually the congruence (7) of Theorem 1.2. This completes the proof. □

Proof of Corollary 1.3. Taking $m = 0$ and $m = 1$ into the congruence (7) of Theorem 1.2, we immediately give the congruences (8) and (9), respectively.

Taking $m = 2$ into the congruence (7), we find that

$$\sum_{k=2}^{p-1}\binom{k}{2}H_k \equiv \frac{1}{3}\left(1 - \frac{11p}{6} + p^2\right) \pmod{p^3},$$

which can be written as

$$\sum_{k=2}^{p-1}\frac{k^2H_k}{2} - \sum_{k=2}^{p-1}\frac{kH_k}{2} \equiv \frac{1}{3}\left(1 - \frac{11p}{6} + p^2\right) \pmod{p^3}. \qquad (27)$$

By using the congruences (27) and (9), we obtain

$$\begin{aligned}\sum_{k=1}^{p-1} k^2 H_k &\equiv \sum_{k=1}^{p-1} kH_k + \frac{2}{3}\left(1 - \frac{11p}{6} + p^2\right) \pmod{p^3} \\ &\equiv -\frac{p^2-3p+2}{4} + \frac{2}{3}\left(1 - \frac{11p}{6} + p^2\right) \pmod{p^3} \\ &= \frac{15p^2-17p+6}{36} \pmod{p^3}.\end{aligned}$$

The above congruence is in fact the congruence (10) of Corollary 1.3.

Finally, in order to prove the congruence (11), we put $m = 3$ into the congruence (7). This immediately yields

$$\sum_{k=3}^{p-1} \binom{k}{3} H_k \equiv -\frac{1}{4}\left(1 - \frac{25p}{12} + \frac{35p^2}{24}\right) \pmod{p^3}.$$

By substituting $\binom{k}{3} = \frac{k^3-3k^2+2k}{6}$ into above congruence, it can be written as

$$\sum_{k=3}^{p-1} \frac{k^3 H_k}{6} - \sum_{k=3}^{p-1} \frac{k^2 H_k}{2} + \sum_{k=3}^{p-1} \frac{kH_k}{3} \equiv -\frac{1}{4}\left(1 - \frac{25p}{12} + \frac{35p^2}{24}\right) \pmod{p^3}. \tag{28}$$

By using the congruences (28), (9) and (10), we have

$$\begin{aligned}\sum_{k=1}^{p-1} k^3 H_k &\equiv 3\sum_{k=1}^{p-1} k^2 H_k - 2\sum_{k=1}^{p-1} kH_k - \frac{3}{2}\left(1 - \frac{25p}{12} + \frac{35p^2}{24}\right) \pmod{p^3} \\ &\equiv \frac{15p^2-17p+6}{12} + \frac{p^2-3p+2}{2} - \frac{35p^2-50p+24}{16} \pmod{p^3} \\ &= -\frac{21p^2-10p}{48} \pmod{p^3}.\end{aligned}$$

The above congruence coincides with the congruence (11) of Corollary 1.3, and thus, the proof is completed. □

Remark 2.4. Of course, by applying the recursive method used in proof of Corollary 1.3, it is possible to determine the expression for $\sum_{k=1}^{p-1} k^m H_k \pmod{p^3}$ for each positive integer m, where $p > 3$ is a prime. Furthermore, it is obvious that each of these congruences can be written in the form

$$\sum_{k=1}^{p-1} k^m H_k \equiv a_m p^2 + b_m p + c_m \pmod{p^3},$$

where a_m, b_m and c_m are rational numbers depending on m whose denominators are not divisible by p.

REFERENCES

[1] R.L. Graham, D.E. Knuth and O. Patashnik, *Concrete Mathematics: a foundation for computer science*, Addison-Wesley Publishing Company, Amsterdam, 2nd edition (1994).
[2] A. Granville, *Arithmetic properties of binomial coe_cients. I. Binomial coe_cients modulo prime powers,* in: Organic Mathematics (Burnaby, BC, 1995), 253-276, CMS Conf. Proc., 20, American Mathematical Society, Providence, RI (1997).
[3] K. Ireland and M. Rosen, *A Classical Introduction to Modern Number Theory*, Springer-Verlag, New York (1982).
[4] R. Meštrović, "Proof of a congruence for harmonic numbers conjectured by Z.W. Sun", *Int. J. Number Theory,* **8**, 1081-1085 (2012); *preprint arXiv:1108.1171v1* [math.NT] (2011).
[5] R. Meštrović, "Wolstenholme's theorem: its generalizations and extensions in the last hundred and fifty years (1862-2012)", *preprint arXiv*:*1111.3057v2* [math.NT] (2011).
[6] R. Meštrović, "On the mod p^2 determination of $\sum_{k=1}^{p-1} H_k \Big/ \left(k \cdot 2^k\right)$: another proof of a conjecture by Sun", *Publ. Math. Debrecen,* **82**, 107-123 (2013); *preprint arXiv*:*1108.3197* [math.NT] (2011).
[7] R. Meštrović, "An extension of Sury's identity and related congruences", *Bull. Aust. Math. Soc.,* **85**, 482-496 (2012).
[8] R. Meštrović, "An extension of a congruence by Tauraso", *ISRN Combinatorics*, **2013**, Article ID 363724, 7 pages (2013); *preprint arXiv:1109.3155v1* [math.NT] (2011).
[9] R. Meštrović, "Some Wolstenholme type congruences", *Math. Appl.*, **2**, 35-42 (2013)
[10] R. Meštrović, "On the mod p^7 determination of $\binom{2p-1}{p-1}$", *Rocky Mount. J. Math.*, **44**, 633-648 (2014); *preprint arXiv:1108.1174* [math.NT] (2011).
[11] C. Schneider, "Symbolic summation assists combinatorics", *Sèminaire Lotharingien de Combinatoire,* **56**, Article B56b (2007).
[12] Z.W. Sun, "Arithmetic theory of harmonic numbers", *Proc. Amer. Math. Soc.*, **140**, 415-428 (2012).
[13] Z.W. Sun, "On harmonic numbers and Lucas sequences", *Publ. Math. Debrecen*, **80**, 25-41 (2012); *preprint arXiv:1001.0348v2* [math.NT] (2011).
[14] Z.W. Sun and L.L. Zhao, "Arithmetic theory of harmonic numbers (II)", *Colloq. Math.*, **130** 67-78 (2013); *preprint arXiv:0911.4433v6* [math.NT] (2011).
[15] Z.W. Sun and R. Tauraso, "New congruences for central binomial coefficients", *Adv. Appl. Math.,* **45**, 125-148 (2010).
[16] R. Tauraso, "New harmonic number identities with applications", *Sèm. Lothar. Combin.*, **63**, Article B63g (2010).
[17] J. Wolstenholme, "On certain properties of prime numbers", *Quart. J. Pure Appl. Math.*, **5**, 35-39 (1862).
[18] J. Zhao, "Wolstenholme type theorem for multiple harmonic sum", *Int. J. Number Theory*, **4**, 73-106 (2008).
[19] X. Zhou and T. Cai, "A generalization of a curious congruence on harmonic sums", *Proc. Amer. Math. Soc.*, **135**, 1329-1333 (2007).

Received January 10, 2017

STOCHASTIC-THERMODYNAMIC MODELING OF THE DEVELOPED STRUCTURED TURBULENCE

A.V. KOLESNICHENKO[*] AND M.YA. MAROV[**]

[*]Keldysh Institute of Applied Mathematics of the Russian Academy of Sciences,
Moscow, Russia;
e-mail: kolesn@keldysh.ru

[**]Vernadsky Institute of Geochemistry and Analytical Chemistry of Russian Academy of Sciences
Moscow, Russia;
e-mail: marovmail@yandex.ru

Summary. The paper deals with a phenomenological model of the developed turbulence in a compressible homogeneous medium with an account for nonlinear cooperative processes. The bottom line is representation of turbulized fluid motion as a thermodynamic system consisting of two continua, the subsystem of averaged motion and the subsystem of turbulent chaos, the latter addressing as conglomerate of vortex structures of various spatiotemporal scales. We develop the ideas of a stationary non-equilibrium state of the dissipative active subsystem of turbulent chaos that emerges due to influx of negentropy from external medium (the subsystem of averaged motion) and the appearance of relatively stable coherent vortex structures in the system when the flow control parameters are varied. This allows us to consider some of the turbulent field rearrangements as self-organization processes in an open system. Methods of the stochastic theory of irreversible processes and extended irreversible thermodynamics are used to derive the defining relations for the turbulent fluxes and forces to close the system of averaged hydrodynamic equations and describe the transport and self-organization processes in the stationary non-equilibrium case sufficiently to be used in some practical applications.

1 INTRODUCTION

Turbulence is regarded as the most common type of fluid motion in nature. Traditionally, it was mainly represented as a fine-grained fluctuating continuum in a state of total stochastic chaos. However, a different viewpoint on turbulence that was probably first put forward explicitly by Prigogine[1] is also admissible. According to this approach, a real turbulent fluid flow is a less-random and macroscopically more organized process than it seems at the first glance: transition from a laminar flow to a turbulent one is regarded as the process of self-organization whereby part of the energy of turbulent chaos corresponding to small-scale fluctuations of thermo-hydrodynamic fluid parameters passes into a macroscopically organized motion of vortex coherent structures (CSs). This increases the internal order of the turbulized hydrodynamic system compared to molecular chaos (laminar fluid motion). In particular, the cascade fragmentation of vortices in fully developed turbulence can also be interpreted as an unbounded sequence of self-organization processes. In this case, the set of spatiotemporal scales on which such a process unfolds corresponds to a coherent behavior of an enormous

2010 Mathematics Subject Classification: 00A69, 00A79, 00A71.
Key words and Phrases: Structured turbulence, Irreversible thermodynamics, Defining relations, self-organization processes, Fokker–Planck equations

number of particles exhibited in the formation of relatively stable mesoscale super-molecular structures (when molecules are involved in collective, coordinated, and interrelated motions corresponding to different-scale vortices continuously distributed in a real fluid flow). This change of the view on turbulence is clearly expressed in Prigogine's utterance[2], who "could predict thirty years ago that non-equilibrium leads to self-organization in the form in which we observe it in hydrodynamic instabilities like Bernard cells."

As has now become clear, the presence of relatively large coherent vortex structures (turbulent filaments, rings, vortex spirals, etc.) randomly distributed in space and time is a characteristic feature of many, if not all, developed turbulent flows[3-6]. According to the latest viewpoints[7], hydrodynamic turbulence, which is among the most complex dynamical phenomena, is related, in particular, to the formation and development of an enormous number of organized dissipative vortex structures with various spatiotemporal scales under certain fluid flow conditions in an essentially non-equilibrium open system. For instance, the self-organization processes against the background of a chaotic fluctuating motion of cosmic matter appear to be the most important mechanism that form the peculiar features in astro- and geophysical objects at various stages of their evolution, including formation of galaxies and galaxy clusters, birth of stars from the diffuse medium of gas-dust molecular clouds, formation of protoplanetary disks and subsequent accumulation of planetary systems, formation of planetary and cometary gaseous envelopes (atmospheres), and the different-scale flows in atmospheres and circumplanetary plasma environment, just to mention a few.

Based on the currently available experimental data[8] where a comprehensive overview of the relevant publications is contained), a coherent vortex structure can be defined as a connected, liquid mass with phase-correlated (i.e., coherent) vortices in the entire region of coordinate space occupied by the structure. In the last decade, a large number of various CSs have been discovered and their topological properties firmly established owing to progress achieved in developing the technique for a visual observation of turbulized fluid flows. As examples, we could mention such CSs as vortex filaments, Taylor vortices, turbulent spots, vortex balls, hairpin-like vortices, burstings, vortex spirals, streaks, Brawn–Thomas structures, and mushroom-shaped vortices. The frequency of occurrence of a particular structure depends on the type of flow (a boundary layer, a mixing layer, a jet, etc.) and on the geometry and regime of turbulized fluid motion. As a rule, such vortex structures are localized in space and do not overlap and therefore, they can often be considered as lumped objects–clusters. Their mean free paths is much larger than their own sizes. By definition, the characteristic CS size is the largest spatial scale l on which coherent vorticity exists; the latest results show that l can be much smaller than the characteristic hydrodynamic flow scale L but larger than the Kolmogorov scale η, i.e., it can lie in the inertial range of scales, $\eta < l << L$. Due to the interaction of individual CSs (e.g., according to the Biot–Savart law in the case of two simple vortices), which generally is essentially nonlinear, they combine or break up, i.e., a new single structure (e.g., a spiral vortex) or adjacent similar structures (rings, balls, etc.) set up, which can be connected by ropes – the regions of low coherent vorticity. Below, we will proceed from the idea that the mesoscale spatiotemporal CSs are random in all range of the parameters used for their description.

Unfortunately, a direct numerical simulation of the developed turbulent motion based on exact (instantaneous) hydrodynamic equations encounters great mathematical difficulties, while constructing a full-blown hydromechanics theory of structured turbulence is hardly pos-

sible because mechanisms of the formation, interaction, and evolution of different-scale vortex structures are extremely complex. For this reason, the development of new model approaches (including phenomenological ones) to describing fully developed turbulence, the introduction of additional internal parameters of a medium (including those characterizing small-scale flow structures), the introduction of universal laws and special relations supplementing the known mass, energy, and momentum conservation laws equations are required. Basically, while semiempirical modeling of the structured turbulence is idealized description of a real fluid flow, such an approach is inevitable in order to preserve the main features of the most important hydrodynamic effects and minimize computational efforts.

Hence, to construct an adequate model of "highly organized" turbulent flow, it is generally necessary to incorporate relatively large dissipative coherent structures, along with fine-grained patterns of fluctuating field of thermo-hydrodynamic flow parameters. They should be taken into account when modeling both the process of yet non-turbulized surrounding fluid transfer into turbulized motion and the fully developed turbulent mass, momentum, and heat transport processes. In other words, any efficient continuum model of turbulence cannot be constructed without including explicitly enough spatiotemporal coherent structures and without describing them by some internal state parameters of fluctuating flow. According to Frisch[9], such regular vortex structures are, in a sense, the "sinews" of turbulence. Consequently, the true possibilities to overcome efficiently various mechanical and mathematical problems when dealing with their formulations and numerical implementations become open up only in turbulence modeling with an account of its internal structurization[10-13].

The phenomenon of structured turbulence is rooted in the order–chaos relationship in turbulized fluid flows. Different complex patterns in the behavior of open fluctuating hydrodynamic systems form spatiotemporal vortex structures with no specific impact from outside through self-organization, i.e., establish "order through fluctuations" far from local thermodynamic equilibrium. Unfortunately, although more than 30 years has elapsed since the understanding of the synergetic nature of turbulence as a self-organization process, the views of dissipative coherent structures emerging in a flow have not yet been implemented into development of model approaches aimed at creating practical (engineering) methods of turbulence calculation based, as a rule, on hydrodynamic equations. At the same time, extending the formalism of non-equilibrium thermodynamics to media with excited internal degrees of freedom of macromolecules (which can be described by additional parameters characterizing the internal microstructure of the medium) probably allows us to extend this approach to modeling the cascade transport of kinetic energy by vortices of various sizes formed by their successive fragmentation in the developed turbulent flow.

Here we consider a synergetic approach to the phenomenological modeling the developed turbulence in a compressible homogeneous fluid with an account for the nonlinear cooperative processes. The goal of this study is an attempt to construct a phenomenological hydrodynamic model of stationary non-equilibrium turbulence using the methods of extended irreversible thermodynamics with internal variables[14,15] and statistical thermodynamics of irreversible processes[16,17]. It turned out very efficient in the study of different physical problems, by taking into account the nonlinear cooperative processes in them giving rise to various non-equilibrium dissipative vortex structures far from thermodynamic equilibrium[18]. In other words, we will attempt to obtain in phenomenological way a closed system of averaged hydrodynamic equations which would described self-consistently the various turbulent transport and self-organization processes. In this approach, the vortex CSs belonging to the strongly

localized regions of small-scale motion of the subsystem of turbulent chaos should be taken into account both at the stage of laminar flow turbulization due to the development of a hierarchy of some type instabilities (e.g., the Kelvin–Helmholtz instability in free shear flows — in mixing layers, jets, wakes, etc., or the Taylor–Gertler instability in the sublayer of a turbulent boundary layer where longitudinal vortices can appear in near-wall layers) and at the stage of developed turbulence given all possible resonant situations associated, for example, with the synchronization of small-scale vorticity in a strongly turbulized fluid flow. Herewith, by the synchronization of regular and chaotic (stochastic) oscillations we mean the establishment of some relations between the characteristic frequencies and phases of self-oscillating systems as a result of their mutual influence.

We will also discuss the synergetic approach to constructing a phenomenological model of the developed turbulence in a compressible homogeneous fluid by taking into account the nonlinear cooperative processes. Including a set of random variables in the model as the internal parameters of the subsystem of turbulent chaos related to its microstructure allows us in this case to derive the Fokker–Planck–Kolmogorov (FPK) kinetic equations in configuration space by thermodynamic methods. These equations are designed to determine the temporal evolution of the conditional probability density for the random structural parameters of chaos (referring, in particular, to the cascade fragmentation of large-scale vortices or temperature inhomogeneities). They will be also used to analyze the Markovian stochastic processes of the transition from one quasi-non-equilibrium state of turbulent chaos to another through a successive loss of fluid flow stability when varying the corresponding control parameters. As it will be shown, stabilization of the subsystem of chaos near a subsequent stationary-non-equilibrium state in configuration space corresponds to the transition of turbulized system to a new state appropriate to the formation of complex spatiotemporal CSs in a turbulized flow.

2 SYSTEM OF HYDRODYNAMIC EQUATIONS OF THE MEAN MOTION FOR A SINGLE-COMPONENT COMPRESSIBLE FLUID

Developed turbulence is known to be realized at the finite but fairly large Reynolds number and is characterized by continuous Fourier spectra (both temporal and spatial ones) suggesting an existence of multiscale structure in the field of hydro-thermodynamic parameters. Basically, multiscale structure of a fluid flow when an enormous number of degrees of freedom are excited is a key signature of the developed turbulence. Therefore, any model approach to describing fully developed turbulence is regarded as one or another way of limiting the degrees of freedom.

In this study, when phenomenologically constructing the model of structured turbulence (aimed at describing "regular" fields of hydro-thermodynamic parameters), we will represent a moving fluctuating fluid as a hydro-thermodynamic system consisting of two interrelated continua (subsystems) that simultaneously fill the same volume of coordinate space continuously − the subsystem of averaged motion and the subsystem of turbulent spatiotemporal chaos[19-21]. The continuum of averaged motion obtained by the probability-theoretical averaging of the instantaneous hydrodynamic equations for a fluid is designed mainly to investigate the evolution of the averaged fields of hydro-thermodynamic parameters (including the description of large vortex structures). In turn, the subsystem of turbulent chaos (turbulent "superstructure") consists of two components (phases): proper turbulent chaos (the so-called incoherent turbulence) associated with the stochastic small-scale fluctuating motion of a

turbulized fluid, and a coherent component associated with mesoscale vortex structures in a turbulized fluid flow embedded in this almost uniform (fine-grained) fluctuating field of t hydro-thermodynamic parameters and generally having the topology of a fractal set. In the thermodynamic description of the subsystem of turbulent chaos, we will include the set of internal coordinates that ultimately correspond to excited macroscopic degrees of freedom of a turbulized fluid. This makes it possible to use the generalized Onsager formalism when modeling the processes of turbulent transport and kinetics in the total continuum. In the case under consideration, this theory describes not only the linear relaxation of the averaged extensive thermodynamic parameters to their stationary values but also the behavior of the turbulent fluctuations in the neighborhood of stationary non-equilibrium states of chaos[17]. By applying the well-known extension of the formalism of non-equilibrium thermodynamics to systems with internal degrees of freedom[22], we can obtain the FPK kinetic equations for the distribution functions of the characteristic parameters of small-scale turbulence and on their basis to model the Richardson–Kolmogorov cascade process.

It should be noted that our separation of a real fluctuating fluid flow into imaginary (averaged and turbulent) ones, in general, depends on the choice of the spatiotemporal region for which the mean values of the local physical variables that are continuous functions of the coordinates $\mathbf{r}$ and time t have been established, i.e., to some extent, it is arbitrary. Below, we will assume the hydrodynamic scale of averaged motion L (the Obukhov[23,24] scale of observation or the resolution step of the finite-difference grid) lying in the inertial range $\eta < \Lambda << L$ and determined by the size $d\mathbf{r} \sim \Lambda^3$ of the averaging region G to be such that the subsystem of turbulent chaos contains the entire set of mesoscale CSs whose size is smaller than the averaging region, $l < \Lambda$. Here, $\eta = (\nu^3 / \varepsilon_b)^{1/4}$ is the Kolmogorov length scale that characterizes the effect of viscous dissipation on the structure of small-scale turbulence; L is the external or integral scale of turbulence characterizing its generation mechanism; ε_b is a key parameter of the Richardson–Kolmogorov cascade vortex fragmentation process that is the mean dissipation rate of turbulent energy per unit fluid mass per unit time and simultaneously (under quasi-equilibrium conditions) the transfer rate of the kinetic energy of fluctuating motion over the hierarchy of vortices. According to the existing estimates, for the averaged flow to contain the bulk (80 or 90 %) of the total energy of a turbulized flow, the averaging scale Λ must be smaller than the integral turbulence scale L by a factor of 10–20. Note that the specificity of the two-phase structure of turbulent chaos manifests itself in the additional turbulent momentum and energy transport by vortex coherent structures. This slightly modifies the known closure models (defining relations) and necessitates refining the effective (given the presence of CSs in the flow) turbulent viscosity and thermal conductivity coefficients.

We will follow the classical approach to the phenomenology of fully developed turbulence. It is based on Reynolds' idea of averaging the instantaneous equations of fluid motion for fluctuating hydro-thermodynamic parameters over space and/or time or through a different equivalent procedure, for example, through the probability-theoretical averaging over an ensemble of statistically similar hydrodynamic systems under identical external conditions adopted in statistical hydrodynamics[25]. Under the standard in statistical physics assumption about the system's ergodicity, when the time (space) average of any physical variable can be identified with its probability-theoretic average, these averaging's filter out the modes of mo-

tion whose scale is smaller than the spatiotemporal averaging interval. These small-scale fluctuating motions excluded in the averaging process are assumed to contribute to the turbulent fluid motion determined by the fluctuations of hydrodynamic parameters with respect to the corresponding average values. Actually, it is this small-scale turbulent motion that is modeled below by the subsystem of turbulent chaos.

It is important to notice that the averaging problem is a central one in the mechanics of natural media. In the case of such a complex system as structured turbulence, the construction of its macroscopic model itself often depends precisely on the averaging method. Bearing in mind the various applications of the turbulence model being developed, in particular, to astrophysical phenomena in which the ratio of the characteristic fluid velocity to the average speed of sound (a measure of significance of the fluid density fluctuations) is much greater than unity, we will assume the system's mass density $\rho(\mathbf{r},t)$ to be variable. As is known, the averaging's in classical theories of turbulence with a constant mass density usually for all physical parameters of the medium without exception are introduced in some identical way, as a rule, without any weight coefficients. At the same time, such an identical averaging for all physical parameters in the case of a fluid with a variable mass density leads not only to cumbersome hydrodynamic equations of mean motion but also to difficulties in the physical interpretation of some individual terms in them. Therefore, when constructing a phenomenological model of structured turbulence in a compressible medium, in addition to the "ordinary" means $f(\mathbf{r},t)$ of some hydro-thermodynamic variables $\overline{f(\mathbf{r},t)}$ (e.g., the density or pressure), we will also use the Favre means[26] for some other parameters $g(\mathbf{r},t)$ (e.g., the temperature or hydrodynamic velocity) specified by the relation

$$\langle g(\mathbf{r},t)\rangle = \overline{\rho g(\mathbf{r},t)} / \overline{\rho} = \lim_{M\to\infty} \frac{1}{M}\sum_{p=1}^{M} \rho^{[p]} g^{[p]} / \lim_{M\to\infty} \frac{1}{M}\sum_{p=1}^{M} \rho^{[p]} \ . \qquad (1)$$

Here, the summation is over the set of possible realizations $[p]$ $(1 \le [p] \le M)$ [or a stochastic hydrodynamic system; $f(\mathbf{r},t) = \overline{f} + f'$, $g(\mathbf{r},t) = \langle g\rangle + g''$, where g'' and f' are the corresponding turbulent fluctuation, with $\overline{g''} \ne 0$ and $\overline{f'} = 0$. Below, unless stated otherwise, the letter in angle brackets will denote the weighted-mean averaging of the corresponding physical quantity. Let us write out here the properties of the weighted-mean averaging of physical quantities that are often used in this paper:

$$\overline{\rho g f} = \overline{\rho}\langle g\rangle\langle f\rangle + \overline{\rho g'' f''}, \quad \overline{\rho g''} = 0, \quad \overline{g''} = -\overline{\rho' g''} / \overline{\rho},$$

$$\overline{\rho\left\{\frac{\partial f}{\partial t} + \mathbf{u}\cdot\frac{\partial f}{\partial \mathbf{r}}\right\}} = \overline{\rho}\left\{\frac{\partial\langle f\rangle}{\partial t} + \langle\mathbf{u}\rangle\cdot\frac{\partial\langle f\rangle}{\partial\mathbf{r}}\right\} + \frac{\partial}{\partial\mathbf{r}}\left(\overline{\rho f''\mathbf{u}''}\right) = \overline{\rho}\frac{D\langle f\rangle}{Dt} + \frac{\partial}{\partial\mathbf{r}}\mathbf{J}_f^{turb},$$

$$\frac{D}{Dt}(..) = \frac{\partial}{\partial t}(..) + \langle\mathbf{u}\rangle\cdot\frac{\partial}{\partial\mathbf{r}}(..).$$

Here, the turbulent flux of an attribute $f(\mathbf{r},t)$ is denoted by

$$\mathbf{J}_f^{turb}(\mathbf{r},t) \equiv \overline{\rho f''\mathbf{u}''} = \overline{\rho}\langle f''\mathbf{u}''\rangle .$$

These relations can be easily derived from definition (1) and the Reynolds averaging postulates.

The system of exact hydrodynamic equations of mean motion for a single component compressible fluid obtained by the probability-theoretical averaging of the corresponding instantaneous hydrodynamic equations which is valid on the microscale is as follows:

$$\overline{\rho}\frac{D\langle v\rangle}{Dt} = div\langle \mathbf{u}\rangle , \quad (\langle v\rangle = 1/\overline{\rho}), \tag{2}$$

$$\overline{\rho}\frac{D\langle \mathbf{u}\rangle}{Dt} = -\frac{\partial \overline{p}}{\partial \mathbf{r}} + \left(\frac{\partial}{\partial \mathbf{r}}\cdot \mathbf{P}^{\Sigma}\right) + \overline{\rho}\mathbf{F}, \tag{3}$$

$$\overline{\rho}\frac{D\langle E\rangle}{Dt} = -div\left(\overline{\mathbf{q}} + \mathbf{q}^{turb} - \overline{p'\mathbf{u}''}\right) - \overline{p}div\langle \mathbf{u}\rangle + \left(\overline{\mathbf{P}} : \frac{\partial\langle \mathbf{u}\rangle}{\partial \mathbf{r}}\right) -$$
$$- \overline{p'div\,\mathbf{u}''} + \left(\mathbf{J}_v^{turb}\cdot\frac{\partial \overline{p}}{\partial \mathbf{r}}\right) + \overline{\rho}\langle \varepsilon_b\rangle , \tag{4}$$

$$\overline{p} = \overline{\rho}\mathsf{R}\langle T\rangle . \tag{5}$$

Here, $\mathbf{u}(\mathbf{r},t)$; $p(\mathbf{r},t)$, $v(\mathbf{r},t)$; $E(\mathbf{r},t)$ are, respectively, the instantaneous values of the hydrodynamic velocity, pressure, specific volume ($v = 1/\rho$), and specific internal energy for a fluid particle; $\langle \mathbf{u}\rangle = \overline{\rho\mathbf{u}}/\overline{\rho}$ is the Favre-averaged hydrodynamic velocity of the medium; $D(..)/Dt = \partial(..)/\partial t + \langle \mathbf{u}\rangle\cdot\partial(..)/\partial\mathbf{r}$ is the total time derivative relative to the averaged velocity field; $\overline{p}(\mathbf{r},t)$ is the average pressure; R is the gas constant; $\mathbf{F}(\mathbf{r},t)$ is the external force acting on a unit mass (in this section, we neglect the fluctuations in mass force); $\mathbf{P}^{\Sigma}(\mathbf{r},t) = \overline{\mathbf{P}}(\mathbf{r},t) + \mathbf{R}(\mathbf{r},t)$ is the total stress tensor in a turbulent flow; $\overline{\mathbf{P}}(\mathbf{r},t)$ is the average molecular viscous stress tensor; $\mathbf{R}(\mathbf{r},t) \equiv -\overline{\rho\mathbf{u}''\mathbf{u}''}$ is the turbulent (Reynolds) stress tensor; $\overline{\mathbf{q}}(\mathbf{r},t)$ is the average molecular heat flux; $\mathbf{q}^{turb}(\mathbf{r},t) = \overline{\rho H''\mathbf{u}''}$ and $\mathbf{J}_v^{turb}(\mathbf{r},t) = -\overline{\rho'\mathbf{u}''}/\overline{\rho}$ are, respectively, the turbulent heat and specific volume fluxes (here, we use the relation $\rho v'' = -\rho'/\overline{\rho}$; $H(\mathbf{r},t) = E + p/\rho$ is the instantaneous value of the specific fluid enthalpy; $\langle \varepsilon_b(\mathbf{r},t)\rangle \equiv \overline{\rho\varepsilon_b}/\overline{\rho} = \overline{(\mathbf{P} : \partial\mathbf{u}''/\partial\mathbf{r})}/\overline{\rho}$ is the weighted-mean value of the specific dissipation rate of turbulent kinetic energy into heat due to molecular viscosity ν.

It can be seen from the system of equations (2)–(5) that the averaged motion of a turbulized homogeneous fluid is characterized by: 1) the average molecular thermodynamic fluxes $\overline{\mathbf{q}}(\mathbf{r},t)$ and $\overline{\mathbf{P}}(\mathbf{r},t)$ for which the corresponding defining relations are needed (they are derived for a turbulized medium using the thermodynamic approach, for example[27]); and 2) the as yet indefinite mixed one-point one-time correlations (second-order moments) $\mathbf{R}(\mathbf{r},t)$,

$\mathbf{q}^{turb}(\mathbf{r},t)$, and $\mathbf{J}_v^{turb}(\mathbf{r},t)$, which represent the so-called turbulent fluxes of the fluid characteristics related to the fluctuations of hydro-thermodynamic parameters. The correlation terms including pressure fluctuations $\overline{p'div\,\mathbf{u}''}$ and $\overline{div(p'\mathbf{u}'')}$ as well as the weighted-mean viscous dissipation rate of turbulent energy $\langle\varepsilon_b\rangle$ should also be determined. When the model of developed turbulence is constructed phenomenologically, the defining (constitutive) relations closing the system (2)–(5) can be established by the same method as in the laminar case, i.e., in accordance with the thermodynamic rules of continuum mechanics by the Onsager method. However, the additional basic idea that the corresponding thermodynamic forces are also responsible for the linear relaxation of the fluctuating characteristics of turbulized chaos to its stable stationary non-equilibrium state[17] will be further used as well.

3 THERMODYNAMICS OF THE STRUCTURED TURBULENCE. INTERNAL FLUCTUATING COORDINATES OF THE SUBSYSTEM OF TURBULENT CHAOS

An important task we face is to suggest a concept that would allow us to go beyond the classical formalism of irreversible thermodynamics. This goal can be achieved by expanding the space of independent basic variables by introducing the internal coordinates defining the microstructure of the subsystem of turbulent chaos. The subsequent step involves finding the evolutionary equations for these additional state parameters.

Within the framework of the complete model of structured turbulence, the system of equations (2)–(5) obtained by the probability-theoretical averaging of the instantaneous hydrodynamic equations for a single-component fluid is designed to study the spatiotemporal evolution of the averaged fields of hydrodynamic quantities, including various large vortex structures. Following Prigogine's viewpoint on hydrodynamic turbulence as a macroscopically highly organized flow we will address the subsystem of turbulent (vortex) chaos as a continuum with a certain internal microstructure. Moreover, recalling the above said, we will assume that the vortex continuum consists of two components: proper turbulent chaos (the so called incoherent turbulence) associated with the stochastic small-scale fluctuating motion of a turbulized fluid, and a coherent component embedded in this almost uniform fluctuating field of hydrodynamic parameters. The latter component is an ensemble of mesoscale vortex structures (multi-molecular structures) whose images in the phase space of an equivalent dynamical system are classical attractors (e.g., limit cycles) or strange attractors (having a fractal structure). Each of these two subsystems is thermodynamically open, i.e., capable to exchange energy and entropy (but not mass) with the adjacent subsystem. We also assume the hydrodynamic velocity fields for the subsystems of averaged motion and turbulent chaos to be coincident, because no separation of the corresponding Lagrangian volumes (diffusion effect) occurs in the process of a real turbulent fluid motion, i.e. the subsystem of turbulent chaos has no macroscopic hydrodynamic velocity relative to the subsystem of averaged motion. Let us note that a different approach to modeling structured turbulence associated, in particular, with the triple decomposition of the instantaneous motion of a fluid into an averaged motion and coherent and incoherent fluctuations is also known. The hydrodynamic equations with double averaging over time and over a specially chosen ensemble determined by some features char-

acteristic of CSs, serve as a basis for such models. However, this procedure encounters some internal inconsistencies[8].

It should be emphasized once again that our artificial separation of a real turbulized fluid flow into imaginary averaged and turbulent (vortex, fluctuating) ones is just a way of pictorially describing the phenomenon to be convenient for modeling. For any elementary volume $d\mathbf{r}$ of the medium in each of these subsystems, we determine local "coarse-grained" thermodynamic parameters (which are continuous functions of the coordinates $\mathbf{r}$ and time t), such as density, pressure, temperature, internal energy, and entropy[i]. Furthermore, we additionally characterize the subsystem of turbulent chaos by a number of internal coordinates that are ultimately related to its microstructure. Note that such primary concepts as the generalized temperature and entropy of the subsystem of turbulent chaos have no precise physical interpretation and they are introduced only to ensure coherence of the theory[15].

It is also assumed that the generalized thermodynamic state parameters characterizing the stationary non-equilibrium vortex structure of turbulent chaos are related by ordinary relations in the local equilibrium thermodynamics such as the Gibbs and Gibbs–Dugham relations. They serve exclusively as a constraint on the form of the derived defining (constitutive) relations. In other words, such identities also remain valid far from local thermodynamic equilibrium of the subsystem of chaos provided that chaos is in a stable stationary non-equilibrium state choosing as a reference one. This fundamental assumption is a kind of new postulate[22] underlying the thermodynamic approach to description of the fully developed turbulence. One should be aware that since the energy of turbulent motions continuously dissipates due to molecular viscosity, it is impossible to reach the situation when the subsystem of turbulent chaos comes to a local statistically equilibrium state in principle. At the same time, for a stationary turbulized fluid flow, where the viscous energy dissipation is, on average, compensated for by the energy from the external source on a long time scale, the stationary non-equilibrium transport processes in the subsystem of turbulent chaos are affordable and do not differ much in physical sense from the local equilibrium processes in a dissipative system. Let us note that in the case under consideration, the *H*-theorem is valid since any initial state of turbulent chaos approaches a stationary non-equilibrium state in sufficiently long time.

In constructing our turbulence model, key concept of the Kolmogorov[28] theory was used. In the limit of very large $\mathbf{Re} = Lu_0 / \nu$ and Peclet $\mathbf{Pe} = L_T u_{T0} / \chi$ numbers corresponding to large-scale motions in anisotropic, inhomogeneity, and non-stationary averaged flow, the randomness of the fragmentation of vortices (or macrostructural temperature inhomogeneities) and the chaoticity of their energy transfer over the cascade downward are assumed to cause the statistical regime of turbulent fluctuations within the small spatiotemporal averaging region G of the instantaneous values of hydrodynamic parameters to be almost locally isotropic−homogeneous, isotropic, and quasi-stationary. This allows us to varying only with control parameters and primarily with the Reynolds number $\mathbf{Re}$ which eventually determines the number of cascades in the hierarchy of vortices of various order. Basically, there can be no

[i] In this connection, it is pertinent to recall the following: according to Onsager[29], the methods of statistical mechanics can be used to describe turbulent chaos in which different-scale vortices are well mixed and, hence, the methods of statistical thermodynamics of irreversible processes are also applicable.

complete local isotropy due to the presence of mesoscale vortex structures. Here, u_0 and u_{T0} are typical changes in the mean velocity at distances $\sim L$ and L_T, respectively; χ and ν are the molecular thermal diffusivity and kinematic viscosity, respectively; L_T is the distance at which the mean temperature changes noticeably. It is also assumed, for simplicity, that the Prandtl number $\mathbf{Pr} = \nu / \chi$ is of the order of unity and $L \approx L_T$; in this case, boundaries of the inertial and convective ranges within which the molecular viscosity and molecular heat conduction effects are significant may be considered to be coincident.

Let us now use the methods of extended irreversible thermodynamics[15] and non-equilibrium statistical thermodynamics[17] to obtain the defining (closing) relations for the thermodynamic fluxes and forces that describe the various turbulent transport processes in coordinate space and self-organization processes in phase space with an efficiency sufficient for practical purposes.

3.1 Thermodynamics of the Subsystem of Averaged Motion

We will begin by analyzing the balance equations for the average entropy $\langle S\rangle(\mathbf{r},t)$ of a turbulized homogeneous fluid. The probability-theoretical averaging of the Gibbs identity, which is assumed to be valid for micromotions

$$T\delta S = \delta E - p\delta v\,,$$

where $T(\mathbf{r},t)$, $S(\mathbf{r},t)$ are the instantaneous values of the absolute temperature and specific entropy in a fluid particle, respectively, leads to the fundamental Gibbs identity for the subsystem of averaged motion. This identity written along the averaged trajectory of the center of mass of a physically elementary volume $d\mathbf{r}$ takes the form

$$\frac{D\langle S\rangle}{Dt} = \frac{1}{\langle T\rangle}\frac{D\langle E\rangle}{Dt} + \frac{p}{\langle T\rangle}\frac{D\langle v\rangle}{Dt}\,. \tag{6}$$

Identity (6) can be rewritten in the form of a local balance equation for the system's average entropy $\langle S\rangle(\mathbf{r},t)$ if we eliminate the substantial time derivatives of the parameters $\langle E\rangle(\mathbf{r},t)$ and $\langle v\rangle(\mathbf{r},t)$ from it using the averaged hydrodynamic equations (2) and (4). This results in

$$\overline{\rho}\frac{D\langle S\rangle}{Dt} + div\left(\frac{\mathbf{q}^{\Sigma}}{\langle T\rangle}\right) = \sigma_{\langle S\rangle} \equiv \sigma^{(i)}_{\langle S\rangle} + \sigma^{(e)}_{\langle S\rangle}\,, \tag{7}$$

where

$$0 \le \sigma^{(i)}_{\langle S\rangle}(\mathbf{r},t) \equiv \frac{1}{\langle T\rangle}\left\{-\left(\mathbf{q}^{\Sigma}\cdot\frac{\partial \ln\langle T\rangle}{\partial \mathbf{r}}\right) + \overline{\pi}\, div\langle \mathbf{u}\rangle + \left(\overset{\circ}{\overline{\mathbf{P}}}{}^{s} : \overset{\circ}{\overline{\mathbf{D}}}\right)\right\}, \tag{8}$$

$$\sigma^{(e)}_{\langle S\rangle}(\mathbf{r},t) \equiv \frac{1}{\langle T\rangle}\left\{-\overline{p' div \mathbf{u}''} + \left(\mathbf{J}^{turb}_{(v)} \cdot \frac{\partial \overline{p}}{\partial \mathbf{r}}\right) + \overline{\rho}\langle \varepsilon_b \rangle\right\} \equiv \frac{\mathfrak{I}}{\langle T\rangle}. \qquad (9)$$

Here, $\overline{\mathbf{P}}^{s}(\mathbf{r},t)$ is the (average) shear rate tensor and $\overline{\pi}(\mathbf{r},t) \equiv \frac{1}{3}\overline{\mathbf{P}} : \mathbf{I}$ is the average viscous pressure. The positive quantity $\sigma^{(i)}_{\langle S\rangle}(\mathbf{r},t)$ defines the local production rate of the system's average entropy $\langle S\rangle(\mathbf{r},t)$ due to dissipative transport processes inside the subsystem of averaged fluid motion; as will be seen from the subsequent analysis, the quantity $\sigma^{(e)}_{\langle S\rangle}(\mathbf{r},t) \equiv \mathfrak{I} / \langle T\rangle$ (the entropy sink or source) reflects the entropy exchange between the subsystems of turbulent chaos and averaged motion. It is important to note that the quantity $\sigma^{(e)}_{\langle S\rangle}(\mathbf{r},t)$ can be different in sign depending on the specific regime of fluid motion. Indeed, the turbulent energy dissipation rate $\langle \varepsilon_b\rangle(\mathbf{r},t)$ is always positive quantity. However, the energy transition rate $\overline{p' div \mathbf{u}''}$ (the work done on turbulent vortices by the environment per unit time per unit volume due to pressure fluctuations and the expansion ($div\mathbf{u}'' > 0$) or compression ($div\mathbf{u}'' < 0$) of turbulent vortices) can be different in sign. The $\mathbf{J}^{turb}_{(v)} \cdot (\partial \overline{p} / \partial \mathbf{r})$ is positive for small-scale turbulence, but it can be both positive and negative for large-scale and mesoscale vortices[11]. Thus, it follows from (7) that, generally, the average entropy of a turbulized medium $\langle S\rangle(\mathbf{r},t)$ can both increase and decrease. This is a characteristic feature of any thermodynamically open systems.

This implies that there is some internal openness in an externally closed turbulized system modeled by two continua. It stems from the fact that the averaged motion of a turbulized fluid is described only by one of the two continua. At the same time, each physically infinitesimal volume element $d\mathbf{r} \sim \Lambda^3$ (where Λ is the averaging scale) of the medium is still assumed to be so large that the additional information about the pattern of the fluctuating motion (turbulent superstructure) on scales smaller than or equal to the size of a "mathematical point" can be taken into account in the model. Hence it follows, in particular, that the average entropy alone is clearly not enough for an adequate description of all features of structured turbulence because this quantity is not related to any parameters characterizing the internal structure and thermodynamics of the subsystem of turbulent chaos and, in particular, to such a key parameter of the theory as the turbulence energy (the average fluctuation kinetic energy per unit mass of the medium)

$$\langle b\rangle(\mathbf{r},t) = \overline{\rho(\mathbf{u}'')^2} / 2\overline{\rho}. \qquad (10)$$

For this reason, to macroscopically describe structured turbulence and, in particular, the cascade transport of turbulent energy by vortices of various scales (downward over the range of sizes), we will use a well-known generalization of the formalism of irreversible thermodynamics to media with an internal structure by introducing for this purpose generalized extensive thermodynamic parameters (internal energy $E_{turb}(\mathbf{r},t)$, generalized chemical potentials $\mu(\mathbf{q},\mathbf{r},t)$, etc.) of the subsystem of turbulent chaos related to the fluctuating fluid motion[30]

and the so-called internal coordinates corresponding to the system's microstructure. In other words, we will proceed just as has long been done in non-equilibrium thermodynamics, for example, in order to take into account various transformations in the internal degrees of freedom of molecules, in particular, to take into account the orientation of polar molecules relative to the external electric field[ii] when the formalism of a generalized chemical potential equal to the standard chemical potential and the field term dependent on the internal coordinate ϑ is used[22].

3.2 Internal Coordinates of the Subsystem of Turbulent Chaos

Thus, when modeling the stochastic system corresponding to the subsystem of turbulent chaos, we use the formalism of generalized statistical thermodynamics[16,17]. It suggests the study of a statistical ensemble of macroscopically identical subsystems of chaos with the same generalized extensive state parameters such as the average specific volume $v(\mathbf{r},t)$, internal energy $E_{turb}(\mathbf{r},t)$, and entropy $S_{turb}(\mathbf{r},t)$ of chaos and some infinite sequence of internal variables $n(\mathbf{q},\mathbf{r},t)$. The internal variables $n(\mathbf{q},\mathbf{r},t)$ can be the number densities of small-scale vortices or temperature inhomogeneities in states characterized by specified values of the parameters $\mathbf{q}$ – the internal coordinates defining the system's microstructure. We assume that the vortex structures of chaos are somehow localized in both coordinate space $\mathbf{r}$ and configuration space $\mathbf{q}$.The internal coordinates $q_k(\mathbf{r},t)$ ($k=1,...n$), which are some characteristics of the ensemble of vortex (or temperature) chaos corresponding to small-scale turbulent fluctuations, are generally random (stochastic) variables fluctuating relative to their mean (stationary) values q_k^{st}. They serve as a measure of the differences in any set of thermodynamically identical subsystems of the vortex ensemble. Allowance for the fluctuations in the internal coordinates describing the state of chaos in purely dynamical modeling refines its statistical description and leads to a more adequate reflection of reality.

The continuously changing local random parameters that adequately characterize the evolution of a turbulized fluid, including the spatiotemporal evolution of various mesoscale coherent structures, can be attributed to the stochastic internal coordinates describing the macroscopic state of turbulent chaos. Thus, some of the internal coordinates q_k can refer to the incoherent component of the subsystem of turbulent chaos, while others can characterize individual CSs. In particular, the following positive definite quantities (or their logarithms) can be chosen as the stochastic coordinates $q_k(\mathbf{r},t)$: the kinetic energy of vortices, $b=\left|\mathbf{u}''\right|^2/2$; the dissipation rate of turbulent energy into heat, $\varepsilon(\mathbf{r},t)=\frac{1}{2}\nu\sum_{i,j}(\partial u_i''/\partial r_j+\partial u_j''/\partial r_i)^2$; the scalar dissipation of temperature inhomogeneities, $\varepsilon_T(\mathbf{r},t)=\chi\sum_j(\partial T''/\partial r_j)^2$; the mixing rate of a substance with a concentration $\theta(\mathbf{r},t)$ to the molecular level (which does not affect the flow

[ii] As it is well known, this can be done by introducing an internal coordinate ϑ, the angle between the field and dipole directions.

dynamics), $\varepsilon_\theta(\mathbf{r},t) = \chi\sum_j (\partial\theta''/\partial r_j)^2$ [iii]; the system's enstrophy (in the case of 2D turbulence); the mean vorticities of the field of velocity fluctuations referring to k-th type mesoscale vortex structures (the fundamental quantities to characterize CSs), etc.

As will be further shown, using the internal coordinates as additional macroscopic parameters of turbulent chaos allows us to obtain thermodynamically the evolutionary Fokker–Planck–Kolmogorov (FPK) equations in the space of configurations $\mathbf{q}$ given in this approach Prigogine's central postulate concerning the direction of irreversible processes in any local volume of the space of internal coordinates[22] (see *Chap. 3, Sect. 11*). These kinetic equations are designed to determine the temporal evolution of the probability density function for various stochastic small-scale turbulence characteristics. They also allow one to analyze the conditions for the transition from one stable stationary non-equilibrium state of turbulent chaos to another that are eventually caused by a successive loss of fluid flow stability when changing the parameters controlling the regime of turbulent motion as a whole.

The purely classical (i.e., without any introduction of internal stochastic coordinates) thermodynamic approach to modeling turbulence seems not quite adequate in the case of a structured vortex continuum, because any two realizations of the ensemble (the set of subsystems of chaos with the same set of extensive thermodynamic state parameters) are identical in all respects when applying it, which does not correspond to the real situation. This is attributable to turbulent fluctuations in the internal coordinates of the state of chaos, which ultimately serve as a measure of the differences in any ensemble of thermodynamically identical subsystems of chaos. Actually, it is these turbulent fluctuations which are not suppressed under strongly non-equilibrium conditions but, on the contrary, are enhanced in certain situations by internal irreversible processes within the vortex subsystem at the so called bifurcation points (at which the subsystem "can choose" between various states), that lead to various mechanical manifestations of a real turbulized flow. In particular, the subsystem of turbulent chaos in some stable stationary state (far from the local thermodynamic equilibrium) at certain values of control parameters can shift to a new stationary state with a neutral stability (associated with the so-called critical point of stability loss) and, subsequently, abruptly pass to another asymptotically stable stationary state corresponding to one or another form of the supramolecular coherent behavior of a large number of particles (e.g., the oscillations of different scale vortices). Here it worth to recall that, according to Prigogine[2], this ability to bring order via fluctuations is a fundamental property of any open strongly non-equilibrium thermodynamic systems. Thus, because of the continuous turbulent fluctuations, it is convenient to imagine any quasi-stationary state of turbulent chaos as a state of not one individual subsystem but the whole physical ensemble of subsystems. That is why it is necessary to refine the thermodynamic description of a turbulized flow so as to be able to take into account in modeling the effects of stochasticity of the vortex continuum[20].

Thus, in accordance with the stochastic-thermodynamic approach we assume that for a complete statistical description of the random vector process $\mathbf{q}(\mathbf{r},t)$ in a turbulized continuum (the set of structural small-scale characteristics of chaos $\mathrm{q}_k(\mathbf{r},t)$, where $k = 1,...n$, which

[iii] The quantity ε_θ is a measure of the concentration field inhomogeneity disappearing per unit time through molecular diffusion $D \approx \chi$.

is often convenient to gather into one column vector $\mathbf{q}$ in n-dimensional configuration space), it is sufficient to keep the one-point probability density $W_1(\mathbf{q},t)$ and the joint two-point probability density $W_2(\mathbf{q}_0,t_0;\mathbf{q},t)$. The random processes that are completely described only by these two distribution functions are known to be the Markovian ones. This key assumption determines the class of random processes (turbulent fluctuations) to which the analyzed stochastic-thermodynamic model of developed turbulence is applicable. We will also use below the two-point conditional probability density, $P_2(\mathbf{q}_0,t_0;\mathbf{q},t)$, which allows the probable value of the parameter $\mathbf{q}$ at time t to be found if $\mathbf{q}=\mathbf{q}_0$ at time t_0 with a probability equal to unity. These probability densities can be used to obtain the mean values of various functions $f(\mathbf{q}(t))$ of the random state vector $\mathbf{q}(t)$; in particular, the formula $\overline{f(\mathbf{q}(t))}=\int f(\mathbf{q}(t))W_1(\mathbf{q},t)d\mathbf{q}$ defines the unconditional mean of $f(\mathbf{q}(t))$ and the formula $\overline{f(\mathbf{q}(t))}^{0}=\int f(\mathbf{q})P_2(\mathbf{q}_0|\mathbf{q},t)d\mathbf{q}$ introduces the mean of $f(\mathbf{q}(t))$ at time t provided that $f(\mathbf{q}(t_0))=f(\mathbf{q}_0)$ (conditional mean). The relationship between the means over the conditional sub-ensemble $\overline{f(\mathbf{q}(t))}^{0}$ and over the entire physical ensemble $\overline{f(\mathbf{q}(t))}$ is implicitly contained in the relation

$$P_2(\mathbf{q}_0|\mathbf{q},t)=W_2(\mathbf{q}_0,t_0;\mathbf{q},t)/W_1(\mathbf{q}_0,t_0),$$

which actually defines the so-called transition probability function P_2.

Our analysis is restricted to the so-called stationary physical ensemble of turbulent chaos consisting of adequate (in the above mentioned sense) sub-systems maintained by continuously acting external sources of turbulence in a state in which the random variables $\mathbf{q}(t)$ are invariant with respect to a shift along the time axis, i.e., $\mathbf{q}(t_p+\tau)=\mathbf{q}(t_p)$ for all p and τ. Clearly, in this case, the one-time probability density $W_1(\mathbf{q})$ will not depend on time, while the joint probability densities will be determined only by the difference $t-t_0$; for example, $P_2(\mathbf{q}_0,t_0|\mathbf{q},t)=P_2(\mathbf{q}_0,0|\mathbf{q},t-t_0)$. Bearing this in mind, we omit the initial time in the expressions for W_2 and P_2 and write them in an abridged form: $P_2(\mathbf{q}_0|\mathbf{q},t)$ etc. Also, in the case under consideration, the positive function P_2 has the following properties[17]:

$$\int P_2(\mathbf{q}_0|\mathbf{q},t)\,d\mathbf{q}=1,\quad \int W_1(\mathbf{q}_0)P_2(\mathbf{q}_0|\mathbf{q},t)\,d\mathbf{q}_0=W_1(\mathbf{q}),$$

$$\lim_{t\to\infty}P_2(\mathbf{q}_0|\mathbf{q},t)=W_1(\mathbf{q}), \tag{11}$$

the latter relation implying that the conditional probability density for stationary processes ceases to depend on the initial condition asymptotically with time.

3.3 Basic Kinetic Equation

The key proposition of the Kolmogorov[28] theory for the generation of small-scale turbulence is that the excitation of vortex structures, their non-linear interactions, and the viscous dissipation of turbulent energy are strictly separated in the space of wave numbers, when the energy influx into a turbulized flow occurs near the wave number k_L corresponding to the turbulence macroscale L, while the energy dissipation becomes efficient near the wave number k_η where η is the turbulence microscale often called the Kolmogorov's scale. In other words, the existence of an inertial range of scales ($k_L << k << k_\eta$) is characteristic signature of the developed turbulence. The energy transfer from large-scale turbulent vortices to small-scale ones can be imagined as a cascade process of their fragmentation.[iv]

For our analysis, we need the so-called basic kinetic equation for the rate of change in the number of vortex moles $n(\mathbf{q})$ in the cascade interaction between turbulent motions of different scales or for the function $P_2(\mathbf{q},t) \equiv n(\mathbf{q}) / n_\Sigma$. The latter is the (conditional) probability density to detect the system in the interval $(\mathbf{q}, \mathbf{q} + d\mathbf{q})$ at time t if it was in a state $\mathbf{q}^{st}$ at the initial time $t = 0$ with a probability equal to unity. Here,

$$n_\Sigma(\mathbf{r},t) = \int n(\mathbf{q},\mathbf{r},t) d\mathbf{q} \tag{12}$$

is the total number of vortex structures with an attribute $\mathbf{q}$ in the volume $d\mathbf{r}$.

When deriving the equation for the rate of change in the number of vortex moles $n(\mathbf{q})$ in the cascade interaction between turbulent vortices of different scales, we will assume that the cascade vortex fragmentation mechanism associated with the transition of kinetic energy from large vortices to increasingly small ones is such that the medium "retains memory" only about the last transition (Markovian process). If the number density of vortices $n(\mathbf{q}_i)$ in a state $\mathbf{q}_i$ can be changed only through their transition from the neighboring states $\mathbf{q}_i$ (the decay of large vortices with attributes $\mathbf{q}_{k-1}$ into smaller vortices with attributes $\mathbf{q}_{i-1}$ or to the neighboring states $\mathbf{q}_{i+1}$ (the interaction locality principle), then we have $\partial n / \partial t + (J_i - J_{i-1}) = 0$, where J_i is the rate of the transition $i \to i+1$ and J_{i-1} is the rate of the transition $(i-1) \to i$. Since the distribution of vorticity in a real turbulized fluid flow is continuous[v] we also assume that this transfer of the kinetic energy of averaged motion over the Richardson–Kolmogorov cascade downward can be adequately described in terms of the change in random parameters $\mathbf{q}$ taking on continuous values. In particular, this corresponds to the cascade destruction of large vortices and the formation of small ones whereby only infinitesimal changes in quantities $\mathbf{q}$ occur in a single interaction, while finite changes arise from the cumulative action of a large number of vortex interactions. In terms of chemistry, this process can be considered as a

[iv] The idea of an energy cascade was first put forward by L. Richardson in 1922.

[v] As it is well known, there is a continuum of excited degrees of freedom in the case of developed turbulence[31].

series of consecutive chemical reactions expressed by the scheme $\ldots \to (k-1) \to k \to (k+1) \to \ldots$. Note that the principle of detailed balance can generally break down for thermodynamic systems far from complete thermal equilibrium; this is also true, in particular, for the stationary non-equilibrium cascade formation of vortex structures. Consequently, for a real cascade process, the equation for the rate of change in the number density of turbulent vortices $n(\mathbf{q},t)$ should be rewritten as the standard continuity equation

$$\partial n(\mathbf{q},t)/\partial t = -(\partial/\partial \mathbf{q}) \cdot \mathbf{J}(\mathbf{q},t)$$

in the configurations space. Here, $\mathbf{J}(\mathbf{q},t)$ is the vortex flux in the inertial range corresponding to the number of "vortex moles" that pass from a state $\mathbf{q}$ to a state $\mathbf{q} + d\mathbf{q}$ in a unit time. In the more general case where the number density of turbulent vortices also depends on the spatial coordinate $\mathbf{r}$, the kinetic equation for the rate of change in $n(\mathbf{q},\mathbf{r},t)$ can be written as the continuity equation, both in the coordinate space $\mathbf{r}$ and in the space of internal coordinates $\mathbf{q}$,

$$\frac{\partial n(\mathbf{q},\mathbf{r},t)}{\partial t} + \frac{\partial}{\partial \mathbf{r}} \cdot \left\{ n(\mathbf{q},\mathbf{r},t) \langle \mathbf{u} \rangle \right\} = -\frac{\partial}{\partial \mathbf{q}} \cdot \mathbf{J}(\mathbf{q},\mathbf{r},t), \tag{13}$$

or, in view of (2), as

$$\overline{\rho} \frac{D}{Dt} \left(\frac{n(\mathbf{q},\mathbf{r},t)}{\overline{\rho}} \right) = -\frac{\partial}{\partial \mathbf{q}} \cdot \mathbf{J}(\mathbf{q},\mathbf{r},t). . \tag{13*}$$

Here, $\mathbf{J}(\mathbf{q},\mathbf{r},t)$ is the thermodynamic flux in the space of internal coordinates $\mathbf{q}$ to be determined.

3.4 Thermodynamics of the Subsystem of Structured Chaos

Thus, the transfer of turbulent energy over the cascade of vortices in the case of developed turbulence can be considered as a kind of chemical transformations with the corresponding chemical potential $\mu_{turb}(\mathbf{q},\mathbf{r},t)$ for the internal degrees of freedom $\mathbf{q}$ and the de Donder chemical affinity

$$\mathbf{A}_{turb}(\mathbf{q}) = -(\partial \mu_{turb}/\partial \mathbf{q}).$$

The latter can be treated as the driving force of the cascade process corresponding to one equivalent $n(\mathbf{q}) \to n(\mathbf{q} + \delta\mathbf{q})$ of the vortex fragmentation process. Note that the concept of chemical potential is distinguished by great generality: it is applicable to almost any model of a continuous medium if the concept of thermodynamic temperature (which is generally not the absolute temperature of the medium) can be introduced for it in one or another way.

Basically, extending the formalism of the generous chemical potential to stationary non-equilibrium turbulent chaos, we determine intensive thermodynamic parameters, such as the generalized turbulization temperature $T_{turb}(\mathbf{r},t)$ and pressure $p_{turb}(\mathbf{r},t)$ (which are not related in any way to the molecular temperature and pressure of the underlying flow). Similarly, the turbulent chemical potential $\mu_{turb}(\mathbf{q},\mathbf{r},t)$ for the internal degrees of freedom $\Phi_0(\mathbf{q})$ follows

from the fundamental Gibbs relation for the generalized entropy (specified a priori as the characteristic function)

$$S_{turb}(\mathbf{r},t)=S_{turb}\left(E_{turb}(\mathbf{r},t),\ \langle v\rangle(\mathbf{r},t),\ n(\mathbf{q})/\overline{\rho}\right) \tag{14}$$

using the relations[32]

$$\frac{1}{T_{turb}}=\left(\frac{\partial S_{turb}}{\partial E_{turb}}\right)_{\langle v\rangle,\,n/\overline{\rho}};\quad \frac{p_{turb}}{T_{turb}}=\left(\frac{\partial S_{turb}}{\partial(1/\overline{\rho})}\right)_{E_{turb},\,n/\overline{\rho}};$$

$$\frac{\mu_{turb}(\mathbf{q})}{T_{turb}}=-\left(\frac{\partial S_{turb}}{\partial(n(\mathbf{q})/\overline{\rho})}\right)_{E_{turb},\,1/\overline{\rho}}. \tag{15}$$

The chemical potential $\mu_{turb}(\mathbf{q})$ for the internal degrees of freedom is generally defined as a functional derivative. The turbulization entropy $S_{turb}(\mathbf{r},t)$ is assumed to contain all thermodynamic information about the subsystem of stationary non-equilibrium turbulent chaos, i.e., it is related to the stability, fluctuations, and dynamical changes in a quasi-stationary state in exactly the same way as the equilibrium entropy of some thermodynamic system in a local equilibrium state[17]. A remarkable feature of the entropy $S_{turb}(\mathbf{r},t)$ is that many statistical properties of turbulent chaos in quasi-stationary states can be deduced from this quantity. In particular, it is admissible to interpret the various algebraic relations for the intensive variables $E_{turb}(\mathbf{r},t)$, $T_{turb}(\mathbf{r},t)$, $p_{turb}(\mathbf{r},t)$, and $\mu_{turb}(\mathbf{q},\mathbf{r},t)$ that can be derived in a standard thermodynamic way from (15) as specific "equations of state" for the subsystem of turbulent chaos.

It is worth to emphasize that the concepts of turbulization temperature and entropy are pertinent not only to the state near local thermodynamic equilibrium of the subsystem of turbulent chaos. On the contrary, these quantities are introduced with the goal of describing thermodynamically chaos in stationary non-equilibrium states. Indeed, in this approach, in contrast to the local equilibrium entropy of the subsystem of averaged motion $\langle S\rangle(\mathbf{r},t)$, the generalized turbulence entropy $S_{turb}(\mathbf{r},t)$ generally remains an indefinite quantity. There are no experimental or physical methods to establish its true functional dependence on state parameters. Hence, this quantity is introduced into the theory exclusively with the goal of ensuring its coherence, while the explicit form of the functional equation (14) is postulated depending on the goals of modeling approach.

The differential form of the fundamental Gibbs relation for the turbulization entropy $S_{turb}(\mathbf{r},t)$ written along the trajectory of the center of mass of a physically elementary volume $d\mathbf{r}$ takes the following form[33]

$$\frac{DS_{turb}}{Dt}=\frac{1}{T_{turb}}\frac{DE_{turb}}{Dt}+\frac{p_{turb}}{T_{turb}}\frac{D\langle v\rangle}{Dt}-\frac{1}{T_{turb}}\int_{\mathbf{q}}\mu_{turb}(\mathbf{q})\frac{D}{Dt}\left(n(\mathbf{q})/\overline{\rho}\right)d\mathbf{q}. \tag{16}$$

Here the internal energy of chaos $E_{turb}(\mathbf{r},t)$ is identified with the turbulence energy[20]

$$E_{turb}(\mathbf{r},t) = \langle b \rangle + const = \overline{\rho(\mathbf{u}'')^2} / 2\overline{\rho} + const\,, \tag{17}$$

and it is assumed that the subsystem of turbulent chaos is represented thermodynamically as an ideal gas with three degrees of freedom in which the energy is distributed uniformly. Then the following equations of state can be written in the form

$$\overline{\rho}\langle b \rangle(\mathbf{r},t) = {}^{3}\!/_{2}\, \mathsf{R}\overline{\rho}\, T_{turb}\,, \quad p_{turb}(\mathbf{r},t) = \mathsf{R}\overline{\rho}\, T_{turb}\,,$$

$$\mu_{turb}(\mathbf{q}, T_{turb}) = \mathrm{k_B} T_{turb} \ln n(\mathbf{q}) + \Phi(\mathbf{q}, T_{turb})\,, \tag{18}$$

where $\mathsf{R}(= n_{\Sigma}\, \mathrm{k_B} / \overline{\rho})$ is the "gas constant" for the vortex continuum, $\mathrm{k_B}$ is the Boltzmann constant, and $\Phi(\mathbf{q}, T_{turb})$ is the so-called potential energy in internal coordinate $\mathbf{q}$, which also generally depends on the turbulization temperature $T_{turb}(\mathbf{r},t)$.

An important caveat is that the potential energy $\Phi(\mathbf{q}, T_{turb})$ can be eliminated from (18) using the equilibrium distribution $P_2^{st}(\mathbf{q})$ of internal coordinates $\mathbf{q}$ corresponding to some asymptotically stable stationary state of turbulent chaos specified *a priori*. As it was said above, since the energy of turbulent motions dissipates continuously due to viscosity, it is impossible to accomplish a statistically equilibrium state while, in contrast, the stationary state is usually dissipative. Indeed, as it is well known[33], as some chemically active molecular continuum passes to a stable stationary (but fairly close to equilibrium) state characterized by minimal entropy production, the entropy itself also decreases. By analogy with molecular chemically reacting systems, for a stationary state of the subsystem of turbulent chaos when the internal coordinates $\mathbf{q}$ can fluctuate near some stable stationary value $\mathbf{q}^{st}$ at certain (for a given elementary volume $d\mathbf{r}$) internal energy and specific volume, the turbulization entropy $S_{turb}(\mathbf{r},t)$ must also be minimal among all of the other states with the same values of $E_{turb}(\mathbf{r},t)$ and $\langle v \rangle(\mathbf{r},t)$. Thus, the following condition is valid:

$$\delta S_{turb} = -\frac{1}{\overline{\rho} T_{turb}} \int_{\mathbf{q}} \mu_{turb}(\mathbf{q}) \delta n(\mathbf{q}) d\mathbf{q} = 0\,,$$

where $\delta n(\mathbf{q}) = n(\mathbf{q}) - n(\mathbf{q}^{st})$. Since the total number of vortex moles n_{Σ} is constant, we also have $\int \delta n(\mathbf{q}) d\mathbf{q} = 0$. It follows from these two conditions that the chemical potential $\mu_{turb}(\mathbf{q})$ in internal coordinates for a stable stationary state of turbulent chaos does not depend on the state vector $\mathbf{q}$ ($\mu_{turb}^{st} = const$). Using this fact, we can obtain the expression

$$\mu_{turb}(\mathbf{q},t) = \mathrm{k_B}\, T_{turb} \ln\left\{ n(\mathbf{q}) / n(\mathbf{q}^{st}) \right\} + \mu_{turb}^{st}\,, \tag{19}$$

which allows the chemical potential to be determined from the stationary distribution $n(\mathbf{q}^{st})$ of an attribute $\mathbf{q}$ known in advance. Relation (19) can be rewritten as

$$\mu_{turb}(\mathbf{q},t) = \mathrm{k_B}\, T_{turb} \ln\left\{\frac{P_2(\mathbf{q}_0|\mathbf{q},t)}{W_1^{st}(\mathbf{q})}\right\} + \mu_{turb}^{st}. \qquad (19^*)$$

The latter is a generalization of the well-known Einstein formula (for a statistically equilibrium state) to quasi-stationary states in configuration space $\mathbf{q}$; in writing(19*), we used the expression

$$\mathbf{f}(\mathbf{q},T_{turb}) = -\frac{\partial}{\partial \mathbf{q}}\Phi(\mathbf{q},T_{turb}) = \mathrm{k_B} T_{turb}\frac{\partial}{\partial \mathbf{q}}\ln W_1^{st}(\mathbf{q}) \qquad (19^{**})$$

for the friction force (in configuration space $\mathbf{q}$) generated by the potential field $\Phi(\mathbf{q},T_{turb})$. The function

$$W_1^{st}(\mathbf{q}) = const \exp\left\{-\frac{\Phi(\mathbf{q},T_{turb})}{\mathrm{k_B}\, T_{turb}}\right\}$$

defines the (maximum) probability of a stable stationary state $\mathbf{q}^{st}$ when the fluctuating internal coordinates $\mathbf{q}$ remain constant, while the function $\Phi(\mathbf{q},T_{turb})$ acts as the thermodynamic potential for a stationary state.

Let us recall that no distinction is made between the two concepts of equilibrium in the equilibrium thermodynamics − the equilibrium state corresponding to maximum entropy and the equilibrium distribution in possible states that are physically almost equivalent[14]. A similar situation also holds for stationary states in the thermodynamics of non-equilibrium processes[17]. This is because the asymptotic probability densities of the states are concentrated in an extremely narrow region and these Gaussian quantities transform into delta functions concentrated in $\mathbf{q}^{st}$ in the thermodynamic limit.

Now, using (13*), let us transform the Gibbs identity (16) by integration by parts and assuming that the flux $\mathbf{J}(\mathbf{q},\mathbf{r},t)$ becomes zero at both boundaries $\mathbf{q}_1$ and $\mathbf{q}_2$ of the domain of definition of the variable $\mathbf{q}$ (a corollary of the condition $\int_{\mathbf{q}_1}^{\mathbf{q}_2}\delta n(\mathbf{q})\,d\mathbf{q} = 0$). This results in

$$\frac{DS_{turb}}{Dt} = \frac{1}{T_{turb}}\frac{DE_{turb}}{Dt} + \frac{p_{turb}}{T_{turb}}\frac{D\langle v\rangle}{Dt} - \frac{1}{T_{turb}}\int_{\mathbf{q}}\mathbf{J}(\mathbf{q})\cdot\frac{\partial\mu_{turb}(\mathbf{q},\mathbf{r},t)}{\partial\mathbf{q}}\,d\mathbf{q}. \qquad (20)$$

The last term in this relation

$$\frac{DS_{turb}}{Dt} = \frac{1}{T_{turb}}\frac{DE_{turb}}{Dt} + \frac{p_{turb}}{T_{turb}}\frac{D\langle v\rangle}{Dt} - \frac{1}{T_{turb}}\int_{\mathbf{q}}\mathbf{J}(\mathbf{q})\cdot\frac{\partial\mu_{turb}(\mathbf{q},\mathbf{r},t)}{\partial\mathbf{q}}\,d\mathbf{q} \qquad (21)$$

describes the total growth of the turbulization entropy $S_{turb}(\mathbf{r},t)$ due to irreversible processes of the formation of various vortex structures characterized by the complete set of internal co-

ordinates $\mathbf{q}$. It can be seen from (21) that the local fluctuation entropy production $\sigma_{\mathbf{q}}(S_{turb})$ corresponding to each part of the space of internal coordinates $\mathbf{q}$ has an ordinary thermodynamic form:

$$\sigma_{\mathbf{q}}(S_{turb}) = -\frac{1}{T_{turb}}\mathbf{J}\cdot\frac{\partial\mu_{turb}}{\partial\mathbf{q}} = \frac{1}{T_{turb}}\mathbf{J}(\mathbf{q},\mathbf{r},t)\cdot\mathbf{A}_{turb}(\mathbf{q},\mathbf{r},t),$$

where

$$\mathbf{A}_{turb} = -\frac{\partial\mu_{turb}}{\partial\mathbf{q}} = \frac{k_B T_{turb}}{n}\frac{\partial n}{\partial\mathbf{q}} - \frac{\partial\Phi}{\partial\mathbf{q}} = \frac{k_B T_{turb}}{n}\exp\left(\frac{\Phi}{k_B T_{turb}}\right)\frac{\partial}{\partial\mathbf{q}}\exp\left(\frac{\mu_{turb}}{k_B T_{turb}}\right) \quad (22)$$

is the generalized de Donder chemical affinity for configuration $\mathbf{q}$ (the state function of the subsystem of turbulent chaos) written here by taking into account (15) for the generalized chemical potential $\mu_{turb}(\mathbf{q},\mathbf{r},t)$.

3.5 Transfer Equation for the Turbulization Entropy

Let us now derive the transfer equation for the turbulization entropy $S_{turb}(\mathbf{r},t)$ by applying the same procedure that led to (7). For this purpose, we will eliminate from (20) the substantial derivatives of the specific volume $\langle v\rangle(\mathbf{r},t)$ and turbulent energy $\langle b\rangle(\mathbf{r},t)$ $(\equiv E_{turb}(\mathbf{r},t))$ for which the differential equation[21] is

$$\overline{\rho}\frac{D}{Dt}\langle b\rangle = -div\mathbf{J}^{turb}_{\langle b\rangle} + \mathbf{R}:\frac{\partial\langle\mathbf{u}\rangle}{\partial\mathbf{r}} + \overline{p'div\mathbf{u}''} - \left(\mathbf{J}^{turb}_{v}\cdot\frac{\partial\overline{p}}{\partial\mathbf{r}}\right) - \overline{\rho}\langle\varepsilon_b\rangle.$$

As a result, we will have

$$\frac{\partial}{\partial t}(\overline{\rho}S_{turb}) + div\left(\overline{\rho}S_{turb}\langle\mathbf{u}\rangle + \mathbf{J}_{(S_{turb})}\right) = \sigma_{(S_{turb})} \equiv \sigma^{(i)}_{(S_{turb})} + \sigma^{(e)}_{(S_{turb})}, \quad (23)$$

where

$$\sigma^{(e)}_{(S_{turb})}(\mathbf{r},t) \equiv \frac{1}{T_{turb}}\left\{\overline{p'div\mathbf{u}''} - \left(\mathbf{J}^{turb}_{v}\cdot\frac{\partial\overline{p}}{\partial\mathbf{r}}\right) - \overline{\rho}\langle\varepsilon_b\rangle\right\} \equiv -\frac{\mathfrak{I}}{T_{turb}}, \quad (24)$$

$$0 \le \sigma^{(i)}_{(S_{turb})}(\mathbf{r},t) = \frac{1}{T_{turb}}\left\{-\left(\mathbf{J}^{turb}_{\langle b\rangle}\cdot\frac{\partial\ln T_{turb}}{\partial\mathbf{r}}\right) - p_{turb}div\langle\mathbf{u}\rangle + \right.$$

$$\left. + \overset{0}{\mathbf{R}}:\overset{0}{\overline{\mathbf{D}}} + \overline{\rho}\int_{\mathbf{q}}\mathbf{J}(\mathbf{q})\cdot\mathbf{A}_{turb}(\mathbf{q})d\mathbf{q}\right\}. \quad (25)$$

Here, $\nu \to 0$ is the so-called turbulent energy diffusion flux; $\overline{\varepsilon}$ is the part with a zero trace of the Reynolds stress tensor;

$$p_{turb}(\mathbf{r},t) = \tfrac{1}{3}(\mathbf{R}:\mathbf{I}), \tag{26}$$

is the turbulization pressure. The quantities $\sigma^{(i)}_{(S_{turb})}(\mathbf{r},t)$ and $\sigma^{(e)}_{(S_{turb})}(\mathbf{r},t)$ are the local production and sink of the entropy $S_{turb}(\mathbf{r},t)$ for the subsystem of turbulent chaos, respectively. Note that the work of turbulent stresses $\overset{0}{\mathbf{R}}:\overset{0}{\overline{\mathbf{D}}}$ causes the entropy of chaos to grow, while the viscous dissipation $\langle \varepsilon_b \rangle > 0$ reduces the turbulization entropy S_{turb}.

4 BALANCE EQUATION FOR THE TOTAL ENTROPY OF THE SUBSYSTEMS OF AVERAGED MOTION AND STRUCTURED TURBULENT CHAOS

Adding (7) and (23) yields the balance equation for the total entropy $S_\Sigma = \langle S \rangle + S_{turb}$ of a turbulized fluid system

$$\overline{\rho}\frac{DS_Y}{Dt} + div\left\{\frac{\mathbf{J}^{turb}_{\langle b\rangle}}{T_{turb}} + \frac{\left(\mathbf{q}^Y - \sum\limits_{\alpha=1}^{N}\langle \mu_\alpha \rangle \mathbf{J}^Y_\alpha\right)}{\langle T\rangle}\right\} = \sigma_Y, \tag{27}$$

where

$$0 \le \sigma_Y \equiv \sigma^{(i)}_{\langle S\rangle} + \sigma^{(i)}_{S_{turb}} + \sigma_{\langle S\rangle, S_{turb}} = \sigma^{(i)}_{\langle S\rangle} + \sigma^{(i)}_{S_{turb}} + \frac{T_{turb} - \langle T\rangle}{\langle T\rangle T_{turb}}\Im_{E,\langle b\rangle} \tag{28}$$

is the local entropy production related to irreversible processes inside the total turbulized continuum. The quantity σ_Y written by taking into account (8), (9) and (24), (25) has the structure of a bilinear form, $\sigma_\Sigma = \sum\limits_\alpha \Im_\alpha(\mathbf{r},t)\mathbf{X}_\alpha(\mathbf{r},t)$,

$$0 \le \sigma_\Sigma(\mathbf{r},t) \equiv \frac{1}{\langle T\rangle}\left\{-\left(\tilde{\mathbf{q}}^\Sigma \cdot \frac{\partial \ln\langle T\rangle}{\partial \mathbf{r}}\right) + \overline{\pi}\, div\langle \mathbf{u}\rangle + \overset{0}{\overline{\mathbf{P}}}:\overset{0}{\overline{\mathbf{D}}} + \right.$$

$$\left. + \frac{1}{T_{turb}}\left\{-\left(\mathbf{J}^{turb}_{\langle b\rangle}\cdot\frac{\partial \ln T_{turb}}{\partial \mathbf{r}}\right) + \overset{0}{\mathbf{R}}:\overset{0}{\mathbf{D}} + \overline{\rho}\int\limits_{\mathbf{q}} \mathbf{J}(\mathbf{q})\cdot\mathbf{A}_{turb}(\mathbf{q})d\mathbf{q}\right\} + \Im\left(\frac{T_{turb}-\langle T\rangle}{T_{turb}\langle T\rangle}\right). \tag{29}$$

According to the basic postulate of the nonlinear thermodynamics of non-equilibrium processes, if the system is near a relatively stable quasi-stationary state, then the thermodynamic fluxes can be represented as linear functions of the conjugate macroscopic forces[17]:

$$\mathfrak{I}_{\alpha i}(\mathbf{r},t)=\sum_{\beta}\Lambda_{\alpha\beta}^{ij}X_{\beta j}(\mathbf{r},t)\quad(\alpha,\beta=1,2,...) \tag{30}$$

It is important to emphasize that the matrix of phenomenological coefficients $\Lambda_{\alpha\beta}^{ij}$ for a turbulized fluid continuum depends not only on the system's average state parameters (i.e., on its average temperature $\langle T\rangle(\mathbf{r},t)$, density $\overline{\rho}(\mathbf{r},t)$, etc.) but also on turbulent superstructure characteristics, i.e., on parameters such as $\langle\varepsilon_b\rangle(\mathbf{r},t)$ $T_{turb}(\mathbf{r},t)$. Such a situation, where there is a functional dependence of the coefficients $\Lambda_{\alpha\beta}^{ij}$ on the thermodynamic fluxes $\mathfrak{I}_{\alpha i}$ themselves (e.g., on the dissipation rate $\langle\varepsilon_b\rangle$, which is also the energy flux over the cascade of vortices in the stationary case), is known to be typical of self-organizing systems[34,35]. Generally, this can lead to the individual terms $\mathfrak{I}_{\alpha}(\mathbf{r},t)\mathbf{X}_{\alpha}(\mathbf{r},t)$ in the sum σ_{Σ} being not positive definite, although the entire sum is always greater than or equal to zero, $\sigma_{\Sigma}\geq 0$. The superposition of various fluxes can then, in principle, lead to negative individual diagonal elements of the matrix $\Lambda_{\alpha\beta}$, which probably explains the negative viscosity effect in some turbulent flows.

As can be seen from (29), the spectrum of possible cross effects for a turbulent flow generally widens compared to a laminar one. Thus, for example, the total heat flux $\mathbf{q}^{\Sigma}(\mathbf{r},t)$ in a turbulized continuum can emerge under the influence of not only its conjugate thermodynamic force $\partial(1/\langle T\rangle)/\partial\mathbf{r}$ but also the force $\partial(1/T_{turb})/\partial\mathbf{r}$ conjugate to the flux $\mathbf{J}_b^{turb}(\mathbf{r},t)$ describing the "diffusive" transport of turbulent kinetic energy. However, at present there are no reliable experimental data which would quantitatively described such cross effects. Besides, the contribution from any cross effects to the total rate of some process is usually an order of magnitude smaller than that from direct ones[14]. Taking this circumstance into account, we use the requirement that the intensities $\sigma_{\Sigma}(\mathbf{r},t)$, $\sigma_{\langle S\rangle}^{i}(\mathbf{r},t)$, $\sigma_{S_{turb}}^{i}(\mathbf{r},t)$ are positive independently of one another and omit a number of cross effects in the linear constitutive relations (30) without special stipulations.

In view of the second law of thermodynamics, the last term on the right-hand side of (29) describing the entropy production within the total continuum through irreversible entropy exchange between the subsystems of turbulent chaos and averaged motion is always positive,

$$\sigma_{\langle S\rangle,S_{turb}}=\mathfrak{I}\left(\frac{T_{turb}-\langle T\rangle}{T_{turb}\langle T\rangle}\right)\geq 0\,. \tag{31}$$

Therefore, the "direction" of the thermodynamic flux $\mathfrak{I}(\mathbf{r},t)$ is determined by the sign of the state function $X_{\mathfrak{I}}(\mathbf{r},t)=\left(1/\langle T\rangle-1/T_{turb}\right)$, which should be considered as the conjugate thermodynamic force (a macroscopic factor) producing the entropy flux $\mathfrak{I}(\mathbf{r},t)$. Such entropy exchange between two mutually open subsystems is known[2] to be an indispensable condition for a structured collective behavior, i.e., it can be a source of self-organization in one of them.

In turn, the dissipative activity of the subsystem of turbulent chaos in the case of stationary non-equilibrium turbulence is determined by the influx of negative entropy ($\sigma^{e}_{S_{turb}} \equiv -\Im / T_{turb} < 0$) from the subsystem of averaged motion.

5 STATIONARY NON-EQUILIBRIUM STATE OF THE TURBULENT FIELD: DEFINING RELATIONS FOR THE STRUCTURED TURBULENCE

Since turbulence is accompanied by the dissipation of kinetic energy, a continuously acting external (relative to the medium under consideration) source is needed to maintain its quasi-stationary regime when the energy input and dissipation are nearly balanced. An energy source could be, e.g., a turbulence-producing wire grid placed perpendicular to the forced fluid flow, stationary boundary conditions causing a large-scale flow velocity shear, a thermal-convective large-scale instability, etc. Such a source should be powerful enough to compensate for the expenditure of turbulent energy dissipated through molecular viscosity. For quasi-stationary turbulence, almost the entire energy being expended will be transferred without any significant (but, in general, existing) losses through the inertial range from the energy range to the viscous one, where it dissipates into heat. The energy transfer from large-scale vortices to small-scale ones can be visualized as a random Richardson–Kolmogorov cascade turbulent vortex fragmentation process.

In the model approach we assume that a continuous process of energy transfer from the subsystem of averaged fluid motion to the subsystem of turbulent chaos corresponds to such quasi-stationary turbulence. Obviously, a stationary non-equilibrium regime between the influx of energy from the "external source" (attributable to the averaged fluid flow) and its dissipation (due to irreversible processes within the subsystem of turbulent chaos itself) is then established in the vortex continuum associated with small-scale turbulence in which $dS_{turb} / dt \cong 0$. Incidentally, the quasi-stationary state in which the entropy production is minimal is an attractor for the open subsystem of turbulent chaos, while the state corresponding to the total entropy maximum serves as an attractor for the turbulized system as a whole. The condition $dS_{turb} / dt \cong 0$ implies that the production $\sigma^{(i)}_{(S_{turb})}(\mathbf{r},t)$ of turbulization entropy S_{turb} is compensated for by its efflux $\sigma^{(e)}_{(S_{turb})}(\mathbf{r},t)$ to such extent that the total generation of entropy S_{turb} is almost absent,

$$\sigma_{(S_{turb})}(\mathbf{r},t) = \sigma^{(e)}_{(S_{turb})}(\mathbf{r},t) + \sigma^{(i)}_{(S_{turb})}(\mathbf{r},t) \simeq 0$$

It should also be kept in mind that the turbulization entropy flux in the stationary case is constant, $\mathbf{J}_{(S_{turb})} = \mathbf{J}^{turb}_{\langle b \rangle} / T_{turb} = const$ ($div \mathbf{J}_{S_{turb}} \approx 0$). Since $\sigma^{(i)}_{(S_{turb})} > 0$, the inequality $0 > \sigma^{e}_{S_{turb}} \cong -\sigma^{i}_{S_{turb}}$ holds, i.e., the subsystem of turbulent chaos must export entropy into the "external medium" in order to compensate for the entropy production through irreversible internal processes within itself. In other words, an influx of negative entropy (negentropy) from the "external medium" is needed to maintain the stationary nonequilibrium state within the subsystem of turbulent chaos,

$$\sigma^e_{S_{turb}}(\mathbf{r},t) \equiv -\Im / T_{turb} = -\langle T\rangle \sigma^e_{\langle S\rangle} / T_{turb} < 0\,.$$

Such a condition is known to be sufficient for the formation of dissipative coherent structures in vortex continuum[1,2]. Indeed, since the entropy efflux from the subsystem of averaged motion in the stationary non-equilibrium state of chaos is positive $(0 < \sigma^e_S \equiv -\Im / \langle T\rangle)$, the rate $\Im(\mathbf{r},t)$ of entropy (heat) exchange between the averaged and turbulent motions is also positive, $\Im \geq 0$. It then follows from inequality (31) that the turbulization temperature $T_{turb}(\mathbf{r},t)$ is higher than the average turbulized fluid temperature ($T_{turb} > \langle T\rangle$), which is in the full agreement with the basic synergetic principle about self-organization of dissipative system. According to this principle, the formation of coherent structures (in our case, the formation of different-scale coherent vortex structures in the subsystem of turbulent chaos) when heat is removed from the system, i.e., when passing to lower temperatures, is a universal property of matter [18].

5.1 Defining Relations for Structured Turbulence

Thus, the negentropy entering the subsystem of turbulent chaos is expended to maintain and improve its internal structure. The relation $0 \leq \sigma^e_{\langle S\rangle} = -T_{turb}\sigma^e_{S_{turb}} / \langle T\rangle \cong T_{turb}\sigma^i_{S_{turb}} / \langle T\rangle$ is then valid and the balance equation (7) for the averaged entropy $\langle S\rangle(\mathbf{r},t)$ of a turbulized fluid system takes the form

$$\overline{\rho}\frac{D\langle S\rangle}{Dt} + div\left(\frac{\mathbf{q}^{\Sigma})}{\langle T\rangle}\right) = \sigma^i_{\langle S\rangle} + \sigma^e_{\langle S\rangle} \cong \sigma^i_{\langle S\rangle} + \frac{T_{turb}}{\langle T\rangle}\sigma^i_{S_{turb}} \cong \sigma_\Sigma\,, \tag{32}$$

where the following expression holds for the local energy dissipation $\langle T\rangle\sigma_\Sigma$:

$$\langle T\rangle\sigma_\Sigma(\mathbf{r},t) \equiv -\left(\mathbf{q}^\Sigma \cdot \frac{\partial \ln\langle T\rangle}{\partial \mathbf{r}}\right) + \overset{\circ}{\mathbf{R}} : \overset{\circ}{\overline{\mathbf{D}}} + \overline{\rho}\int_{\mathbf{q}} \mathbf{J}(\mathbf{q}) \cdot \mathbf{A}_{turb}(\mathbf{q}) d\mathbf{q} \geq 0\,. \tag{33}$$

Here, $\mathbf{q}^\Sigma(\mathbf{r},t) \equiv \mathbf{q}^{turb} - \overline{p'\mathbf{u}''}$ is the total heat flux in the subsystem of averaged motion for the developed turbulence. Based on (33), we can write the following defining (gradient) relations for the turbulent fluxes and their conjugate thermodynamic forces in the linear approximation and using the Curie–Prigogine principle (according to which no relation is possible between tensors of different ranks in locally isotropic medium[14]):

$$\mathbf{q}^\Sigma(\mathbf{r},t) = -\lambda^{turb}\frac{\partial \ln\langle T\rangle}{\partial \mathbf{r}}, \tag{34}$$

$$\mathbf{R}(\mathbf{r},t) = -\tfrac{2}{3}\bar{\rho}\langle b\rangle\,\mathbf{I} + \bar{\rho}\nu^{turb}\left\{\tfrac{1}{2}\left(\frac{\partial\langle\mathbf{u}\rangle}{\partial\mathbf{r}} + \left(\frac{\partial\langle\mathbf{u}\rangle}{\partial\mathbf{r}}\right)^{transp}\right) - \tfrac{1}{3}div\langle\mathbf{u}\rangle\,\mathbf{I}\right\}, \tag{35}$$

$$\mathbf{J}(\mathbf{q},\mathbf{r},t) = \int_{\tilde{\mathbf{q}}} \mathbf{L}(\mathbf{q},\tilde{\mathbf{q}},\mathbf{r},t)\cdot\mathbf{A}(\tilde{\mathbf{q}},\mathbf{r},t)d\tilde{\mathbf{q}}\,. \tag{36}$$

They correspond to the stationary state of the turbulent field. Note that the linearity condition is not strong enough to deprive the case under consideration of practical significance.

Assessing the status of the problem of closing the averaged hydrodynamic equations as a whole, it should be recognized that currently almost all semi-empirical turbulence models are mainly based on the gradient relations. The phenomenological coefficients (turbulent exchange coefficients) $\lambda^{turb}(\mathbf{r},t)$, $\nu^{turb}(\mathbf{r},t)$ in these relations are scalar quantities, because, as has been emphasized above, strong turbulence is locally homogeneous and isotropic. In contrast to the molecular exchange coefficients, these quantities are not material constants. This is because in turbulized continuum the processes of mass, momentum, and energy transfer from one region of the system to another are determined by the collective motions of molecules (vortex structures) and, hence, must depend on turbulence intensity parameters, in particular, on the parameters ε_b and L_1 (or $\langle b\rangle$). For example, in the inertial range of vortex scales $(\eta < k < L_1)$, the turbulent viscosity $\nu^{turb}(\mathbf{r},t)$ corresponding to the Richardson–Obukhov empirical "law of four thirds"[vi] is $\nu^{turb} \sim \langle\varepsilon_b\rangle^{1/3}L_1^{4/3} \sim \langle b\rangle^2/\langle\varepsilon_b\rangle$.

Thus, when stationary-inhomogeneous turbulence is modeled in the system where the energy dissipation processes are important, a heat transfer equation for averaged motion in form (32) should be invoked; this equation should be supplemented by the linear defining relations (34)–(36).

6 PRIGOGINE'S PRINCIPLE: THERMODYNAMIC DERIVATION OF THE FOKKER–PLANCK–KOLMOGOROV EQUATIONS

According to (36), the phenomenological relation for the thermodynamic flux $\mathbf{J}(\mathbf{q},\mathbf{r},t)$ in the space of internal coordinates $\mathbf{q}$ and the corresponding "instantaneous" affinity $\mathbf{A}(\mathbf{q},\mathbf{r},t)$ generally has an integral form. Following Prigogine[22] (see Chap. 3, Sect. 11), we will now assume that the irreversible processes in each part of the internal coordinate space $\mathbf{q}$ proceed in such a way that only positive entropy increment occurs. This implies that not only integral (19) but also the quantity

$$T_{turb}\sigma_{\mathbf{q}}(S_{turb}) = \mathbf{J}(\mathbf{q},\mathbf{r},t)\cdot\mathbf{A}_{turb}(\mathbf{q},\mathbf{r},t) \geq 0\,, \tag{37}$$

which is the energy dissipation per unit volume of configuration space $\mathbf{q}$ will be positive. The defining relation between the flux $\mathbf{J}(\mathbf{q},\mathbf{r},t)$ and affinity $\mathbf{A}_{turb}(\mathbf{q},\mathbf{r},t)$ of a state $\mathbf{q}$ (corresponding to one equivalent of the vortex decay process) is then

[vi] This law follows, in particular, from dimensional and similarity considerations.

$$\mathbf{J}(\mathbf{q},t)=\mathbf{L}_{\mathbf{q}}\cdot\mathbf{A}_{turb}(\mathbf{q},t)=-\mathbf{L}_{\mathbf{q}}\cdot\frac{\partial\mu_{turb}(\mathbf{q},t)}{\partial\mathbf{q}}=\mathbf{L}_{\mathbf{q}}\cdot\left(\frac{\mathrm{k_B}\,T_{turb}}{n(\mathbf{q},t)}\frac{\partial n(\mathbf{q},t)}{\partial\mathbf{r}}+\frac{\partial\Phi(\mathbf{q},t)}{\partial\mathbf{r}}\right). \quad (38)$$

Here, $\mathbf{L}_{\mathbf{q}}$ is the positive definite local matrix of transport coefficients satisfying the Onsager–Casimir reciprocity relation $\mathbf{L}^{transp}=\mathbf{L}$; $n(\mathbf{q},t)$ are the numbers of vortex moles in the cascade interaction between turbulent motions of different scales.

Relation (38) taken together with (13) allows us to derive the following evolutionary Fokker–Planck–Kolmogorov equation in the so-called kinetic form[36] in the space of stochastic variable $\mathbf{q}$ for the distribution functions of various statistical small-scale turbulence characteristics:

$$\frac{\partial P_2(\mathbf{q},\mathbf{r},t)}{\partial t}+\frac{\partial}{\partial\mathbf{x}}\cdot\left(\langle\mathbf{u}\rangle P_2(\mathbf{q},\mathbf{r},t)\right)=$$

$$=\frac{\partial}{\partial\mathbf{q}}\cdot\left\{-\mathbf{K}(\mathbf{q})P_2(\mathbf{q},\mathbf{r},t)+\frac{\varepsilon^2}{2}\mathbf{Q}(\mathbf{q})\cdot\frac{\partial P_2(\mathbf{q},\mathbf{r},t)}{\partial\mathbf{q}}\right\}. \quad (39)$$

Here, the probability flux $\mathbf{J}=\mathbf{J}_{dr}+\mathbf{J}_{dif}$ is the sum of the drift $\mathbf{J}_{dr}$ and diffusion $\mathbf{J}_{dif}$ components: $\mathbf{J}_{dr}=\mathbf{K}P_2$, $\mathbf{J}_{dif}=-\frac{\varepsilon^2}{2}\mathbf{Q}\cdot\frac{\partial P_2}{\partial\mathbf{q}}$, where the following notation is used for the drift vector $\mathbf{K}$ and the matrix of generalized diffusion coefficients $\mathbf{D}$ in the space of stochastic variable $\mathbf{q}$:

$$\mathbf{K}(\mathbf{q})\equiv\text{€}(\mathbf{q})\cdot\mathbf{f}(\mathbf{q}),\quad \mathbf{D}=\varepsilon^2\,\text{€}(\mathbf{q})=\frac{1}{2}\varepsilon^2\,\mathbf{Q},\quad \mathbf{Q}(\mathbf{q})\equiv 2\text{€}(\mathbf{q}). \quad (40)$$

The function $P_2(\mathbf{q},t)=n/n_{\Sigma}$ is the (conditional) probability density to detect the system in an interval $(\mathbf{q},\,\mathbf{q}+d\mathbf{q})$ at a time t if it was in a state $\mathbf{q}^{st}$ at an initial time (at $t=0$) with probability equal to unity. The parameter $\varepsilon\equiv\sqrt{\mathrm{k_B}\,T_{turb}}=\sqrt{\overline{\rho(\mathbf{u}'')^2}/3\overline{\rho}}$ characterizes the total intensity of the action of internal noise in the subsystem of turbulent chaos (generated by its "thermal" structure) on the random process $\mathbf{q}(t)$. In writing (39), we assumed in the first approximation the mobility parameter $\text{€}(\mathbf{q})\equiv\mathbf{L}(\mathbf{q})/n(\mathbf{q})$ in internal coordinate $\mathbf{q}$ to be independent on the density $n(\mathbf{q})$. Generally, the matrix K does not form a vector unless the modeling is confined by only linear transformations of coordinates.

Note that, apart from the kinetic form of the FPK equation (39), other representations of this equation can be also used, Ito's and Stratonovich's representations being the most common. They are based on a different treatment of the so-called stochastic integrals[37] that emerge from the solution of the corresponding nonlinear stochastic Langevin's equations. Although these representations are based on stochastic nearly identical equations [see (86)], they lead to the different form of FPK equations:

$$\frac{\partial P_2(\mathbf{q},\mathbf{r},t)}{\partial t} + div\left(\langle \mathbf{u} \rangle P_2(\mathbf{q},\mathbf{r},t)\right) =$$

$$= \frac{\partial}{\partial \mathbf{q}} \cdot \left\{ -\left(\mathbf{K}(\mathbf{q}) + \mathbf{H}(\mathbf{q})\right) P_2(\mathbf{q},\mathbf{r},t) + \tfrac{1}{2}\varepsilon^2 \frac{\partial}{\partial \mathbf{q}} \cdot \left(\mathbf{Q}(\mathbf{q}) P_2(\mathbf{q},\mathbf{r},t)\right) \right\}, \qquad (39^*)$$

where $\mathbf{H}(\mathbf{q}) \equiv \lambda \frac{\varepsilon^2}{2} \frac{\partial \mathbf{Q}(\mathbf{q})}{\partial \mathbf{q}}$ is a "fictitious force" dependent on the choice of calculus. In the case $\lambda = 0,\ 1/2,\ 1$ Ito's - Stratonovich's, and Klimontovich's representations of the FPK equation, respectively, are the most appropriate.

If response of the subsystem of turbulent chaos to impact of the external medium (the subsystem of averaged motion) does not depend on its internal state specified by stochastic variable $\mathbf{q}$, then the diffusion coefficient does not change with coordinate $\mathbf{q}$ either (i.e., $\mathbf{Q}(\mathbf{q}) = const$). The stochastic system can then be assumed to possess additive noise that, in our case, is just reduced to the intensity $\varepsilon^2 = \mathrm{k_B} T_{turb}$ of the internal noise in the subsystem of turbulent chaos. The fictitious force $\mathbf{H}(\mathbf{q})$ for such systems is identically equal to zero, i.e., they both are completely insensitive to the choice of calculus. In other words, all three forms of the FPK equation take the same simplest form (39). However, a feedback is generally possible between the internal states $\mathbf{q}$ of the stochastic subsystem of chaos and the subsystem of averaged motion. It turns out that not only the external fluctuations (associated, for example, with the degrees of freedom of the turbulent field that are not described by the selected coordinates $\mathbf{q}$) affect the stochastic subsystem of turbulent chaos but also the latter has the reverse effect on their intensity. As applied to the case under consideration, this implies that the diffusion coefficient becomes dependent on the random coordinate $\mathbf{q}$, i.e., the external fluctuations are multiplicative. In the presence of multiplicative noise, when $\mathbf{Q}(\mathbf{q}) \neq const$, the simplest form of the FPK equation (39) holds only in Klimontovich's representation ($\lambda = 1$).

Thus, the problem of choosing calculus arises for systems with multiplicative noise because the force entering into the FPK equation is determined ambiguously. In Ito's calculus, it is reduced to a real force acting on the selected degree of freedom. When using Stratonovich's calculus, an addition proportional to the derivative of the effective diffusion coefficient emerges. The value of this addition doubles in Klimontovich's kinetic representation. It is important to notice that it affects significantly the behavior of the stochastic system. As a result, the question about the physical nature of this addition and the choice of calculus seems topical.

7 EXAMPLES OF THE FOKKER–PLANCK–KOLMOGOROV EQUATIONS DESCRIBING EVOLUTION OF THE FLUCTUATING CHARACTERISTICS OF TURBULENT CHAOS

Now proceeding from simple examples let us show that Prigogine's principle (37) can serve as a basis for deriving the evolutionary partial differential Fokker–Planck–Kolmogorov equations in the space of stochastic variable $\mathbf{q}$ for the distribution functions of various stochastic small-scale turbulence characteristics. This is valid if appropriate hypotheses about the distribution in a stationary non-equilibrium state of the latter are adopted in advance. It should be kept in mind, however, that such hypotheses are almost always not quite rigorous and are a strong idealization related to the simplification of a real turbulent motion under natural conditions [38].

7.1 Evolution of Vortices in the Space of Fluctuating Velocities

Let us first address assumption (37) to derive the kinetic equation describing the change in the probability density function of vortex velocities $P_2(u''\mathbf{r},t)$ $(\equiv n(u'',\mathbf{r},t)/n_\Sigma)$, $n(u'',\mathbf{r},t)$ being the number density of turbulent vortices and n_Σ is the total number of vortex moles, see (12). We consider this function as the internal variable of the subsystem of turbulent chaos and the fluctuating velocity u'' as the internal coordinate $\mathbf{q}$. The probability distribution function for the fluctuating velocity is known to be not universal in the case of developed turbulence because it depends on the mechanism generating the turbulent field. Nonetheless, following Millionshchikov[40], we may use the hypothesis about normal distribution of fluctuating velocities (for a locally isotropic turbulent field) in the stationary case

$$W_1(u'') \equiv n^{stat}(u'')/n_\Sigma = \left(\beta/\sqrt{\pi}\right)\cdot\exp\left(-\beta^{\,2}u''^2\right). \tag{41}$$

Millionshchikov applied such a distribution in the turbulence theory for special purposes that we will not discuss in more detail. Note only that there are many examples where the velocity distribution function is approximately Gaussian, for instance, in turbulence generated by grids in wind tunnels or turbulence in an atmospheric boundary layer [9,41]. For the subsystem of turbulent chaos we accept the constant β in (41) as being related to the turbulization temperature T_{turb} in exactly the same way as it is done in the gas kinetic theory[42]. Then, using (17) and (41), it is easy to find that $\beta^2 = (2\mathsf{R}T_{turb})^{-1}$, whence we obtain a different equivalent expression for the function $n^{stat}(u'')$:

$$n^{stat}(u'') = n_\Sigma\left(\frac{1}{2\pi\mathsf{R}T_{turb}}\right)^{1/2}\exp\left(-\frac{u''^2}{2\mathsf{R}T_{turb}}\right) = const\cdot\exp\left(-\frac{u''^2}{2\mathsf{R}T_{turb}}\right). \tag{41*}$$

Substituting this distribution into (16) yields the following representation of the chemical potential $\mu_{turb}(u'',\mathbf{x},t)$ for the configuration u'':

$$\mu_{turb}(u'',\mathbf{r},t) = \frac{\mathsf{k}_\mathrm{B}}{\mathsf{R}}(u''^2/2) + \mathsf{k}_\mathrm{B}T_{turb}(\mathbf{r},t)\ln\left[n(u'',\mathbf{r},t)\right] + const\,. \tag{42}$$

Given this formula, the phenomenological relation (36) for the probability flux $J(u'', \mathbf{x}, t)$ takes the form

$$J(u'') = -\frac{\overline{\rho}}{n_\Sigma} L_{u''} \left(u'' + \frac{\mathsf{R} T_{turb}}{n(u'')} \frac{\partial n(u'')}{\partial u''} \right) = -\alpha \left(u'' n(u'') + \mathsf{R} T_{turb} \frac{\partial n(u'')}{\partial u''} \right), \tag{43}$$

where $\mathsf{R} (= n_\Sigma \mathrm{k_B} / \overline{\rho})$. Here, we introduce the coefficient $\alpha \equiv \mathrm{k_B} L_{u''} / \mathsf{R} n(u'')$ that can be interpreted as the "mobility" in the space of internal coordinate u'' per unit volume; in the first approximation, this coefficient does not depend on $n(u'')$ and is assumed to be independent of u''. Substituting (43) into (19) yields the sought for kinetic FPK equation for the conditional probability density function of the fluctuating velocity u'':

$$\frac{\partial P_2}{\partial t} + \frac{\partial}{\partial \mathbf{r}} \cdot \left(P_2 \langle \mathbf{u}(\mathbf{r}, t) \rangle \right) - \alpha \frac{\partial}{\partial u''} \left(u'' P_2 + \mathsf{R} T_{turb}(\mathbf{r}, t) \frac{\partial P_2}{\partial u''} \right) = 0 . \tag{44}$$

This dynamical equation supplemented by the initial condition $P_2 = \delta(u'' - 0)$ (the $\delta-$ function concentrated at point «0» appears on the right-hand side) describes the temporal evolution of the probability density function P for the fluctuating velocity u'', in particular, for decaying (so-called degenerating) turbulence. It should be noted that the quantity $K \equiv -\alpha u''$ (the friction coefficient in the corresponding Langevin's equation) acts as the drift coefficient in the FPK equation written in standard form and the quantity

$$D \equiv 2 L_{u''} \mathrm{k_B} T_{turb} / n(u'') = 2\alpha \mathsf{R} T_{turb} = \alpha \beta^{-2}$$

is the diffusion coefficient.

The normal distribution (41), which is a stationary solution of the one-dimensional (in parameter u'') FPK equation (44) can be taken as the initial statistical state of the fluctuating velocity field for the whole class of various motions of degenerating turbulence. A non-stationary solution of this equation can then be obtained in an analytically closed form:

$$P_2(u'', \mathbf{r}, t) = \left\{ \pi a(\mathbf{r}, t) \right\}^{-1/2} \exp\left\{ -\left[u'' - b(\mathbf{r}, t) \right]^2 / a(\mathbf{r}, t) \right\}, \tag{45}$$

where

$$a(\mathbf{r}, t) = \frac{D}{\alpha} \left\{ 1 - \exp(-2\alpha t) \right\} + a_0 \exp(-2\alpha t), \quad b(\mathbf{r}, t) = b_0(\mathbf{r}) \exp(-\alpha t); \tag{46}$$

$a_0(\mathbf{r})$ and $b_0(\mathbf{r})$ are the initial conditions. This solution allows us to calculate the various n-point moments (correlation functions) of the m-th order describing the statistical relation between the random velocities at various points of space-time. In particular, for the quantities $\overline{u''}^0(\mathbf{r}, t)$ (the conditional mean velocity of the ensemble of vortices at a time t) and $\overline{u''(\mathbf{r}, t) u''(\mathbf{r}, t_1)}$ (the two-time one-point correlation function), we have

$$\overline{u''}^{0}(\mathbf{r},t)=\int u''P_2(0|u'',t)du''=b_0(\mathbf{r})\exp(-\alpha t), \tag{47}$$

whence $b(\mathbf{r},t)\equiv\overline{u''}^{0}(\mathbf{r},t)$;

$$\overline{u''(\mathbf{r},t)u_1''(\mathbf{r},t_1)}=\int u''\,du''\int u_1''\,du''\,W_2(u'',t;u_1'',t_1)=$$

$$=\overline{u''^2(\mathbf{r},t)}\;\exp\{-\alpha|t-t_1|\}=\frac{1}{2}\frac{D}{\alpha}\exp\{-\alpha|t-t_1|\}, \tag{48}$$

where the average is taken over the stochastic process[34]. Here, $W_2(u'',t;u_1'',t_1)$ is the joint probability density. Because generation of new modes of fluctuating motion (the fragmentation of vortex structures) is a Markovian process, it is represented as the product of the probability density at time t_1, $W_1(u_1'',t_1)$, and the conditional probability $P_2(u'',t|u_1'',t_1)$ (which is reduced to the δ-function at $t=t_1$):

$$\delta(u''-u_1''))\colon\ W_2(u'',t;u_1'',t_1)=W_1(u_1'',t_1)\,P_2(u'',t|u_1'',t_1).$$

Since $D=2\alpha\,\mathrm{R}T_{turb}=\frac{4}{3}\alpha\langle b\rangle$, then we have: -first, the correct relation $\overline{u''^2}=\frac{2}{3}\langle b\rangle\cong\frac{1}{3}\overline{|\mathbf{u}''|^2}$ is consistent with the assumption about local isotropy of the vortex velocity field in the case of developed turbulence and, -and second, the effective formula for one of the most important correlation quantities in the theory of statistical turbulence

$$\overline{u''(\mathbf{r},t)u''(\mathbf{r},t_1)}=\tfrac{2}{3}\langle b\rangle\exp\left(-\alpha|t-t_1|\right), \tag{49}$$

defining the speed with which the fluctuating velocity "forgets its past" (according to this formula, this occurs in a time $t\cong 1/\alpha$ follow from (48).

Solution (45) at zero values of the parameters a_0 and b_0 takes the form

$$P_2(u'',t)=\left\{2\pi\,\mathrm{R}T_{turb}\left[1-\exp(-2\alpha t)\right]\right\}^{-1/2}\exp\left\{-\frac{u''^2}{2\mathrm{R}T_{turb}\left[1-\exp(-2\alpha t)\right]}\right\}. \tag{50}$$

It allows the temporal evolution of the conditional probability distribution function for the fluctuating velocity to be traced if the velocity distribution was Gaussian in the case of stationary turbulence.

It should be kept in mind that choosing the fluctuating velocity u'' as a suitable characteristic of turbulent vortices (the internal coordinate of the subsystem of turbulent chaos) generally does not justified, because the Gaussian probability distribution of the fluctuating velocity u'' has been confirmed with a sufficient degree of reliability neither experimentally (it was established, for example, that the deviation from "normal behavior" behind the grid increases considerably with increasing Reynolds number **Re**) nor theoretically (the classical "two and

five thirds" laws of turbulence are known to break down for this distribution). Earlier it was pointed out that the most acceptable characteristics of small-scale turbulence to serve as an internal coordinate are non-negative macroscopic variables even functions of rates such as the dissipation rate of turbulent energy[38]. According to Kolmogorov's hypothesis, such random characteristics asymptotically satisfy a log-normal probability distribution. This is because the successive fragmentation of vortex structures is similar to the coagulation of solid particles (the latter is known to lead to a log-normal particle size distribution). We note that the log-normal distribution does not accurately describe the edges of the true distribution of random variable and, hence, can be used to calculate the high order moments only with a great caution.

8 CASCADE PROCESS. THERMODYNAMIC TREATMENT CORRESPONDING TO THE KOLMOGOROV'S ORIGINAL SIMILARITY HYPOTHESES

Let us now apply Prigogine's principle (37) to the derivation of the kinetic equation describing the temporal evolution of the vortex distribution function in the space of kinetic energy. We will describe the Richardson–Kolmogorov cascade process (large vortices towards small vortices and heat) using an analogy with the process of consecutive chemical reactions. In this case, the original kinetic equation (13) for the distribution function $P(0|q;\mathbf{r},t)$ of turbulent vortices in the space of fluctuating energy $q = \rho|\mathbf{u}''|^2/2$ takes the form

$$\frac{\partial P_2(0|q;\mathbf{r},t)}{\partial t} + \frac{\partial}{\partial \mathbf{r}} \cdot \left(P_2(0|q;\mathbf{r},t)\langle \mathbf{u} \rangle \right) = \frac{\partial}{\partial q}\left(P_2(0|q;\mathbf{r},t)\, \varepsilon(q,\mathbf{r},t) \right), \tag{51}$$

where

$$\varepsilon(q,\mathbf{r},t) \equiv -J(q,\mathbf{r},t)/n(q,\mathbf{r},t) \tag{52}$$

is the transition reaction rate from state q to state $q+dq$ corresponding to the probability flux $J(q)$ in state q; n is the number density of turbulent vortices. In other words, relation (51) defines the parameter $\varepsilon(q,\mathbf{r},t)$ that can be interpreted as the transfer rate of kinetic energy $\rho|\mathbf{u}''|^2/2$ over hierarchy of turbulent vortices along the coordinate q. Concurrently, this quantity also defines the kinetic energy dissipation in vortices of type q. Indeed, the equation for the first moment

$$\int q\, P_2(0|q;t)dq = \overline{\rho|\mathbf{u}''|^2/2}^{0} = \overline{\rho}\langle b \rangle .$$

Derived from (51) as a result of integration by parts (and by assuming the flux $J(q,\mathbf{r},t)$ at the boundaries of the domain of integration to be zero) takes the classical form[31]

$$\overline{\rho}\frac{D\langle b \rangle}{Dt} \cong -\int \varepsilon(q,\mathbf{r},t) P_2(0|q;\mathbf{r},t)dq = -\overline{\varepsilon(\mathbf{r},t)}^{0} \cong -\overline{\rho}\langle \varepsilon(\mathbf{r},t) \rangle . \tag{53}$$

Here the conditional average is taken over the stochastic process q, in which parameter $\langle\varepsilon\rangle$ defines the mean turbulent energy dissipation rate at point $(\mathbf{r},t)$. For this reason the quantity $\varepsilon(q)$ can be interpreted as the energy dissipation rate in vortices of type q (at the point $q=\rho\left|\mathbf{u}''\right|^2/2$ of configuration space. Then for the part of the dissipation energy $\langle T\rangle\sigma_\Sigma$ [see (33)] attributable to the transfer of turbulent energy over the cascade, we have

$$\left(\langle T\rangle\sigma_\Sigma\right)^{Ch}\equiv-\overline{\rho}\int_{\mathrm{q}}\varepsilon(\mathrm{q},\mathbf{r},t)\,n(q,\mathbf{r},t)\,A_{turb}(q,\mathbf{r},t)dq\geq 0\,. \tag{54}$$

Hence, a local phenomenological Prigogine-type equation follows:

$$\varepsilon(\mathrm{q},\mathbf{r},t)=L_q A_{turb}(q,\mathbf{r},t)/n(q,\mathbf{r},t)=-\alpha' A_{turb}(q,\mathbf{r},t)\,, \tag{55}$$

in which

$$A_{turb}(q)=-\mathrm{k_B}\,T_{turb}\frac{\partial\ln n(q)}{\partial q}+f(q) \tag{56}$$

is the chemical affinity of the vortex fragmentation process (the state function of the subsystem of turbulent chaos); $f(\mathrm{q})=-\partial\Phi/\partial q$ is the so-called friction force; and $\alpha'=-L_q/n(q)$ is the mobility coefficient, which is assumed to be independent of q.

In the case where a stationary non-equilibrium flow is established in a turbulent medium when the energy transfer rate over the cascade is constant, $\varepsilon(q,\mathbf{r},t)\cong\langle\varepsilon(\mathbf{r},t)\rangle$ [vii] inequality (54) takes the form

$$\langle T\rangle\sigma_\Sigma=-\overline{\rho}\,\langle\varepsilon(\mathbf{r},t)\rangle\,A^{gl}_{turb}(\mathbf{r},t)\geq 0\,. \tag{57}$$

Here,

$$A^{gl}_{turb}\equiv\int_q n(q)A_{\mathrm{turb}}(q)dq=n_\Sigma\overline{A_{\mathrm{turb}}}$$

is the so-called global affinity of the formation of turbulent structures. Given (56), it can be rewritten as

$$\overline{A_{turb}}(\mathbf{r},t)=-\mathrm{k_B}\,T_{turb}\int_q\frac{\partial P_2(0|q;t)}{\partial q}dq+\int_q P_2(0|q;t)f(q)dq=$$

$$=-\mathrm{k_B}\,T_{turb}[P_2(q_{L_1})-P_2(q_\eta)]+\overline{f(\mathbf{r},t)}\cong\overline{f(\mathbf{r},t)}, \tag{58}$$

because P_2 becomes zero at the boundaries of the domain of integration (here, η is the local value of the Kolmogorov's microscale; $\overline{\tilde{\mathbf{F}}(\mathbf{q},t_1)\tilde{\mathbf{F}}^T(\mathbf{q},t)}^0=RT_{\mathrm{turb}}\mathbf{Q}(\mathbf{q})\delta(t-t_1)$ is the total

[vii] This assumption was first adopted in the original formulation of the well-known Kolmogorov[28] hypotheses.

number of vortex moles). Thus, the production σ_Σ of averaged entropy in such a stationary process is the product of total energy transfer rate over the cascade $\langle\varepsilon\rangle$ and the global affinity A_{turb}^{gl} is referring to the entire cascade fragmentation of large vortices into small ones. In this case, the linear phenomenological relation

$$\langle\varepsilon(\mathbf{r},t)\rangle = -\alpha' A_{turb}^{gl}(\mathbf{r},t) \tag{59}$$

is valid, in complete agreement with the results of irreversible thermodynamics for consecutive chain of chemical reactions.

On the other hand, we can adopt the more realistic condition

$$J(q,\mathbf{r},t) \cong J(\mathbf{r}) \equiv -n_\Sigma(\mathbf{r})\langle\varepsilon(\mathbf{r})\rangle$$

for the thermodynamic kinetic energy flux $J(q,\mathbf{r},t)$ over the cascade of vortices being quasi-stationary, i.e., for the flux J on various scales of motion being independent of the parameter $q = \rho|\mathbf{u}''|^2/2$. This assumption considered together with the linear relation (55) leads to a more general (than 59) form accounting for non-linear relation between ε and the chemical affinity

$$\tilde{A}(\mathbf{r},t) \equiv \int_q A(q)dq = \mu(q_{L_1},\mathbf{r}) - \mu(q_\eta,\mathbf{r})\,. \tag{60}$$

for the cascade process as a whole. The non-linear defining relation in the case can be easily obtained by applying the second formula in (22) for the "local affinity" $A_{\text{turb}}(q,\mathbf{r},t)$ and as a result, we have for the chemical reaction rate

$$\langle\varepsilon\rangle \cong \gamma\left[1 - \exp\left(-\frac{\tilde{A}}{\mathrm{k_B}\,T_{turb}}\right)\right], \tag{61}$$

where

$$\gamma = \frac{\left(\alpha'\dfrac{\mathrm{k_B}\,T_{turb}}{n_\Sigma}\right)\exp\left(\dfrac{\mu(q_\eta)}{\mathrm{k_B}\,T_{turb}}\right)}{\displaystyle\int_{q_\eta}^{q_{L_1}} \exp\left(\frac{\Phi(q)}{\mathrm{k_B}\,T_{turb}}\right)dq}\,. \tag{62}$$

Thus, the existing deep analogy between the consecutive chemical reactions ($A \to B \to C \to$ etc.) and the Richardson–Kolmogorov cascade fragmentation of vortices with the corresponding chemical potential and chemical affinity allows us to describe macroscopically structured turbulence by the methods of extended irreversible thermodynamics and represent it as self-organization process in an open system. Using the two interpretations of Kolmogorov's parameter ε as the quantity describing the dissipation rate of energy into heat and, simultaneously, as the transfer rate of turbulent energy over the cascade of vortices in the stationary-equilibrium case, we have been able to obtain the defining relations for a key characteristic of the turbulent field - the turbulent energy dissipation rate $\langle\varepsilon\rangle$ by means of thermodynam-

ical modeling structured turbulence. We may recall that in the Kolmogorov[28] theory this quantity is constant and is called Kolmogorov's parameter. Relations (59) and (60) closing the system of hydrodynamic equations (2)–(5) make the thermodynamic approach to modeling the developed turbulence to a certain extent self-sufficient. Obviously, when addressing various problems of numerical simulations including broad class of natural phenomena synergetic approach to describing stationary non-equilibrium turbulence should be further refined.

An additional important remark is worth to mention. By analogy with a laminar fluid motion, the condition for increase in total continuum entropy (33) seems would place some constraints on the turbulent transport coefficients in the defining relations (34), (35), and (59). Positiveness of the direct molecular exchange coefficients is known to follow precisely from such conditions whereas the cross coefficients can be different in sign[31]. Substituting relations (34), (35), and (59) into (33) for the total entropy production of turbulent system, we obtain

$$0 \le \sigma_\Sigma \equiv \frac{1}{\langle T\rangle}\left\{\lambda^{turb}\left(\frac{\partial \ln\langle T\rangle}{\partial \mathbf{r}}\right)^2 + \bar{\rho}\nu^{turb}\left(\mathbf{D}-\frac{1}{3}(\mathrm{div}\langle \mathbf{u}\rangle)\mathbf{U}\right)^2 + \bar{\rho}\alpha'\left(A^{gl}_{turb}\right)^2\right\}. \qquad (63)$$

Specificity of interactions associated with the functional dependence of the turbulent transport coefficients on parameters $\langle\varepsilon\rangle$ and $\langle b\rangle$ between various dissipative processes in a turbulized continuum is such that "switching off" one of the thermodynamic forces (e.g., the affinity A^{gl}_{turb}) can change (or even "switch off") other processes (e.g., the viscous ones). This implies that the second law of thermodynamics, which requires that the entire sum (63) is to be positive, in general, cannot be applied to its individual terms. For example, it could happen that the quantity

$$\bar{\rho}\nu^{turb}\left(\mathbf{D}-\frac{1}{3}(\mathrm{div}\langle \mathbf{u}\rangle)\mathbf{U}\right)^2 < 0,$$

provided that the $\sigma_\Sigma \ge 0$. This indicates that turbulent flows with a negative turbulent viscosity, $\nu^{turb} < 0$, can appear under certain peculiar conditions. The above considerations serves as thermodynamic justification for the possibility that a negative viscosity can appear in turbulent fluid flows.

12 CONCLUSIONS

We performed a stochastic-thermodynamic analysis of developed turbulence in a homogeneous fluid and constructed a phenomenological model of structured turbulence as a self-organization process in an open system based on our previous study summarized in the works[11,27,40,43]. A turbulized continuum was represented as a thermodynamic complex consisting of two mutually open subsystems − the subsystem of averaged motion and the subsystem of turbulent chaos, which, in turn, is considered as an ensemble of vortices with various spatiotemporal scales. This representation allowed us to obtain the defining relations for the turbulent fluxes and forces in the subsystem of turbulent chaos in a non-equilibrium stationary state by the methods of thermodynamics with internal variables. By introducing a number of additional random parameters for the medium characterizing the excited macroscopic degrees of freedom of a strongly turbulized continuum, we obtained various Fokker–Planck–

Kolmogorov equations for the distribution functions of small-scale turbulence characteristics using Prigogine's postulate concerning the direction of the irreversible processes localized in the space of configurations. We also described thermodynamically Kolmogorov's cascade process. At the same time, a deeper understanding of the phenomenology of Kolmogorov's cascade is possible only by taking into account a large number of statistically correlated stochastic processes **q** that comprehensively characterize vortex spatiotemporal structures. Nonetheless, the simplified thermodynamic analysis of quasi-stationary turbulence performed here and the idealized macroscopic model constructed on its basis allow us to extend further our original views of the properties of open dissipative hydrodynamic systems. The latter is a "hot spot" in one of the most important and rapidly developing branches of nonlinear dynamics including evolution of chaotic motions and the formation of ordered dissipative structures.

The dual nature of the irreversible processes leading to disordering near equilibrium and ordering far from equilibrium clearly manifests itself when analyzing the current problems of turbulence, specifically in natural environment and outer space, in the entire variety of spatiotemporal scales. They involve origin and evolution of the Universe, stellar and planetary objects formation and evolution, the processes in the gaseous envelopes of celestial bodies, as well as different patterns of ecosystems in which the cascades of spatiotemporal configurations are created. From our viewpoint, the concept of entropy itself becomes much more substantive and deeper owing to the approach to modeling structured turbulent chaos being developed here. One of the main objectives of this study was the development of theoretical approach to the stationary non-equilibrium state of turbulent chaos using stochastic-thermodynamic methods and finding conditions of self-organization in such open systems.

Acknowledgements. This study was supported by the Russian Fund for Basic Research, Grants № 17-02-00507(a) and № 15-01-03490 (a), and by the Program for Fundamental Research of the Russian Academy of Science № 7 for 2017.

REFERENCES

[1] I. Prigogine, I. Stengers, *Order out of chaos*. Heinemann, London, (1984).

[2] I. Prigogine, I. Stengers. *Vremia. Khaos. Kvant. K resheniiu paradoksa vremeni*. Progress Publishing House, Moscow, (1994).

[3] S.C. Crow, F.H. Champagne, "Orderly structures in jet turbulence", *J. Fluid Mech*. **48**, 547-591 (1971).

[4] G.L. Brown, A. Roshko, "On density effects and large structures in turbulent mixing layers", *J. Fluid Mech*. **64**, 775-816 (1974).

[5] M.I. Rabinovich, M.M. Sushchik, "Regular and chaotic dynamics of structures in fluid flows". *Usp. Fiz. Nauk,* **160 (**1**),** 3-64 (1990).

[6] A.S. Monin, A.M. Yaglom. *Statistical Fluid Mechanics*, *Vol*. 2. Cambridge, Mass., USA: MITPress, (1975).

[7] Yu. L. Klimontovich, *Statistical Theory of Open Systems.* Kluwer academic publishers, Dordrecht, (1995).

[8] Y.I. Khlopkov, V.A. Zharov, S.L. Gorelov, *Kogerentnye Struktury v Turbulentnom Pogranichnom Sloe,* Moskwa, MFTI, (2002).

[9] U. Frisch, *The Legacy of A.N. Kolmogorov*. Cambridge University Press, Cambridge, (1995).

[10] L.I. Sedov, *O perspektivnykh napravleniiakh i zadachakh v mekhanike sploshnykh sred*. Nauka, Moskwa, (1980).

[11] M.Y. Marov, A.V. Kolesnichenko, *Mechanics of Turbulence of Multicomponent Gases*. KluwerAcademic, Dordrecht-Boston-London, (2001).

[12] A.V. Kolesnichenko, «K teorii inversnogo energeticheskogo kaskada v zerkalno-nesemetrichnoi turbulentnosti nemagnitnogo astrofizicheskogo diska» *Mathematica Montisnigrix*, **29**, 11-37 (2014).

[13] A.V. Kolesnichenko, «K MGD -modelirovaniiu struktury i evoliutsii turbulentnogo akkretsionnogo diska protozvezdy», *Mathematica Montisnigrix*, **25**, 65-93 (2012).

[14] S. de Groot, P. Mazur, *Non-equilibrium Thermodynamics*. North-Holland Publishing Company, Amsterdam, (1962).

[15] D. Jou, J. Casas-Vazquez, G. Lebon, *Extended Irreversible Thermodynamics*, Springer, Verlag Berlin Heidelberg, (2001).

[16] R.L. Stratonovich, *Nelineinoia neravnovesnaia termodinamika,* Nauka, Moskwa, (1994).

[17] J. Keizer, *Statistical Thermodynamics of Nonequilibrium Processes,* Springer, Verlag New York, (1987).

[18] W. Ebeling, A. Engel, R. Feistel, *Fizika evoliutsionnykh protsessov*. *Sinergeticheskie prilozheniia*, Editorial USSR, Moscow, (2001).

[19] A.V. Kolesnichenko, M.Ya. Marov, *Turbulentnost mnogokomponentnykh sred*, MAIK-Nauka, Moskwa, (1999).

[20] A.V Kolesnichenko, "Synergetic approach to describing developed turbulence", *Astron, Vestn*., **36(2)**, 121-139 (2002).

[21] A.V. Kolesnichenko, "Thermodynamic modeling of developed structured turbulence with energydissipation fluctuations", *Astron. Vestn*., **38**(2), 144-170 (2004).

[22] I. Prigogine, *Introduction to Thermodynamics of Irreversible Processes,* John Wiley & Sons, New York, (1967).

[23] A. M. Obukhov, "On the energy distribution in the spectrum of turbulent flow", *Izv. Akad. Nauk USSR, Serg. Geogr. Geophys,* **5**, 453-466 (1941)

[24] A.M. Obukhov, "Some specific features of atmospheric turbulence", *J. Fluid Mech*., **13**, 77-81 (1962).

[25] A.S. Monin, A.M. Yaglom, *Statisticheskaia gidrodinamika, Tom* 1, Gidrometeoizdat, St. Petersburg, (1992).

[26] A. Favre, "Statistical Equations of Turbulents Gases", *In: Problems of Hydrodynamics and Continuum Mechanics, SIAM, Philadelphia,* 231-267 (1969)

[27] A.V. Kolesnichenko, "Sootnosheniia Stefana-Maksvella I potok tepla dlia turbulentnoy mnogokomponentnoy sredy", *V zb.: Problemy sovremennoi mekhaniki, Moskwa, Moskovskii Gosudarstvennyi Universitet,* 52-75 (1998).

[28] A.N. Kolmogorov, "Local structure of turbulence in an incompressible fluid at very large Reynolds numbers", *Dokl. Akad. Nauk USSR,* **30**, 299-303 (1941).

[29] L. Onsager, "Statistical hydrodynamics", *Nuovo Cimento (Suppltmtnt),* **6**, 279-287 (1949).

[30] A.K. Blackadar, "Extension of the laws of thermodynamics to turbulent system", *J. Meteorol.*, **12**, 165 -175(1955).

[31] L.D. Landau, V.M. Lifshitz, *Gidrodinamika,* Nauka, Moskwa, (1988).

[32] A. Munster, *Khemicheskaia Termodinamika,* Editorial URSS, Moscow, (2002).

[33] D. Kondepudi, I. Prigogine, *Modern Thermodynamics, from Heat Engines to Dissipative Structures,* John Wiley and Sons, New York, Weinheim, Brisbane, Toronto, Singapore, (1999).

[34] H. Haken, *Synergetics*, Springer, Heidelberg-Berlin-New York, (1981).

[35] H. Haken, *Information and Self-Organization*. Springer, Berlin- Heidelberg- New York, (1988).

[36] Yu. L. Klimontovich, *Turbulent motion and Structure of Chaos,* Kluwer academic Publishers, Dordrecht, (1991).

[37] V.I. Tikhonov, M.A. Mironov, *Markovskie Protsessy*, Sov. Radio, Moskwa, (1977).

[38] A.S. Monin, A.M Yaglom, *Statisticheskaia gidrodinamika, tom* 2. Gidrometeoizdat, St. Petersburg, (1996).

[39] M.D. Millionshchikov, "To the theory of homogeneous and isotropic turbulence", *Izv. Akad. Nauk USSR, Ser. Geogr. Geoph*, **5**(4/5), 433-446 (1941).

[40] M. Ya. Marov, A. V. Kolesnichenko. *Turbulence and Self-Organization: Modelling Astrophysical Objects*, Springer, ASSL, New York-Helderberg-Dordrecht-London, (2013).

[41] G.K. Batchelor, *The Theory of Homogeneous Turbulence*, Cambridge University Press, Cambridge, (1953).

[42] J. Ferziger, H. Kaper, *Mathematical Theory of Transport Processes in Gases*, North-Holland Publishing Company, Amsterdam-London, (1972).

[43] A. V. Kolesnichenko, M. Y. Marov, "Methods of nonequilibrium thermodynamics for description of multicomponent turbulent gas mixtures", *Arch. Mech*., **37**(1/2), 3-19 (1985).

Received December 2, 2016

CALCULATION OF SILICON BAND GAP BY MEANS OF FERMI-DIRAC INTEGRALS

O.N. KOROLEVA [1,2], V.I. MAZHUKIN[1,2], A.V. MAZHUKIN [1,2]

[1] Keldysh Institute of Applied Mathematics of RAS, Moscow, Russia
email: vim@modhef.ru

[2]National Research Nuclear University MEPhI, Moscow, Russia

Summary. The article by mathematical simulation using quantum statistics and Fermi-Dirac integrals investigated narrowing band gap of silicon. As well as its dependence on the temperature and carrier density effects on the change in the carrier density in the conduction band. Particular attention is paid to the determination of the equilibrium concentration of charge carriers in the conduction band and the influence of the narrowing of the band gap on it. The narrowing values of the band gap, calculated using the theoretical model, are compared with the experimental results.

1 INTRODUCTION

The wide use of silicon in numerous technological applications, such as the creation of nanoparticles and nanostructures [1,2], metamaterials [3], the modification of the surface of semiconductors by laser pulses, which has aroused special interest in bio- [4] and IT-technologies [5,6] causes interest in the properties of this semiconductor. Studies of the melting mechanisms of semiconductors and the properties of high-density electron-hole plasma remain topical. Numerous experiments [7-12] have shown that in the process of melting in silicon, covalent bonds are destroyed, with a change in the short-range order, accompanied by a sharp increase in the concentration of conduction electrons and leading to the transition of silicon to the metallic state. However, the role and influence of one of the most important fundamental characteristics of silicon of the band gap on the processes associated with the phase transition and in the region of higher temperatures have remained uncovered both experimentally and theoretically.

The notion of a band gap arose within the framework of quantum theory [13-18] in connection with the need to explain the differences in the physical properties of metals and semiconductors in solid state physics. The most important property of both metals and semiconductors is electrical conductivity and its characteristic - carrier concentration. In determining the carrier concentration necessary to describe all the properties of semiconductors, the width (energy) of the band gap E_g is of great importance, since it is the most important characteristic of the energy structure of semiconductors. For use in mathematical modeling, the band gap should be represented in the form of a temperature dependence $E_g(T)$ (or baric $E_g(P)$). In accordance with the concepts of quantum theory, when a crystal is formed from individual atoms, the interatomic distances decrease, and due to the action of the Pauli principle, allowed bands arise in which electrons can be located. The allowed bands are characterized by the density of electronic states. The most "deep" allowed bands, i.e. energy bands formed by the electrons of the deep-lying shells are the same for all substances. The uppermost of them - the valence band E_v in semiconductors is completely

2010 Mathematics Subject Classification: 82D37, 82B05, 82B10.
Key words and Phrases: Silicon, Narrowing of the Band Gap, Fermi-Dirac integrals, Degenerate carrier gas, Quantum and Classical Statistics

filled with electrons at zero absolute temperature (T=0 °K). The next allowed zone behind it is not filled with electrons at the same temperature. This band is called the conduction band E_c. The allowed bands of a crystal are separated by band gaps, the density of electronic states in which is zero. The band gap largely determines the nature of the chemical bond in the material. To characterize the filling of electronic bands we introduce the concept of Fermi energy (level) E_F, which separates on the energy scale the filled electronic states of the crystal from free ones at zero absolute temperature. Depending on the position of the Fermi level the allowed bands of the crystal can be filled completely or partially by electrons, or remain unfilled. The location of the Fermi level E_F with respect to the edges of these zones determines the electronic nature and physical properties of the crystal. Indeed, the valence electrons of the crystal in the filled bands are bound and do not participate in the conductivity. Electrons can participate in electronic conduction, becoming free, only if they are in an unfilled zone [16]. Accordingly, substances in which the valence band is partially filled, or the conduction band and the valence band overlap, are metals. Substances in which the valence and conduction bands do not overlap at zero absolute temperature (T=0 °K) are semiconductors or dielectrics [15, 16, 17, 18]. Semiconductors and dielectrics differ in the value of E_g. Conditionally, dielectrics include substances with a band gap E_g>2-3 eV (1 eV= 1.6021×10-12 Erg = 1.6021 × 10-19 J), to semiconductors with a bandgap E_g <2-3 eV. Wide-band (1.0 eV <Eg <2-3 eV) and narrow-gap (Eg <0.1 - 0.2 eV) semiconductors are distinguished by the width of band gap. Substances with Eg≈0 are attributed to gapless semiconductors, substances with $E_g \leq 0$ (band overlap) to semimetals, the Fermi level in these substances is located deep in the conduction bands or in the valence band [13, 16, 17, 18].

For semiconductors, including silicon, were carried out experiments to determine the width of the band gap [19-24], which for Si was determined in the temperature range from 4.2 °K to 800 °K. Experimental studies have shown that the narrowing of the band gap depends not only on temperature [19-22], but also on carrier concentration [23-24]. However, a number of limitations of the experimental approach do not make it possible to obtain the necessary characteristics in the melting temperature range and, therefore, theoretical studies are required to determine the band gap and the carrier concentration over a wide temperature range.

In this paper, mathematical modeling will be used - a recognized tool for theoretical studies of problems accompanying the use of silicon in numerous technological applications [25-30]. In the conditions of temperature increase, the band gap $E_g(T)$ narrows, the carrier concentration reaches high values of $N(T) \approx 10^{18}$ cm^{-3} and higher, which is confirmed by experimental studies [7-12], the electron gas degenerates, the values of $Eg(T)$, $EF(T)$, $N(T)$ become interdependent, the classical Maxwell-Boltzmann statistics becomes unjust, which greatly complicates the calculation of all quantities. To solve this problem, the use of Fermi-Dirac quantum statistics becomes fundamental. Therefore, the basis of mathematical modeling is the use of quantum statistics and Fermi-Dirac integrals (F-D) to take into account the degeneracy of the electron gas.

This article is devoted to the study of the behavior of the band gap with increasing temperature and carrier concentration and its role in processes associated with a phase transition in the region of the equilibrium melting temperature of silicon and higher temperatures. Particular attention is paid to the determination of the equilibrium concentration of charge carriers in the conduction band and the impact on it of narrowing the band gap. We consider silicon with intrinsic conductivity under conditions of thermodynamic equilibrium and electroneutrality in the temperature range 300 °K <T <1.5×Tm.

2 QUANTUM APPROACH

In the mathematical modeling of the band gap of silicon, using the statistics of electron gas, the central place is occupied by the law of the distribution of charge carriers over energy states.

In semiconductors, unlike metals, the number of charge carriers and their mobility depend on temperature, defects and the presence of impurities. Under thermodynamic equilibrium conditions at a temperature $T=T_{lat}=T_e$ (T_{lat} is the lattice temperature, T_e is the electron temperature), the probability of the electron filling the state with energy E is determined by the Fermi-Dirac distribution law using the Fermi level E_F

$$f(\mathrm{E},\mathrm{T}) = \frac{1}{\left(1+\exp\left(\frac{E-E_F}{k_B T}\right)\right)} \tag{1}$$

where k_B - Boltzmann constant. At low temperatures, the valence band of the semiconductor is completely occupied and, according to the Pauli principle, charge carriers cannot move inside the valence band. In connection with this, at low temperatures in semiconductors the concentration of conduction electrons is so small that they behave like a gas of noninteracting particles, the Fermi energy exceeds the electron energy $(E-E_F)<0$ and the electron gas is nondegenerate. In this case (1) reduces to the Maxwell-Boltzmann distribution function

$$f(\mathrm{E},\mathrm{T}) = \exp\left(\frac{E_F-E}{k_B T_e}\right) \tag{2}$$

To move free carriers from the valence band to unoccupied conduction band, an additional finite energy is required and it exceeds the energy of the band gap, which for silicon E_g=1.17 eV for at T = 0 °K [13]. With increasing temperature, hot electrons give off energy to the lattice, while the width of band gap decreases, and the concentration of free charge carriers in the conduction band increases, determined by the processes of generation and recombination of electrons from the conduction band and holes from the valence band, which occur continuously and in parallel, the electron gas degenerates and $(E-E_F)> 0$. In a state of thermodynamic equilibrium, these opposite processes must coincide in speed, both in the whole and in each region of the spectrum. Such a detailed equilibrium exists when the phonon energy is converted into the energy of electrons and back and in any other process of energy transformation that can occur in a solid. From the principle of detailed balance it follows that there is a unique electron energy distribution characterized by a single Fermi level E_F for a material of a given composition at a given temperature T.

As we can see, the distribution function has the necessary minimum information for describing the processes taking place inside a solid body with an acceptable accuracy.

By integrating the distribution function of the carriers (1), one can obtain many characteristics of the electron gas. Therefore, in determining the properties of silicon in an arbitrary degeneracy range from the classical Boltzmann limit to the degenerate Fermi-Dirac, including the weak degeneracy range ($E\sim E_F$), a large role is played by the Fermi-Dirac integrals

$$\mathcal{F}_j(\eta_c) = \frac{1}{\Gamma(j+1)} \int_0^\infty \frac{\varepsilon^j}{1+exp(\varepsilon-\eta_c)} d\varepsilon \tag{3}$$

where $\Gamma(x)$ is the gamma function, j is the index of the Fermi-Dirac integral, c=e for electrons and c=h for holes, ε is the reduced electron energy (hole), the reduced Fermi level for electrons

$$\eta_e = \frac{E_F - E_C}{k_B T} \tag{4}$$

for holes

$$\eta_h = \frac{E_V - E_F}{k_B T}. \tag{5}$$

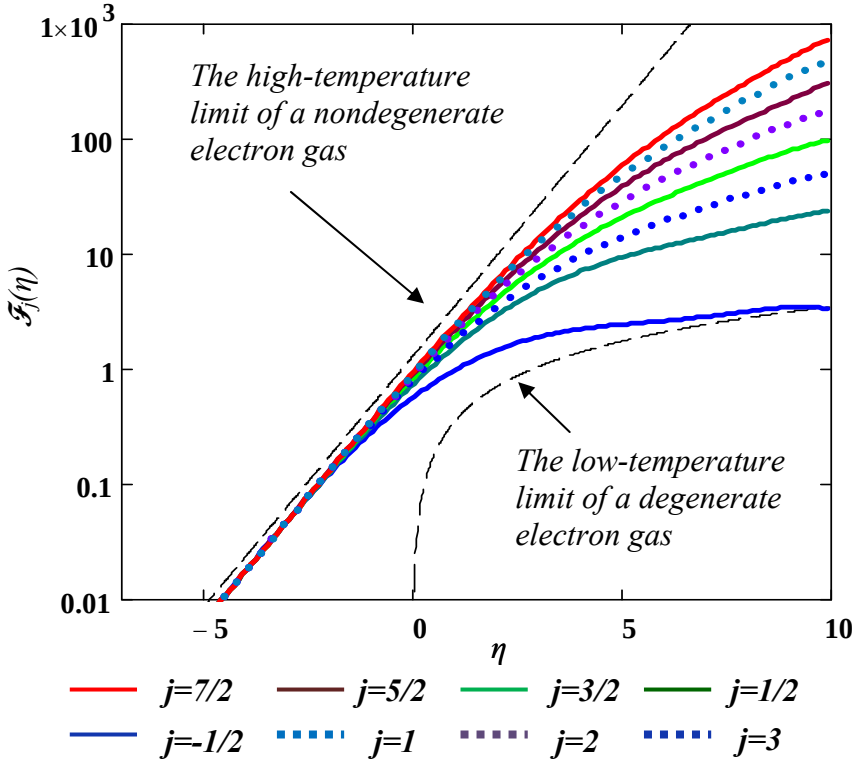

Fig. 1. Approximating functions of Fermi-Dirac integrals $\mathcal{F}_j(\eta)$ of order j.

To determine the carrier concentration and the band gap of semiconductors we use F-D integral with the index j=1/2. The integral (3) with the exception of an integral with order $j=0$, cannot be calculated analytically. This involves a variety of methods for approximate calculation and approximation of Fermi integrals [30], among them: expansion in series [31-33], numerical quadratures [33-35], recurrence relations and interpolation of tabulated values [36-38], piecewise polynomials and rational functions [39-41]. In [42,43] Fermi-Dirac integrals of orders j=-1/2, 1/2, 1, 3/2, 2, 5/2, 3 and 7/2, continuous analytic expressions that unique for each order were obtained in a wide range of degeneracy -10 ≤η≤ 10. The

approximating function of F-D integral with order j=1/2 from [42,43] will be used to calculate the properties of the electron gas of silicon.

Figure 1 shows the dependences of the Fermi-Dirac function of integers j and half-integral *j/2* orders, for different values of η. The dotted lines in the figure show the high-temperature limit for the nondegenerate ($\eta<0$) and low-temperature limit for the degenerate ($\eta>0$) electron gas. It is seen that the use of approximating functions makes it possible to carry out a smooth, continuous transition from the domain of nondegeneracy to the degeneracy region, which is very important for obtaining smooth functional dependences of the properties of the electron gas of silicon.

3 CALCULATION OF THE BAND GAP OF SILICON

The band gap of silicon E_g, like other semiconductors, depends on external parameters such as temperature, pressure, electric, magnetic, gravitational fields, and others [13-18]. With increasing temperature and an increase in the concentration of charge carriers, the energy of band gap tends to decrease [12, 13, 19-24].

Narrowing of the band gap for wide-gap semiconductors was studied by optical methods and by photoluminescence spectroscopy. The experimental data give an idea of narrowing of the band gap in the range of carrier concentrations from 4×10^8 -10^{20} cm^{-3} and temperatures of 20-300 K [19, 23-24]. In [10], it was suggested that the width of the forbidden band at the melting temperature T_m abruptly becomes zero.

In this paper, it is of interest to investigate the influence of the band gap of silicon on processes associated with the phase transition and in the region of higher temperatures. It is known that upon melting silicon acquires metallic properties, so the width of the forbidden band in the vicinity of the melting temperature should become close to or equal to zero. These arguments form the basis of our assumption about the observance at the equilibrium melting temperature of the condition

$$E_g(T_m)\approx 0, \text{ при } T_m = 1687°\text{K} \qquad (6)$$

Let us consider the basic mechanisms that affect the temperature dependence of the width of the band gap.

The first mechanism is associated with the expansion of the lattice when the temperature rises causing displacement of position relatively the conduction band and the valence band. The second mechanism is associated with the enhancement of electron-lattice interaction with an increase in temperature [44-50]. In low-temperature region these effects make a significant contribution to the change in the energy of the band gap. The temperature dependence of the width of the band gap at low temperature is nonlinear. In high-temperature region according to estimates made in Ref. [48], the contribution of these mechanisms is approximately 20-25% of total change in the energy of the band gap and temperature dependence is linear

$$T << \theta, \quad \Delta E_g \infty T^2; \quad T >> \theta, \quad \Delta E_g \infty T \quad , \qquad (7)$$

where θ is the Debye temperature (for Si θ = 640 °K).

At present, empirical and semiempirical dependences are used to describe the temperature changes in the band gap E_g (T) [44-51]. They usually use linear coefficients (for example, temperature coefficient [48] - $\alpha_T = -\frac{\partial E_g}{\partial T}$ and baric [56] - $\alpha_P \approx -\frac{\partial E_g}{\partial P}$, here T and P are the

absolute temperature and hydrostatic pressure). The most common is the Varshni approximation [48], which describes well first two mechanisms of narrowing of the band gap

$$E_g(T) = E_{g,0} - \frac{\alpha T^2}{T+\beta} \tag{8}$$

where $E_{g,0}$ is the band gap at 0 °K, α and β are constants that have been evaluated experimentally and for silicon are: α=7.021×10-4 eV/T, β=1108K. The constant β is comparable with the Debye temperature with a coefficient ≈2.5 for silicon [48]. At high temperatures T>>β, it follows from (8), that $\alpha \approx -\frac{\partial E_g}{\partial T}$, so it is temperature coefficient of the width of band gap.

The third mechanism of narrowing of band gap is related to the effects of collective interactions and operates at sufficiently high carrier concentrations and degeneracy of the electron gas. The most significant contribution to narrowing the width of the band gap is due to the exchange interaction which leads to an empirical dependence of the form $\Delta E_g \sim \gamma \times N(T)^{1/3}$, where γ is a parameter that has the behavior of a fitting to this experiment. In [51-55], the parameter γ is defined in the range $1\times10^{-8} \div 7.3\times10^{-8}$ eV×cm.

Thermal and quantum mechanisms are taken into account in the relation of [26], which represents the modification of (8)

$$E_g(T,N) = E_{g,0} - \frac{\alpha T^2}{T+\beta} - \gamma \cdot N^{1/3}(T) \tag{9}$$

where α, β are the constants that coincide with the corresponding constants from (8), the constant γ=1.5×10^{-8} eV×cm, $N(T)$ is the concentration of charge carriers in the conduction band, and T is the temperature. In this paper, two values of the fitting parameter γ were chosen. The first - $\gamma = 8.35\times10^{-8}$ eV×cm - was chosen from the condition that the width of the band gap should be zero at equilibrium melting point $E_g(T_m)=0$. The second value - γ=4.2×10^{-8} eV×cm was chosen as a half of first one.

4 CARRIER CONCENTRATION AND FERMI LEVEL

In metals the carrier concentration is constant and can be characterized by a definite value of the electrochemical potential (Fermi energy), the value of which can be obtained from the experimental data [17]. In semimetals which have a band gap $E_g \leq 0$, the Fermi level is located in conduction band or in valence band, and the carrier concentration is about 10^{18}-10^{20} cm^{-3}, several orders of magnitude lower than typical for metals of 1022 cm-3. With increasing temperature, the number of carriers in semimetals increases, and the electrical conductivity increases [18].

In semiconductors, unlike metals, the carrier concentration and their mobility depends on the temperature and on the presence of defects and impurities. For any semiconductor, the most important characteristic is the concentration of electrons N_e in the conduction band or holes N_h in the valence band. For an intrinsic semiconductor that does not contain impurities, the equality of the concentrations $N_e=N_h$ is observed.

The temperature dependences of the carrier concentrations in the conduction band and holes in the valence band are determined by integrating the distribution function of the carriers (1)

$$N_e(T) = N_C \mathcal{F}_{1/2}(\eta_e) \tag{10}$$

$$N_h(T) = N_V \mathcal{F}_{1/2}(\eta_h) \tag{11}$$

where $\mathcal{F}_{1/2}(\eta_e), \mathcal{F}_{1/2}(\eta_h)$ - the Fermi-Dirac integrals (3) of order j=1/2 for electrons and holes, η_e and η_h are the reduced Fermi energy $E_F(T)$ for electrons (4) and holes (5), N_C and N_V are the density of states in the conduction band and valence band

$$N_C = 2\left(\frac{m_e k_B T}{2\pi\hbar^2}\right)^{3/2}, \; N_V = 2\left(\frac{m_h k_B T}{2\pi\hbar^2}\right)^{3/2} \tag{12}$$

where $m_e = M^{2/3}\left(m_l \cdot m_t^2\right)^{1/3}$ - the effective mass of the density of states of electrons in the conduction band, taking into account the contribution from the total set of ellipsoids M - the number of equivalent energy minima in the conduction band (for silicon M=6) [14, 18], m_l, m_t are respectively longitudinal and transverse masses, m_h is the effective mass of the density of states of holes in the valence band.

Since in thermodynamic equilibrium the probability of filling all electronic states with any energy can be expressed using a single normalization parameter-the Fermi level E_F, then the temperature dependence of $E_F(T)$ is necessary to determine the carrier concentration and other properties of silicon. The position of the Fermi level is determined from the condition of electroneutrality.

Taking into account (10) and (11), the electroneutrality condition takes the form

$$N_C \cdot \mathcal{F}_{1/2}(\eta_e) = N_V \cdot \mathcal{F}_{1/2}(\eta_h) \tag{13}$$

Equation (13) is greatly simplified when approximating expressions are used for integrals $\mathcal{F}_{1/2}(\eta_e), \mathcal{F}_{1/2}(\eta_h)$ [27, 28]

$$\mathcal{F}_{1/2}(\eta_c) = \exp\left(\sum_{i=0}^{7} a_i \eta_c^i\right)_{c=e,h} \tag{14}$$

where a_i - coefficients of the polynomial [42,43]. The use of a continuous analytic expression approximating F-D integral allows us to calculate carrier concentrations and energy of the Fermi level with an arbitrary degeneracy degree of the electron gas.

Taking (14) into account, equation (13) takes the form

$$N_C \cdot exp\left(\sum_{i=0}^{7} a_i \eta_e^i\right) = N_V \cdot exp\left(\sum_{i=0}^{7} a_i \eta_h^i\right) \tag{15}$$

Formulated equations (9) - (15) represent a mathematical description of the interrelated variables $E_F(T)$, $N(T)$, $E_g(T,N)$ that vary with temperature, the derivation of which in this paper was carried out from a numerical solution of equations using a computational procedure consisting of 2 nested iteration cycles. At one step in temperature $[T_i, T_{i+1}]$, the sequence of

calculations looks like this. In the inner cycle, the energy of the Fermi level $E_F(T_{i+1})$ is determined from the condition of electroneutrality (15) of the intrinsic semiconductor using the iterative Newton method [57]. In the outer cycle, taking into account the new value $E_F(T_{i+1})$, the values are determined by the simple iteration method. The procedure is repeated until complete convergence.

The results of the calculations are shown in Figures 2-6.

5 MODELING RESULTS

Figure 2 shows the temperature dependences of the band gap calculated for the Fermi-Dirac distribution (9) with both values of the parameter γ (curves 1, 2) and for the Maxwell-Boltzmann distribution (curve 3). In the temperature range from 300 ° K to θ, where the influence of quantum mechanisms is weak, the width of band gap is equally well approximated by all the dependences and completely coincide with the experiment [22]. Above the Debye temperature, the contribution of collective interaction mechanisms to the width of the forbidden band becomes appreciable, which is reflected in the behavior of the dependences. The width of the forbidden band, calculated with the Maxwell-Boltzmann statistics (curve 3), depends only on the temperature remains positive longer than others. The condition $E_g(T)=0$ for this dependence is satisfied at T=2400K, and at the melting point - $E_g(T_m)$=0.5 eV. The dependences calculated with Fermi-Dirac statistics (curves 1, 2), which take into account the effect of temperature and carrier concentration, narrow more strongly. For the value of parameter $\gamma=4.2\times10^{-8}$ eV×cm, $E_g(T)=0$ at T=2000 K, $E_g(T_m)$=0.248 eV. For the value of parameter $\gamma=8.35\times10^{-8}$ eV×cm, the width of band gap at temperature $T>Tm$ becomes negative.

Figure 3 gives a clear picture of the shape and velocity of the narrowing of the band gap $E_g(T,N)$ and the position of the Fermi energy level $E_F(T)$, calculated with quantum statistics, relative to the edges of the valence $E_V(T)$ and conduction $E_C(T)$ bands and intrinsic Fermi level located in the middle of the band gap. With increasing temperature the Fermi energy $E_F(T)$ deviates from its own level toward the edge of the valence band $E_V(T)$, which is determined by lower effective mass of the density of states of the valence band. For silicon, the ratio of the effective masses of the electron and hole states is m_{de}/m_{dh}=1.89. Because of this, the degeneracy of the hole gas ($\eta_h=0$) occurs earlier than the degeneracy of the electron gas ($\eta_e=0$) (Fig. 5).

Beginning with T=1000K the carrier concentration and the width of the forbidden band, calculated with quantum and classical statistics begin to differ: for Fermi-Dirac – $N(T)=1.5\times10^{18}$ cm^{-3}, for Maxwell-Boltzmann - $N(T)=9.1\times10^{17}$ cm^{-3}, $E_g(T,N)$=0.81 eV. Obtained data corresponds to appearance of a weak degeneracy, to which the values $\eta_h\approx-4$ correspond (Fig. 5).

The region of strong degeneracy arises when the curves $E_F(T)$ and $E_V(T)$ (Figure 3), which corresponds to $\eta_h=0$ and to the values T=1600K, $N(T)=1.1\times10^{20}$ cm^{-3} (Fig. 4), $E_g(T,N)$=0.083 eV for Fermi-Dirac distribution and $N_{M\text{-}B}(T)=3.8\times10^{19}$ cm^{-3} (Fig. 4), $E_g(T)$=0.48 eV for Maxwell-Boltzmann.

The same picture, with a certain shift to higher temperatures, is observed with degeneracy of the electron gas. Weak degeneracy: $\eta_e\approx-4$, T=1090K (Fig.5), $N(T)=4.5\times10^{18}$ cm^{-3}, $E_g(T,N)$=0.61 eV (Fig. 3, 4), strong degeneracy: $\eta_e\approx-0$ (Fig.5), T=1920K, $E_g(T,N)$=-0.28 eV (Fig. 3, 4).

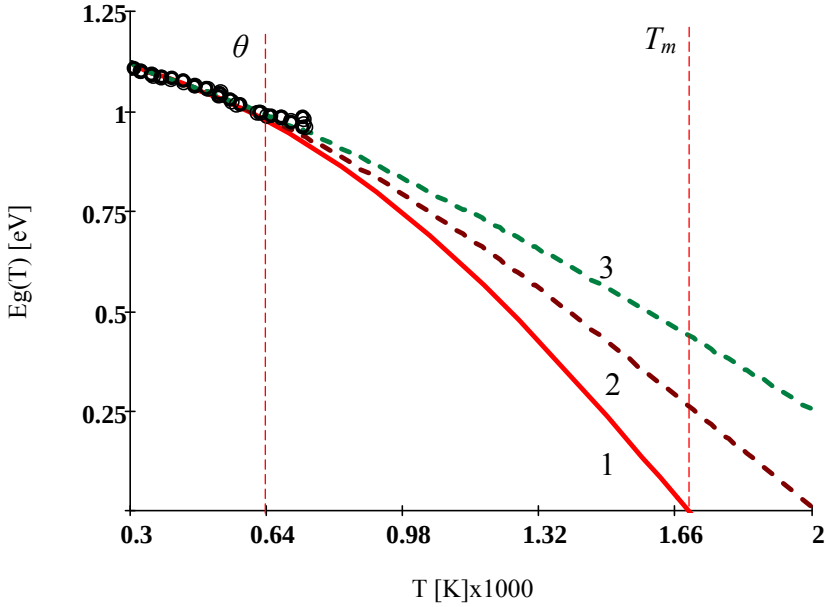

Fig. 2. Temperature dependence of the width of band gap of silicon. The calculation was carried out using: 1 - quantum statistics with $\gamma=8.35\times10^{-8}$ in (10); 2 - quantum statistics with $\gamma=4.2\times10^{-8}$ in (10); 3 - Maxwell-Boltzmann statistics and Varshni relation [48]. Experimental data are marked by unpainted circles [22].

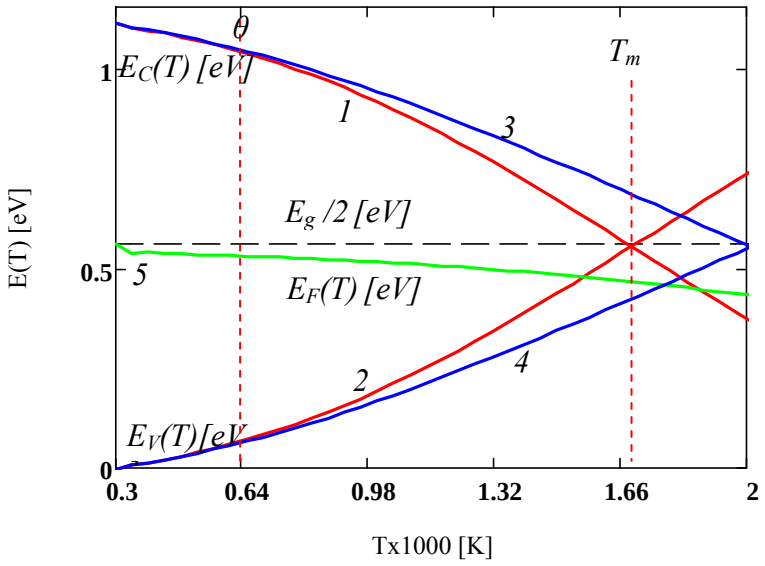

Fig. 3. Temperature dependence of edges of the conduction band $E_C(T)$ and the valence band for various degrees of narrowing of band gap: (1), (2) - $\gamma=8.35\times10^{-8}$ eV×cm, (3), (4) - $\gamma=4.2\times10^{-8}$ eV×cm; (5) is the temperature dependence of Fermi energy $E_F(T)$.

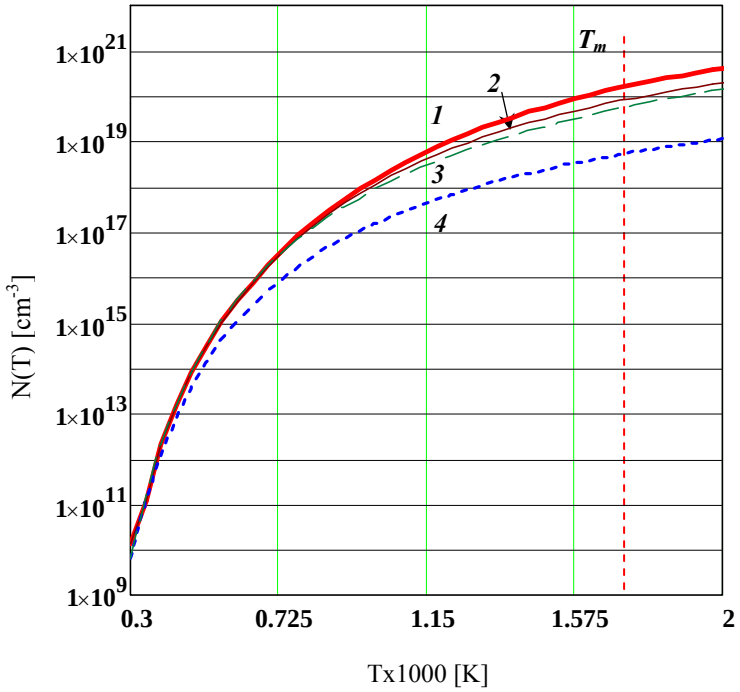

Fig. 4. The temperature dependences of the carrier concentration calculated using the Fermi-Dirac statistics (1) - γ = 8.35 × 10-8 eV × cm, (2) γ = 4.2 × 10-8 eV × cm; and Maxwell-Boltzmann (3) - the temperature dependence, (4) - the constant Eg = 1.12 eV.

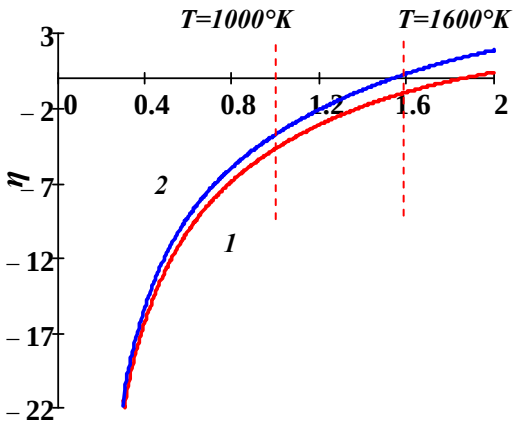

Fig. 5. Temperature dependences of the electron (1) and hole (2) reduced levels of the Fermi energy.

At the equilibrium melting temperature $T=T_m$=1687K in the variant with quantum statistics and fitting parameter $\gamma=8.35\times10^{-8}$ eV×cm the width of the forbidden band vanishes $E_g(T,N)=0$ with the carrier density $N(T)=1.7\times10^{20}$ cm^{-3}.

With further heating up to T=2000K, the width of the forbidden band becomes negative, and the carrier concentration continues to increase, (Fig. 3, 4) $N(T)=4.2\times10^{20}$ cm^{-3}, $E_g(T,N)$=-0.38 eV. With the Maxwell-Boltzmann statistics (Figure 2), the width of the forbidden band still remains positive, and the concentration is much lower than in the Fermi-Dirac statistics: $E_g(T,N)$=0.24 (Fig. 2), $N_{M\text{-}B}=1.4\times10^{20}$ cm^{-3} (Fig. 4).

As the fitting parameter decreases by a factor of 2 $\gamma=4.2\times10^{-8}$ eV×cm, the width of the forbidden band vanishes $E_g(T,N)$=0 (Fig. 3) at a temperature T=2000K with a concentration $N(T)=2.05\times10^{20}$ cm^{-3} (Fig. 4).

6 CONCLUSIONS

- Under the conditions of thermodynamic equilibrium, the degeneracy of charge carriers in silicon with intrinsic conductivity begins at a temperature which is considerably below the equilibrium melting point. This requires the use of quantum statistics and Fermi-Dirac integrals calculation technique when determining the properties of solid-state silicon.
- The width of the band gap and its variation is one of the most important fundamental characteristics of silicon, which affects substantially on the concentration of electrons and holes and, therefore, all properties and characteristics of a solid-state semiconductor.
- Concentrations of both types of carriers indicate their strong degeneracy in the temperature range T=1600÷2500K. Taking into accoun quantum effects allow one to vanish the width of the forbidden band at the point of equilibrium melting point or its vicinity. However, the concentrations are in the range $N(T)=4.2\times10^{20}\div 10^{21}$ cm^{-3}, which is typical for semimetals with a negative band gap [18], but several orders of magnitude lower than the values typical for metals $10^{22}\div 10^{23}$ cm^{-3}.
- The thermodynamic equilibrium melting of pure crystalline silicon occurs in two stages. First, the melt acquires the properties of a semimetal with growing with a temperature number of carriers, and then reaching a certain temperature T>Tm~3000K, the molten silicon acquires metallic properties with a constant concentration of electrons and holes.
- The above analysis is very important for a better understanding of the processes of nonequilibrium heating and melting of pure crystalline silicon, for example by ultrashort femtosecond laser pulses [7]. Under the condition $\hbar\omega_L > E_g(T)$, where $\hbar\omega_L$ is the energy of the quantum of laser radiation, in solid silicon due to photoeffects, the electron and hole concentrations can reached the values $N(T)\approx10^{22}$ cm^{-3} without the lattice reaching the melting temperature, but with the achievement of metal properties. In the physical literature, this phenomenon was called pre-melting or softening of the lattice up to the melting. However, these concepts are given without proper quantitative characteristics.
- The acquisition of metallic properties by a semiconductor (silicon) depends on specific situation, in particular, related to the certain mode of action, and can occur before melting, at the moment of melting or after the melting.

This work was supported by RSF (project № 15-11-00032).

REFERENCES

[1] U. Zywietz, A.B. Evlyukhin, C. Reinhardt, B.N. Chichkov, “Laser printing of silicon nanoparticles with resonant optical electric and magnetic responses”, *Nat. Commun.*, **5**, 3402 - 3405 (2014).

[2] A. Mene´ndez-Manjo´n, S. Barcikowski, G.A. Shafeev, V.I. Mazhukin, B.N. Chichkov, “Influence of beam intensity profile on the aerodynamic particle size distributions generated by femtosecond laser ablation”, *Laser and Particle Beams*, **28**, 45–52 (2010).

[3] L. Shi, T.U. Tuzer, R. Fenollosa, F. Meseguer, "A new dielectric metamaterial building block with a strong magnetic response in the sub-1.5-micrometer region: silicon colloid nanocavities", *Adv. Mater*., **24**, 5934−5938 (2012).
[4] E. Stratakis, A. Ranella, and C. Fotakis, "Biomimetic micro/nanostructured functional surfaces for microfluidic and tissue engineering applications", *Biomicrofluidics*, **5** (1), 013411, (2011).
[5] A. Mathis, F. Courvoisier, L. Froehly, L. Furfaro, M. Jacquot, P. A. Lacourt, and J.M. Dudley, "Micromachining along a curve: Femtosecond laser micromachining of curved profiles in diamond and silicon using accelerating beams", *Appl. Phys. Lett.*, 101 (7), 071110 (2012).
[6] M. K. Bhuyan, F. Courvoisier, P. A. Lacourt, M. Jacquot, R. Salut, L. Furfaro, and J. M. Dudley, "High aspect ratio nanochannel machining using single shot femtosecond Bessel beams", *Appl. Phys. Lett.*, **97** (8), 081102 (2010).
[7] K. Sokolowski-Tinten and D. von der Linde, "Generation of dense electron-hole plasmas in silicon", Phys. Rev. B, **61** (4), 2643-2650 (2000).
[8] Ia.B. Magometov, G.G. Gadzhiev, Z.M. Omarov. "Vliianie temperatury na termoelektricheskie parametry kremniia", *Fazovye perehody, uporiadochennye sostoianiia i novye materialy*, 1-3 (2009).
[9] S. Nakamura, T. Hibiya. "Thermophysical properties data on molten semiconductors", *International Journal of Thermophysics*, **13** (6), 1061–1084 (1992).
[10] C. J. Glassbrennert and Glen A. Slack, "Thermal Conductivity of Silicon and Germanium from 3K to the Melting Point", *Phys. Rev.*, **134** (4a), A1058-A1069 (1964).
[11] D.R. Hamilton and R.G. Seidensticker, "Association in Melted Semiconductors", *J. Appl. Phys.*, **34** (9), 2697-2699 (1963).
[12] P. J. Morin and J. P. Maita, "Electrical Properties of Silicon Containing Arsenic and Boron". *Phys. Rev.*, **96** (1), 28-35 (1954).
[13] L.S. Stilbans, *Semiconductor Physics*, M.: Sov. radio, (1967).
[14] S. M. Sze, K. Ng. Kwok, *Physics of Semiconductor Devices*, John Wiley & Sons, (2007).
[15] A.H. Wilson, *The Theory of Metals*, Cambridge, (1953).
[16] C. Kittel, *Introduction to Solid State Physics*, *8th Edition*, John Wiley & Sons, (2005).
[17] J.S. Blakemore, *Solid State Physics, 2nd ed.*, Cambridge University Press, New York, (1985).
[18] Neil W. Ashcroft, N. David Mermin, *Solid state physics*, Saunders College, Vol. 1, (1976).
[19] G.G. Macfarlane, T.P. McLean, J.E. Quarrington, and V. Roberts, "Fine Structure in the Absorption-Edge Spectrum of Si", *Phys. Rev.,* **111** (5), 1245-1254 (1958).
[20] J.R. Haynes, M. Lax, and W.F. Flood, "Analysis of intrinsic recombination radiation from silicon and germanium", *J. Phys. Chem. Solids,* **8**, 392-396 (1959).
[21] A.M. Emelianov, "Opredelenie izmenenii shiriny zapreshchennoi zony nepriamozonnykh poluprovodnikov po spektram kraevoi liuminescentcii", *Pisma v ZHTF*, **35** (6), 9-16 (2009).
[22] V. Alex, S. Finkbeiner, and J. Weber, "Temperature dependence of the indirect energy gap in crystalline silicon", *J. Appl. Phys*. **79** (9), 6943-6946 (1996).
[23] Joachim Wagner, Jesus A. del Alamo. "Band - gap narrowing in heavily doped silicon: A comparison of optical and electrical data", *J. Appl. Phys.*, **63** (2), 425-429 (1988).
[24] Diego Olego and Manuel Cardona, "Photoluminescence in heavily doped GaAs. I. Temperature and hole-concentration dependence", *Phys. Rev. B*, **22** (2), 886-893 (1980).

[25] V.I. Mazhukin, V.V. Nosov. U. Zemmler, "Issledovanie teplovykh i termouprugikh polei v poluprovodnikakh pri impulsnoi obrabotke", *Matematicheskoe modelirovanie*, **12** (2), 75-83 (2000).

[26] Henry M. van Driel, "Kinetics of high-density plasmas generated in Si by 1.06-and 0.53-pm picosecond laser pulses", *Phys. Rev. B*, **35** (11), 8166-8176 (1987).

[27] A. Lietoila and J.F. Gibbons, "Computer modeling of the temperature rise and carrier concentration induced in silicon by nanosecond laser pulses", *J. Appl .Phys.*, **53**(4), 3207-3213 (1982).

[28] J.K. Chen, D.Y. Tzou, J.E. Beraun, "Numerical investigation of ultrashort laser damage in semiconductors", *International Journal of Heat and Mass Transfer*, **48,** 501–509 (2005).

[29] A. Rämer, O. Osmani, and B. Rethfeld," Laser damage in silicon: Energy absorption, relaxation, and transport", *J. Appl. Phys.*, **116**, 053508(1-12) (2014).

[30] J.S. Blakemore, "Approximations for Fermi-Dirac integrals, especially the function $\Im_{1/2}(\eta)$, used to describe electron density in a semiconductor", *Solid-State Electronics*, **25** (11), 1067-1076 (1982).

[31] P. Van Halen and D. L. Pulfrey, "Accurate, short series approximations to Fermi-Dirac integrals of order -1/2, 1/2, 1, 3/2, 2, 5/2, 3, and 7/2", *J. Appl. Phys.*, **57**, 5271-5274 (1985).
P. Van Halen and D. L. Pulfrey, Erratum: "Accurate, short series approximation to Fermi-Dirac integrals of order -1/2, 1/2, 1, 3/2, 2, 5/2, 3, and 7/2", [*J. Appl. Phys.*, **57**, 5271 (1985)], *J. Appl. Phys.*, **59** (6), 2264 (1986).

[32] F.G. Lether, "Variable precision algorithm for the numerical computation of the Fermi-Dirac function $F_j(x)$ of order $j = -3/2$", *J. Sci. Comput.*, **16**, 69–79 (2001).

[33] Bernard Pichon, "Numerical calculation of the generalized Fermi-Dirac integrals", *Comput. Phys. Com.*, **55**, 127-136 (1989).

[34] W. H. Press, S. A. Teukolsky, W. T. Vetterling, and B. P. Flannery, *Numerical Recipes: The Art of Scientific Computing. 3rd ed*, New York: Cambridge University Press, (2007).

[35] A.W. Smith, A. Rothary, "Reevaluation of the derivatives of the half order Fermi integrals", *J. Appl. Phys.*, **73**, 7030–7034 (1993).

[36] J. McDougall and E.C. Stoner, "The computation of Fermi-Dirac functions", *Philosophical Transactions of the Royal Society of London. Series A, Mathematical and Physical Sciences*, **237**, 67-104, (1938).

[37] A. C. Beer, M. N. Chase, and P. F. Choquard, "Extension of McDougall-Stoner tables of the Fermi-Dirac functions", *Helvetica Physica Acta*, **28**, 529 - 542 (1955).

[38] R.B. Dingle, "The Fermi-Dirac integrals $\Im_p(\eta) = (p!)^{-1}\int_0^\infty \varepsilon^p \left(e^{\varepsilon-\eta}+1\right)^{-1} d\varepsilon$.", *Applied Scientific Research*, **6**, 225-239 (1957).

[39] D. Bednarczyk and J. Bednarczyk, "The approximation of the Fermi-Dirac integral $\Im 1/2(\eta)$", *Phys. Lett.*, **64A** (4), (1978).

[40] X. Aymerich-Humet, F. Serra-Mestres and J. Millan, "An analytical approximation for the Fermi-Dirac integral F1/2(η)", *Solid-St. Electron*, **24**, 981 (1981).

[41] E. L. Jones, "Rational Chebyshev Approximation of the Fermi-Dirac Integrals", *Proc. IEEE*, **54**, 708-709 (1966).

[42] O.N. Koroleva, A.V. Mazhukin, V.I. Mazhukin, P.V. Breslavskiy, "Approximation of Fermi-Dirac integrals of different orders used to determine the thermal properties of metals and semiconductors", *Mathematica Montisnigri*, **35**, 37-53 (2016).

[43] O.N. Koroleva, A.V. Mazhukin, V.I. Mazhukin, and P.V. Breslavskiy, "Analytical Approximation of the Fermi-Dirac Integrals of Half-Integer and Integer Orders", *Mathematical Models and Computer Simulations*, **9** (3), 383–389 (2017).
[44] K.P. O'Donnell and X. Chen, "Temperature dependence of semiconductor band gaps", *Appl. Phys. Lett.*, **58** (25), 2924-2926 (1991).
[45] J. Bhosale and A. K. Ramdas, A. Burger, A. Munoz, A. H. Romero, M. Cardona, R. Lauck, and R. K. Kremer, "Temperature dependence of band gaps in semiconductor: electron-phonon interaction", *Phys. Rev. B*, **86**, 195208 (1-10) (2012).
[46] M. Klenner, C. Falter, and W. Ludwig, "Temperature dependence of band gaps in Si and Ge in the quasi-ion model", *Ann. Physik*, **1**, 34-38 (1992)
[47] W. Bludau and A. Onton, W. Heinke, "Temperature dependence of the band gap of silicon", *J. Appl. Phys.*, **45** (4), 1846-1848 (1974).
[48] Y. P. Varshni, "Temperature dependence of the energy gap in semiconductors", *Physica*, **34** (1), 149-154 (1967).
[49] H.Y. Fan, "Temperature Dependence of the Energy Gap in Semiconductors", *Phys. Rev.*, **82** (6), 902-905 (1951).
[50] H.D. Vasileff, "Electron Self-Energy and Temperature-Dependent Effective Masses in Semiconductors: n-Type Ge and Si", *Phys. Rev.*, **105** (2), 441-446 (1957).
[51] V.K. Kononenko, E.V. Lucenko, "Suzhenie shiriny zapreshchennoi zony nitrida galliia", *Aktualnye problemy fiziki tverdogo tela, sb. docl. Mezhdunar. nauch. konf., Minsk*, (2009).
[52] S.C. Jain, J.M. McGregor, and D.J. Roulston, "Band-gap narrowing in novel III-V semiconductors", *J. Appl. Phys.*, **68** (7), 3747-3749 (1990).
[53] S. C. Jain And D. J. Roulston, "A simple expression for band gap narrowing (BGN) in heavily doped Si, Ge, GaAs and Ge,Si, _-x strained layers", *Solid-State Electronics*, **34** (5), 453-465 (1991).
[54] S. C. Jain, J. M. Mcgregor, D. J. Roulston and P. Balk, "Modified Simple Expression For Bandgap Narrowing in n-type GaAs", *Solid-State Electronics*, **35** (5), 639-642 (1992).
[55] H.D.P. Lanyon, R.A. Tuft, "Bandgap Narrowing in Moderately to Heavily Doped Silicon", *IEEE Transactions on Electron Devices*, **ED-26** (7), (1979*)*.
[56] A.R. Goni, K. Syassen, K. Strossner, M. Cardona, "Pressure dependence of the direct optical gap and refractive index of Ge and GaAs", *Semicond. Sci. Technol*., **4**, 246-247 (1989).
[57] A.A. Samarskii, A.I. Gulin, *Chislennye metody*, M.: Fizmatlit, (1989).

Received December 20, 2017

ON EXACT SOLUTION ENCLOSURE ON ENSEMBLE OF NUMERICAL SIMULATIONS

A.K. ALEXEEV[1], **A.E. BONDAREV**[2]

[1] Moscow Institute of Physics and Technology
Moscow, Russia
e-mail: aleksey.k.alekseev@gmail.com
[2] Keldysh Institute of Applied Mathematics Russian Academy of Sciences
Moscow, Russia
e-mail: bond@keldysh.ru

Summary. The estimation of a vicinity of the approximate solution that contains the exact one (*exact solution enclosure*) may be performed using an ensemble of numerical solutions if the information on their error ranging is available *a priori*. A posteriori analysis of distances between numerical solutions enables error ranging by magnitudes, if the ensemble of numerical solutions separates into clusters of "accurate" and "inaccurate" solutions. For nonlinear problems this enclosure may serve as the computational proof of the exact solution existence. The impact of metric selection on the solution enclosure is observed. The numerical tests for the supersonic flows, governed by two dimensional Euler equations, demonstrate the exact solution enclosure using the set of solvers that have different orders of accuracy.

1 INTRODUCTION

We consider some additional opportunities for analysis of CFD results that may be provided by the abundant set of numerical methods with wide range of orders of approximation, which is available at present.

Usually, the order of approximation of the finite-difference/finite volume scheme is related with the truncation error order. The truncation error δu is obtained via Taylor series decomposition of the discrete operator $A_h u_h = f_h$, which approximates the system of PDE, formally noted herein as $Au = f$. The truncation error dependence on the spatial step h is usually presented as $\delta u = O(h^n)$, where the order n is equal to the minor order of series terms.

The approximation error $\Delta u = u_h - u$ is caused by the truncation error and is of the real practical interest. It may be described by the tangent linear equation $A\Delta u = \delta u$ having the formal solution $\Delta u = A^{-1}\delta u$.

For linear problems, the approximation error $\|\Delta u\| = O(h^n)$ tends to zero as h decreases with the same order n (Lax theorem, [1]) if the discrete operator is well-posed (the inverse operator is uniformly bounded, $\|A_h^{-1}\| < C$).

For the case of nonlinear equations with discontinuities [2,3,4,5], the error order is essentially local and varies significantly depending on the type of flow structure elements. In

2010 Mathematics Subject Classification: 35Q93, 35R30, 94A15.
Key words and Phrases: truncation error, discretization error, ensemble of numerical solutions, distance matrix, Euler equations, exact solution enclosure

this event, the observed order of convergence may be not equal to the nominal order of the approximation error even in the asymptotic range.

Two single-grid based approaches to the discretization error estimation are of interest herein.

A priori error estimation is the common approach to the error analysis and may be expressed in the form $\|\Delta u\| < C \cdot h^n$, which contains unknown constants independent on current numerical solution. A priori error estimation justifies the common practice to stop the mesh refining when the dependence of numerical solution on the step size becomes unobservable. This technique may be used for the proof of the exact solution existence [6] for linear problems.

A posteriori error estimation [7,8,9] has the form $\|\Delta u\| \le C_h e_h$, where C_h is the computable stability constant, which depends on the numerical solution, and e_h is the computable indicator of the truncation error. At present, the most successes in this direction are achieved for elliptic equations and finite element methods starting from the work by Babushka [7]. In most of practical applications the stability constant is not estimated, while the error indicator is used for the mesh adaptation.

The feasibility for rigorous estimations of the exact solution without mesh refinement is the significant merit of this approach. This is another way if compare with the standard mesh refinement approach, the Richardson extrapolation [12,13] and a multigrid approach, presented, for example, by [14].

However, *a posteriori* error estimation may provide more information regarding the exact solution, for example, [10,11]. *A posteriori* check that can be applied to a numerical solution of Navier-Stokes equations to guarantee the existence for the sufficiently smooth solution of the exact problem is considered in [10]. The paper [11] demonstrated for nonlinear elliptic equations that the estimation of the stability constant (inverse operator norm $\|A_h^{-1}\|$) and the residual may be used for the determination of the vicinity of the numerical solution, which contains the exact solution. The results [11] are interpreted as the proof of the existence of the exact nonlinear solution nearby the approximate solution. This information may be of use due to problems with the existence for the compressible multidimensional Euler equations [15]. According [15] the standard weak solution may not exist for the compressible multidimensional Euler equations. The use of the measure-valued solutions (in Young measures), considered in [15], may cause unacceptable computational burden. So, the a posteriori proof of exact solution existence (even local) in the vicinity of the ensemble of numerical solutions may be of practical interest.

We consider a single-grid analysis of another type, if compare with [10,11] herein.

The truncation error δu may be computed by the action of the high order scheme stencil on the precomputed flowfield [16, 17], by the action of the differential operator on the interpolation of the numerical solution [18] or via the differential approximation [19,20]. The practical application of the truncation error δu implies the calculation of the discretization (global) error $\Delta u = A^{-1}\delta u$. The surveys of the global error calculation methods may be found in [21, 22]. In the simplest option, the estimation of this error may be performed using defect correction [16] or nearby equation methods [22,23]. In defect correction frame, the truncation error δu is used as the source term inserted in the discrete algorithm in order to correct the

solution. However, the total subtraction of the error implies the elimination of the scheme viscosity that may cause oscillations in the vicinity of discontinuities or activation of some addition dissipation sources, which engenders their own error. Also, the estimation of the error may be performed via the linearized problem [24], complex differentiation [25] or by adjoint equations [17,18,20,26,27]. Usually, adjoint equations are applied to estimation of the uncertainty of certain valuable functional (drag, lift etc.). Nevertheless, the approach described in [20] enables to estimate the norm of the solution error. Unfortunately, it implies the solution of the number of adjoint problems that is proportional to the number of grid nodes that causes the extremely high computational burden.

The unknown components of truncation error causes the general disadvantage of above discussed residual-based methods for the error estimation. The differential approximation based methods using Taylor series [20] do not account for senior terms of expansion. The postprocessor based methods do not account for the higher scheme truncation errors [17] or the interpolation errors [18].

Herein, the analysis is conducted in the space of numerical solutions, so, the truncation error is accounted implicitly and completely. The feasibility to find the vicinity of the numerical solution that contains an exact solution using the ensemble of calculations performed by the solvers of different approximation order is addressed. In contrast to above mentioned norm oriented approaches, the current analysis is addressed to the ensemble of distances (distance matrix) in different metrics. The Multidimensional Scaling (MDS) [28] concerns similar problems, however, we consider the events when the vector length is much greater the number of vectors, so MDS cannot be applied.

2 EXACT SOLUTION ENCLOSURE VIA THE SET OF NUMERICAL CALCULATIONS WITH RANGED ERRORS

The approximation error is considered herein as the distance between the exact and approximate solutions. Let us consider the ensemble of numerical solutions obtained using finite difference (finite volume) schemes of different order on the same grid. Let the relation of the approximation error of these schemes to be *a priori* known.

We note the numerical solution as the vector $u^{(i)} \in R^N$ (i is the scheme number, N is the number of grid points), values of unknown exact solution at nodes of this grid (further denoted as exact solution) as $\tilde{u} \in R^N$ and use some metrics $d(u,v)$ in the space of solutions. The unknown deviation of exact solution values at grid points $\tilde{u} \in R^N$ from computed solution is estimated using $d(u^{(k)},\tilde{u}) = \delta_{0,k}$ (for example, $d(u^{(k)},\tilde{u}) = \left\| u^{(k)} - \tilde{u} \right\|_{L_2}$). The numerical solutions $u^{(k)}$ are located at surfaces of nested concentric hyperspheres with the centre at $\tilde{u}$ and radii $\delta_{0,k}$.

The following theorem may be stated for two numerical solutions $u^{(1)}$ and $u^{(2)}$ having *a priori* known errors relation $\delta_{0,1} \geq 2 \cdot \delta_{0,2}$.

Theorem 1. *Let the distance $\delta_{1,2}$ between two numerical solutions $u^{(1)} \in R^N$ and $u^{(2)} \in R^N$ be known from computations and there is available a priori information*

$$\delta_{0,1} \geq 2 \cdot \delta_{0,2} \tag{1}$$

then the exact solution is located within the hypersphere of radius $\delta_{1,2}$ *with the centre at* $u^{(2)}$*:*

$$\delta(u^{(2)},\tilde{u}) \le \delta_{1,2} \tag{2}$$

Proof. The analysis is founded on the triangle inequality [29]: $\delta_{ij} \le \delta_{ik} + \delta_{kj}, i \ne j \ne k$. For our problem, (points $u^{(1)}, u^{(2)}, \tilde{u}$ and distances $\delta_{0,1}, \delta_{1,2}, \delta_{0,2}$ between them) it has the form $\delta_{0,1} \le \delta_{1,2} + \delta_{0,2}$, which may be transformed to $\delta_{0,1} - \delta_{0,2} \le \delta_{12}$. By accounting (1) as $\delta_{0,1} - \delta_{0,2} \ge \delta_{0,2}$ one obtains $\delta_{0,2} \le \delta_{0,1} - \delta_{0,2} \le \delta_{12}$ and, finally, the desirable expression $\delta_{0,2} \le \delta_{12}$.

This theorem may be easily stated in L_2 norm, statements in other norms are not straightforward, however, so the general metric based approach is of great advantage. Herein, we usually consider the metrics determined by L_2 and L_1 norm, the metrics of Mahalonobis form [30] is used also in several tests.

3 THE ANALYSIS OF THE ERROR RELATIONS FOR AN ENSEMBLE OF CALCULATIONS

The evident weakness of the *Theorem 1* is the assumption of the existence of solutions with *a priori* ranged error. Despite the widespread opinion that the schemes of higher order are more accurate, it should be checked numerically. Herein, we consider some options for the check of error rating. The collection of distances between solutions $\delta_{i,j}$ enables a detection of the close and distant solutions. For example, if $\delta_{0,1} >> \delta_{0,i}$, the set $\delta_{i,j}$ is split into a cluster of inaccurate solutions with great values $\delta_{1,j}$ and the cluster of more accurate solutions $\delta_{i,j}(i \ne 1)$. It is caused by the asymptotics $\delta_{1,j}/\delta_{0,1} \to 1$ and $\delta_{i,j}(i \ne 1)/\delta_{0,1} \sim (\delta_{0,i} + \delta_{0,j})/\delta_{0,1} \to 0$ at $\delta_{0,i}/\delta_{0,1} \to 0$.

The separation of the collection of distances between solutions into clusters is the evidence of the existence of solutions with significantly different errors that may be considered as a proof of error ranging. The quantitative criterion based on dimension of clusters and the distance between them is of interest. Let us compare the set of distances $\delta_{1,j}$ and $\delta_{k,j}$, where $u^{(1)}$ is maximally incorrect solution and $u^{(k)}$ is the selected accurate solution (the localization of exact solution is performed in its vicinity), $\delta_{i,\max}$ is the maximum error in the subset of accurate solutions.

We state the following heuristical criterion ***(Conjecture 1)***:

The exact solution may be enclosed if the distance between clusters is greater the size of the cluster of accurate solutions. Then the condition (1) is valid and the exact solution is located within a hypersphere of radius $\delta_{i,k}$ *with the center at* $u^{(i)}: \delta_{0,i} \le \delta_{i,k}$*, where* $u^{(i)}$ *belongs to the cluster of more accurate solutions and* $u^{(k)}$ *is maximally inaccurate solution.*

This conjecture is based on the assumptions that the dimension of the accurate cluster to be $r_{i,\max} + r_k$, and a cluster of inaccurate solutions belongs the interval $(\delta_{0,1} - \delta_{i,\max}, \delta_{0,1} + \delta_{i,\max})$,

the relation of accurate cluster dimension and the distance between clusters has an appearance $\delta_{0,1} - 2\delta_{i,\max} - \delta_{i,k} > \delta_{i,\max} + \delta_{i,k}$. This leads to the relation $\delta_{0,1} > 2\delta_{0,k}$, that corresponds condition (1).

This criterion may be rigorous only in the limit of the infinite set of solutions obtained by independent methods. Nevertheless, most numerical tests for two dimensional supersonic inviscid flows confirm the applicability of this heuristic criterion. The violation of the enclosure condition $\left\| \tilde{u} - u^{(i)} \right\|_{L_2} \le \left\| du_{i,k} \right\|_{L_2}$ above 15% was not observed.

4 THE SELECTION OF METRICS

The vector of solution for CFD problems contains elements having different physical meanings, such as density, velocity components, energy, etc. Herein, we consider two dimensional Euler equations with four component $u^{(i)} = \{\rho^{(i)}, U^{(i)}, V^{(i)}, E^{(i)}\}$. We consider the metrics engendered by the simplest L_1 and L_2 norms.

The norm

$$\left\| u^{(i)} - u^{(k)} \right\|_{L_2} = \left\| \{(\rho^{(i)} - \rho^{(k)}), (U^{(i)} - U^{(k)}), (V^{(i)} - V^{(k)}), (e^{(i)} - e^{(k)})\} \right\|_{L_2} \tag{3}$$

enables to calculate the distance between solutions. In parallel to Expression (3), the distance between solutions was calculated using the expression

$$\left\| \{(\rho^{(i)} - \rho^{(k)}) / \left\| \rho^{(i)} \right\|, (U^{(i)} - U^{(k)}) / \left\| U^{(i)} \right\|, (V^{(i)} - V^{(k)}) / \left\| V^{(i)} \right\|, (e^{(i)} - e^{(k)}) / \left\| e^{(i)} \right\|\} \right\|_{L_2}, \tag{4}$$

which imitates a relative error.

It should be noted that expression (4) corresponds not to the norm but to the distance $(\Delta u^{(i)}, M\Delta u^{(i)}) = (M_{j,k} \Delta u_j^{(i)} \Delta u_k^{(i)})^{1/2}$. This distance is determined by a metric tensor with the matrix $M_{j,k}$ of the diagonal form that describes some ellipsoid. With account of the presentation $M = A^* A$ (valid for a metric tensor as the symmetric positively defined matrix, a Mahalanobis distance metric [30]) one can state $(\Delta u^{(i)}, M\Delta u^{(i)}) = (\Delta u^{(i)}, A^* A \Delta u^{(i)})^{1/2} = (A\Delta u^{(i)}, A\Delta u^{(i)})^{1/2} = (\Delta z^{(i)}, \Delta z^{(i)})^{1/2}$. So, we can enclosure the solution in the transformed space $Au^{(i)}$, where the error may have the form of hypersphere.

The search for more complicated metrics, having some physical meaning and illustrative capabilities, is of interest also. The suitable metrics should not compare different variables, i.e. the matrix should have block-diagonal form with blocks related to different variables. It would be useful, if small flowfield deformations (shift by single step of grid, for example) corresponds small distances. So, the comparison of variables at adjacent grid nodes may be of use, i.e. blocks may have a band form.

5 NUMERICAL TESTS

The tests of the exact solution enclosure are presented below for flows governed by two dimensional unsteady Euler equations.

$$\frac{\partial \rho}{\partial t} + \frac{\partial \left(\rho U^k \right)}{\partial x^k} = 0; \tag{5}$$

$$\frac{\partial \left(\rho U^i \right)}{\partial t} + \frac{\partial \left(\rho U^k U^i + P \delta_{ik} \right)}{\partial x^k} = 0; \tag{6}$$

$$\frac{\partial (\rho E)}{\partial t} + \frac{\partial \left(\rho U^k h_0 \right)}{\partial x^k} = 0; \tag{7}$$

The elementary structures such as the single oblique shock wave, the interaction of shock waves of I and VI kinds according Edney classification [31] were used as the test problems. All tests concern the steady state solutions. The analytical solution may be easily constructed for these problems. The values of analytical solution at grid points is considered herein as "exact" solution. The flowfield contains undisturbed domains (nominal order of error is expected), shock waves (error order about $n = 1$ [5]), contact discontinuity line (error order about $n = 1/2$, [4]). In result, one may hope to obtain the nontrivial error composed of components with different orders of accuracy. The estimation of this error and the capture of exact solution in certain hypersphere around a numerical solution are the main purposes of the paper.

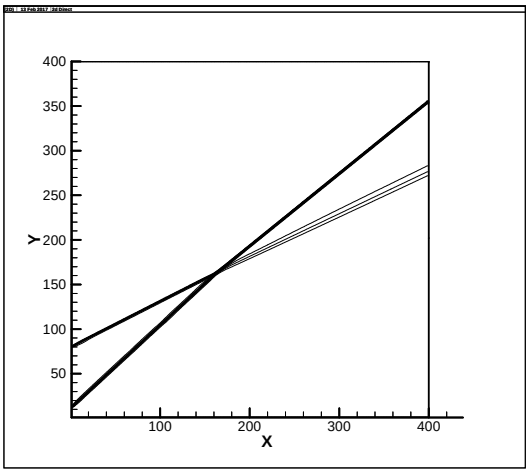

Fig. 1. Edney VI density isolines.

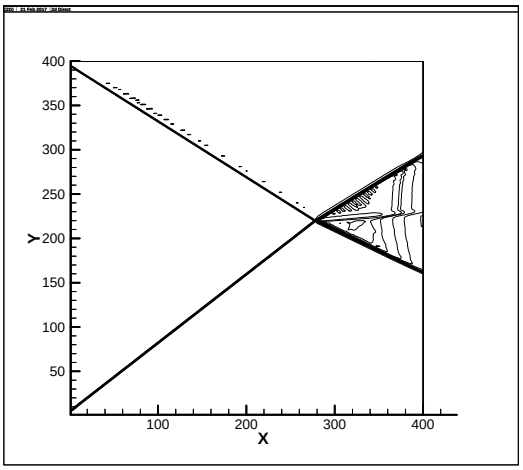

Fig. 2. Edney I density isolines.

The computations were performed for $C_p / C_v = 1.4$, Mach number range $M = 3 \div 5$ and flow deflection angles range $\alpha = 10 - 30^o$. All tests contain discontinuities in the flow field. Fig. 1 presents the density distribution for Edney VI flow structure ($M = 4$, two consequent flow deflection angles $\alpha_1 = 10^o$, $\alpha_2 = 15^o$). The flow is determined by the merging shock waves, the contact line and the expansion fan. Fig. 2 presents the density isolines for Edney I flow structure ($M = 3$ and flow deflection angles $\alpha_1 = 20^o$ and $\alpha_2 = 15^o$). The crossing shock waves and contact discontinuity line, engendered at the shocks crossing point, are the main elements of this flow structure.

The paper presents the analysis of the ensemble of computations performed by methods listed below.

The first order scheme by Courant Isaacson Rees [32] designated as $S1$ was used in the variant described by [33].

The second order scheme based on the MUSCL method [34] and using algorithm by [35] at cell boundaries is noted as $S2$.

Second order TVD scheme of relaxation type by [36], noted as $S2TVD$.

Third order modified Chakravarthy-Osher scheme [37, 38] marked as $S3$.

Fourth order scheme by [39] marked as $S4$.

Computations were performed on uniform grids containing 100×100, 200×200 or 400×400 nodes. The vector of solution of Eq. (5-7) contains four components $u^{(i)}=\{\rho^{(i)},U^{(i)},V^{(i)},E^{(i)}\}$ having different physical meanings and different magnitudes. For example, for Edney VI flow (Fig.2) the norms of component are $\left\|\rho^{(i)}\right\|_{L_2}\approx2.5$, $\left\|U^{(i)}\right\|_{L_2}\approx0.87$, $\left\|V^{(i)}\right\|_{L_2}\approx0.24$, $\left\|e^{(i)}\right\|_{L_2}\approx0.17$, herein

$$\left\|\Delta u\right\|_{L_2}=\left(\frac{1}{N}\left(\sum\Delta\rho_i^2+\sum\Delta U_i^2+\ldots\right)\right)^{1/2}, \tag{8}$$

$$\left\|\Delta u\right\|_{L_1}=\frac{1}{N}\left(\sum\left|\Delta\rho_i\right|+\sum\left|\Delta U_i\right|+\ldots\right). \tag{9}$$

The data under the consideration are extremely bulky, so for convenience of visualization, in Fig. 3-9 the norm of error is marked up along both axes, despite the data are one dimensional.

For the level of error less 0.1 the solutions visually can not be distinguished. The only visually distinguishable solution corresponds the scheme $S1$ (level of error about 0.2) and is specified by high smearing of shock waves. The level of error about 0.1 (400×400) may be related with the shift of incident shock location by a single node.

It should be noted that methods $S1,S2,S3,S4$ (1,2,3 and 4 nominal truncation orders) demonstrated the order of convergence a bit below $n=1/2$ in norm L_2. In norm L_1 the same computations demonstrated the order of convergence a bit higher $n=1/2$. The method S2TVD (nominal order 2) is the only exception with the order about $n\sim3/4$.

In numerical tests, we first check *Conjecture 1* and, second, verify the enclosure. We consider the enclosure to be successful, if the error estimate $\left\|u^{(i)}-u^{(k)}\right\|_{L_2}$ is greater the true error $\left\|u^{(k)}-\widetilde{u}\right\|_{L_2}$, obtained in comparison with the analytical solution $\widetilde{u}$.

The comparison with the analytical solution permits to conclude that using the scheme $S1$ (as “inaccurate”) and schemes $S2$, $S3$, $S4$ (as “accurate”) enables to find the vicinity of numerical solution that contains exact solution.

Second order $S2TVD$ scheme [36] from standpoint of error norm is close to first order scheme $S1$ for 100×100 grid and to high order schemes for grid 400×400. When the clusters are detected, it also enables the enclosure of solutions generated by $S2, S3, S4$. If the clusters are not available, the exact solution is not enclosed. The calculations on the grid 100×100 demonstrated the formation of clusters with "inaccurate" scheme $S2TVD$ and successful enclosure of the exact solution. However, the scheme $S2TVD$ on the grid 400×400 does not form clusters. Paradoxically, the reason for this failure is the relatively rapid convergence of $S2TVD$ in comparison with schemes $S2a, S2c, S3, S4$. In result, the scheme $S2TVD$ on the grid 400×400 transfers from "inaccurate" to "accurate" schemes approaching in error to $S2, S3, S4$.

The comparison of schemes $S2, S3, S4$ ($\left\|u^{(2)}-u^{(4)}\right\|_{L_2}$, $\left\|u^{(3)}-u^{(4)}\right\|_{L_2}$, $\left\|u^{(3)}-u^{(2)}\right\|_{L_2}$) does not enable to enclose the exact solution. Similarly, the enclosure of exact solution by pair $S2TVD, S1$ fails. These schemes have the errors which are close in magnitude and splitting into clusters is not observed.

If the *Conjecture 1* is not satisfied (there are no clusters, or distance between them is less the dimension of the cluster of "accurate" solutions) the enclosure of true solution fails. However, the exact error is about two or three maximum distances between numerical solutions.

The numerical tests for the single oblique shock demonstrate the feasibility for the exact solution enclosure at the significant distance between clusters, if splitting occurs. However, the set of distances between solutions separates into clusters in about half of tests, usually for more fine meshes.

For Edney-VI shock interaction (Fig. 1), the set of distances between solutions also splits into clusters in about half of tests without dependence on the grid size. There is the enclosure of exact solution according expression (3), for the distance between clusters, which approximately equals the dimension of the cluster.

Fig. 3 (with "inaccurate" scheme $S1$, L_2, grid 400×400) demonstrates the collection of distances between numerical solutions $\left\|du_{i,k}\right\|_{L_2}=\left\|u^{(i)}-u^{(k)}\right\|_{L_2}$ to break into two clusters, one of them is related with the "inaccurate" scheme. It enables to enclose an exact solution. Fig. 4 presents results of L_2 error enclosure based on clusters presented in Fig. 3. The norm L_1 presents the same results as L_2 for this test, Fig. 5.

For Edney-I shock interaction (Fig. 2), the set of distances between solutions splits by clusters in about half of tests, usually for more fine meshes. For the distance between clusters, which approximately equals the dimension of the cluster, the enclosure of exact solution for metrics engendered by L_2, L_1 fails, see Figs 6,7.

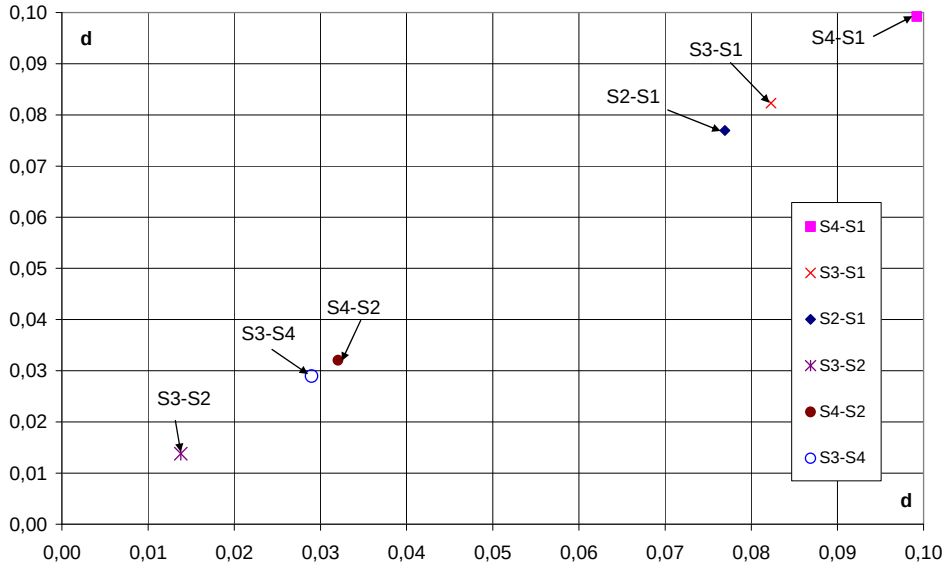

Fig. 3. Clusters related with "inaccurate" scheme S1 for Edney-VI in L_2, grid 400×400.

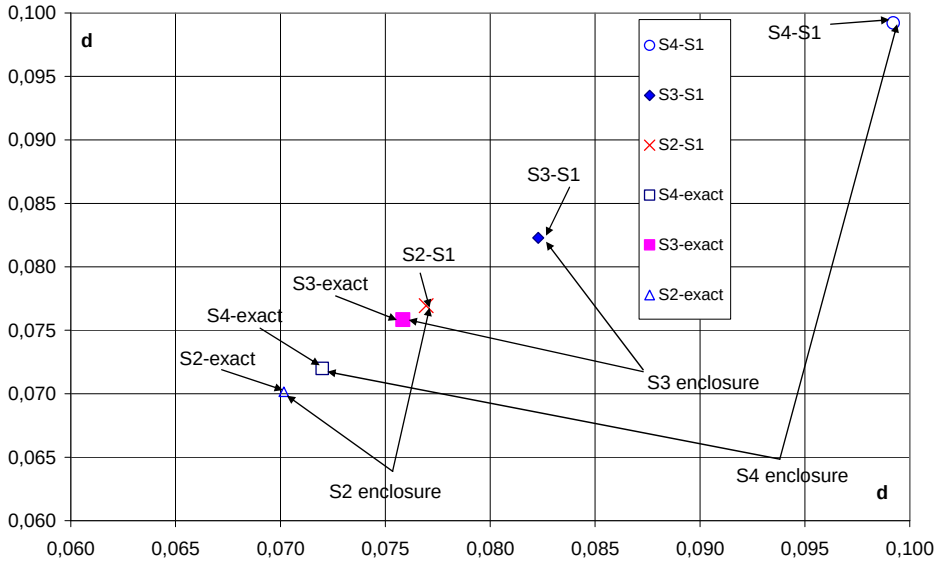

Fig. 4. Exact solution enclosure (Edney-VI) in vicinity of S2, S3, S4 using S1, L_2, grid 400×400.

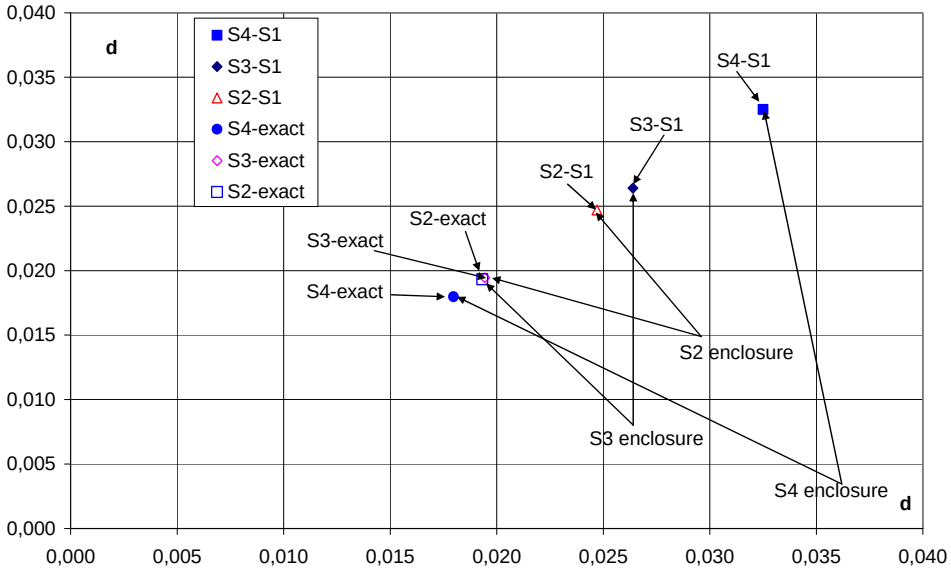

Fig. 5. Exact solution enclosure (Edney-VI) in vicinity of S2, S3, S4 using L_1 norm, grid 400×400.

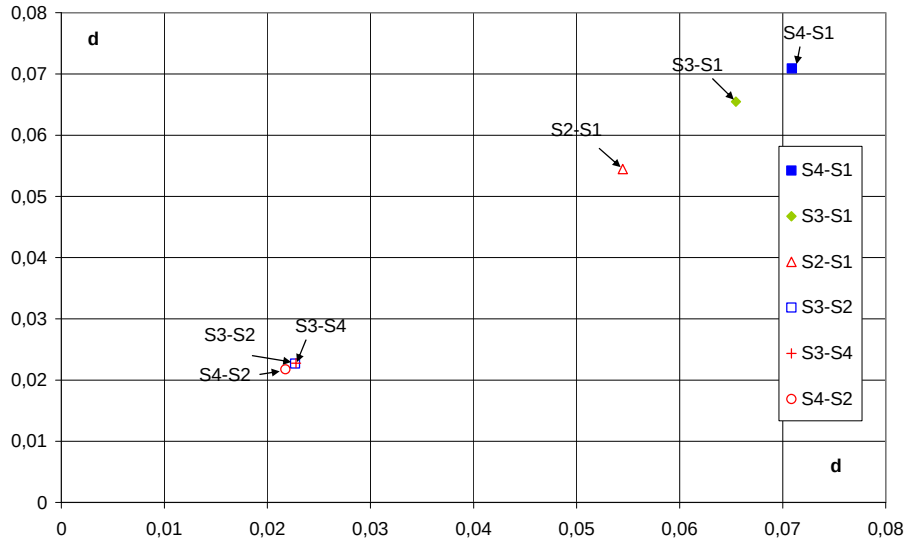

Fig. 6. Clusters related with S1 for Edney-I, L_2, grid 400×400.

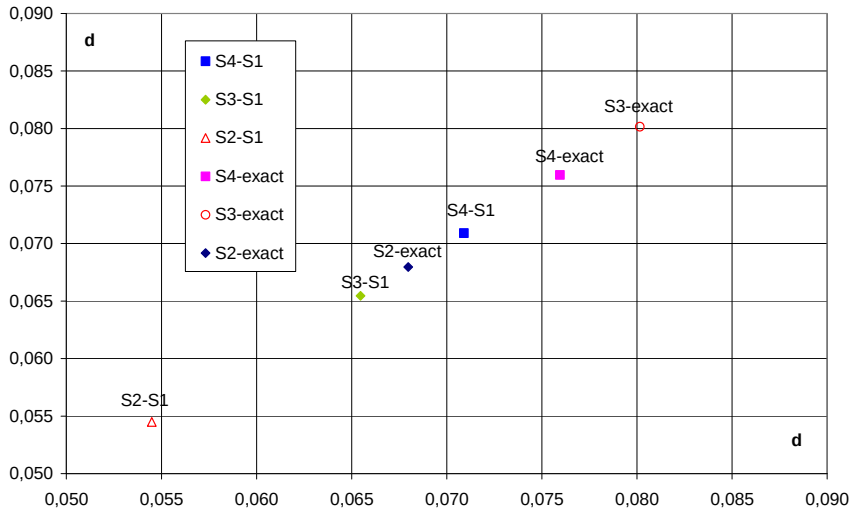

Fig. 7. Exact solution enclosure (Edney-I) in vicinity of S2, S3, S4 using S1, L_2, grid 400×400.

The results are obtained for $M = 3$ and flow deflection angles $\alpha_1 = 20^o$ and $\alpha_2 = 15^o$. The magnitude of capture condition $\left\| \tilde{u} - u^{(2)} \right\|_{L_2} \le \left\| du_{1,2} \right\|_{L_2}$ violation is about 10%. This demonstrates the heuristical, approximate nature of *Conjecture 1*. However, the violation of the enclosure condition is moderate.

The metrics (4) related with relative error enables an more reliable enclosure, Figs. 8,9.

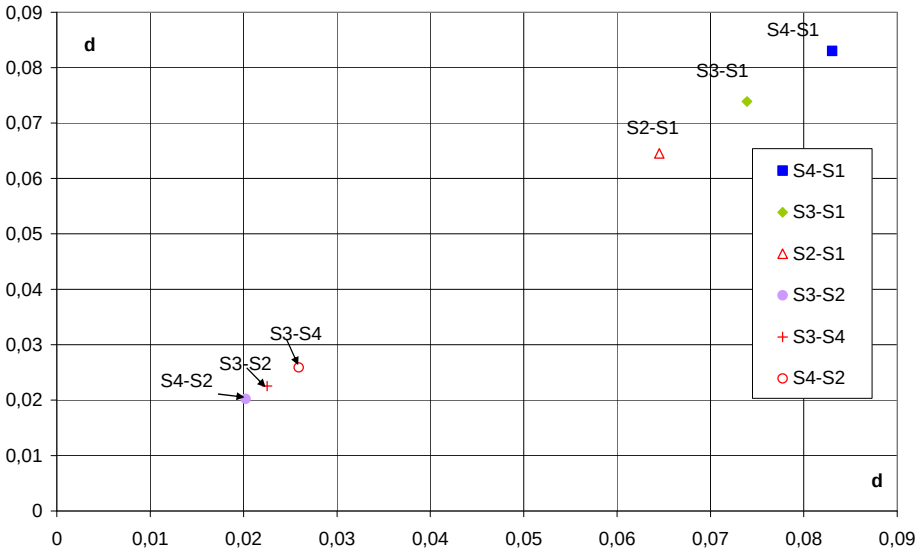

Fig. 8. Clusters related with S1 for Edney-I, grid 400×400.

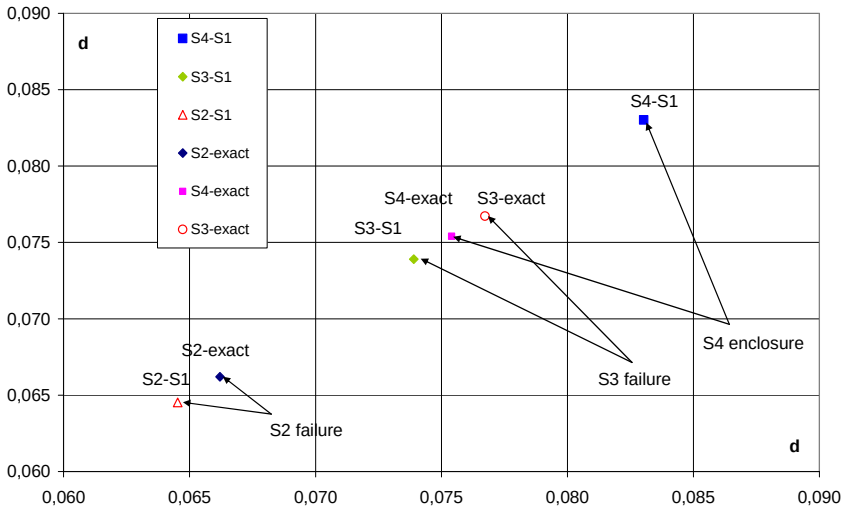

Fig. 9. Exact solution enclosure (Edney-I) in vicinity of S2, S3, S4 using S1, grid 400×400.

Figs. 6-9 demonstrate the visible dependence of the enclosure success on the metrics that is used for the distances calculation.

Thus, in order to enclosure the exact solutions, one should have a priori information *(Theorem 1*) or an ensemble of minimum three solutions with distances split into two clusters. The distance between clusters should be greater the dimension of cluster of more accurate solutions *(Conjecture 1).*

6 DISCUSSION

The relation of errors obtained in the paper is not necessarily attributed to properties of the considered schemes. In the strict sense, it may be caused by the imperfections of numerical realization by authors. So, authors do not pretend on the definitive assessment of considered methods. We only can compare solvers (algorithms realizations) from the viewpoint of numerical results.

The standard check of the grid convergence is based on heuristic rule by C. Runge [9]. From this standpoint, if the difference of two approximate solutions on coarse grid T_h with step h and on the fine grid $T_{h,ref}$ with step h_{ref} is small, then $u_{h,ref}$ and u_h are ***probably*** close to exact solution. From practical needs, one should desire the estimate of the form $\|u_h - \tilde{u}\| \le \delta$ with computable δ**.** The Richardson method [12,13,22] is close to this ideal. It enables to determine the refined solution and the error estimate if the single error order exists in total flowfield. The set of solutions $u_k^{(1)} = \tilde{u}_k + C_k h_1^n$, $u_k^{(2)} = \tilde{u}_k + C_k h_2^n \ldots$ computed on different meshes is used. Unfortunately, in most CFD problems the error order on different flow structures varies that hampers or prohibits the application of the Richardson method.

The present paper concerns a single-grid alternative to the Richardson method and Runge rule. The set of solutions is collected at the same mesh using different methods. Calculations may be terminated if a preassigned error level $\delta(u_h, \tilde{u}) \le \delta$ ($\|u_h - \tilde{u}\| \le \delta$) is achieved.

The existence of “accurate” and “inaccurate” schemes is one of the main postulates of computational mathematics, although having an asymptotic sense. The above results demonstrate the feasibility to distinguish “accurate” and “inaccurate” schemes in the sense of error norm ranging. For the events presented on Figs. 3, 5 the distribution of distances between solutions $\left\| du_{i,j} \right\|_{L_2}$ shows the presence of two clusters corresponding “accurate” and “inaccurate” schemes. This engenders the hope to enclose the exact solution only from observable $\left\| du_{i,j} \right\|_{L_2}$ (without a priori information on errors ranging), that is confirmed by Figs. 4,6,7. If clusters cannot be detected, the exact solution enclosure fails.

The feasibility to estimate the distance from the exact solution to numerical one $\delta(u_h, \tilde{u}) \le \delta$ seems attractive, however, it is difficult to define at what magnitude of δ two solutions can be considered as coinciding (the calculations may be stopped) or describing different flows.

The estimation of uncertainty of certain valuable functionals (drag, lift etc.) is of interest in most of applications. This estimation may be performed using adjoint equations [17,18,20,26,27], nevertheless, it does not describe the flowfield in unique way.

The ensemble based method operates the total error including flowfield error, initial and boundary condition error and round-off errors. It may be used as a postprocessor similar to Richardson extrapolation [12,13,22]. However, it does not need the mesh refinement and may be used away the asymptotic range.

The dependence on the set of numerical methods and analyzed solution is the drawback of ensemble based method. The same set of methods may provide segregation by clusters on one flow pattern and may not provide on another. So, this approach cannot replace the standard accuracy control method (mesh refining) and is assigned to supplement it by non-expensive algorithm.

If there is no breaking into clusters, the distance between numerical solutions and analytical ones is 2-3 times greater the maximum distance between solutions that provide some opportunity for the rough estimation of numerical error.

So, it is feasible to obtain the information on the numerical error and exact solution location using the collection of solution obtained on the same grid by different solvers without mesh refinement.

7 CONCLUSIONS

The information on distances between numerical solutions in some metrics enables the enclosure of the exact solution and the estimation of the discretization error in this metrics.

If two numerical solutions with the discretization error relating twice or more in some metrics are available, the exact solution is located in the hypersphere with the centre at the more accurate solution and with the radius, which equals the distance between solutions.

If there is no *a priori* information on error ranging, the enclosure of the exact solution is feasible if the collection of solutions is available and it is split into separated clusters corresponding “accurate” and “inaccurate” schemes. The distance between clusters should be greater the dimension of "accurate" cluster.

The numerical tests confirmed the efficiency of this heuristic rule in metrics corresponding L_2 and L_1 norms for two dimensional supersonic problems governed by Euler equations. The

success of the enclosure is sensitive to the choice of the metric. The metrics, engendered by the norm, which imitate the relative error, provide an opportunity to enclosure the exact solution in certain events when L_2 and L_1 based enclosure fails. For nonlinear problems, the estimation of the vicinity of the numerical solution, which contains the exact solution, may be interpreted as the proof of the existence of the exact solution nearby the approximate solution.

Acknowledgements

Authors acknowledge the partial support by grants of RFBR № 16-01-00553A and № 17-01-00444A.

REFERENCES

[1] R.D. Richtmyer and K.W. Morton, *Difference Methods for Initial Value Problems, John Wiley and Sons*, NY (1967).

[2] N.N. Kuznetsov, "Accuracy of some approximate methods for computing the weak solutions of a first-order quasi-linear equation", *USSR Comp. Math. and Math. Phys.*, **16**, 105-119 (1976).

[3] T. Tang and Z.H. Teng, "The sharpness of Kuznetsov's $O(\sqrt{\Delta x})$ L^1 error estimate for monotone difference schemes", *Math.Comput.*, **64**, 581-589 (1995).

[4] J.W. Banks, T. Aslam, and W.J. Rider, "On Sub-linear Convergence for Linearly Degenerate Waves in Capturing Schemes", *JCP*, **227**, 6985-7002 (2008).

[5] M.H. Carpenter and J.H. Casper, "Accuracy of Shock Capturing in Two spatial Dimensions", *AIAA J*, **37** (9), 1072-1079 (1999).

[6] O.A. Ladyzhenskaya, "The Boundary Value Problems of Mathematical Physics", *Applied Mathematical Sciences*, *Springer*, **49,** 1-43 (1985).

[7] I. Babushka and W. Rheinboldt, "A Posteriori error estimates for the finite element method", *Int. J. Numer. Methods Eng.*, **12**, 1597–1615 (1978).

[8] I. Babushka and A.D. Miller, "The post-processing approach in the finite element method, III", "A Posteriori error estimation and adaptive mesh selection", *Int. J. Numer. Meth. Eng.*, **20**, 2311–2324 (1984).

[9] S.I. Repin, *A Posteriori estimates for partial differential equations*, 4, Walter de Gruyter, Berlin-New York, (2008).

[10] S.I. Chernyshenko, P. Constantin, J.C. Robinson, E.S. Titi, "A Posteriori regularity of the three-dimensional Navier-Stokes equations from numerical computations", *J. of Mathematical Physics*, **48**, 065204 (2007).

[11] C. Ortner, "A Posteriori Existence in Numerical Computations", *SIAM Journal on Numerical Analysis*, **47**(4), 2550-2577 (2009).

[12] G.I. Marchuk and V.V. Shaidurov, *Difference methods and their extrapolations*, Springer, N.Y. (1983).

[13] Z. Zlatev, I. Dimov, I. Farago, K. Georgiev, A. Havasic, T. Ostromsky, "Application of Richardson extrapolation for multi-dimensional advection equations", *Computers and Mathematics with Applications*, **67**, 2279–2293 (2014).

[14] O.B. Feodoritova, N.D. Novikova, V.T. Zhukov, "Multigrid method for diffusion equations based on adaptive smoothing", *Mathematica Montisnigri*, **XXXVI,** 14-26 (2016).

[15] U.S. Fjordholm, S. Mishra, E. Tadmor, "On the computation of measure-valued solutions", *Acta Numerica*, 567–679 (2016).

[16] T. Linss and N. Kopteva, "A Posteriori Error Estimation for a Defect-Correction Method Applied to Convection-Diffusion Problems", *Int. J. of Numerical Analysis and Modeling*, **1** (1), 1–16, (2009).

[17] A.K. Alekseev, I.M. Navon, "A Posteriori Error Estimation by Postprocessor Independent of

Flowfield Calculation Method", *Computers & Mathematics with Applications*, **51**, 397-404 (2006).
[18] M.B. Giles and E. Suli, "Adjoint methods for PDEs: a posteriori error analysis and postprocessing by duality", *Acta numerica*, 145-206 (2002).
[19] Yu.I. Shokin, *Method of differential approximation*, Springer-Verlag, (1983).
[20] A.K. Alekseev, I.M. Navon, "Adjoint Correction and Bounding of Error Using Lagrange Form of Truncation Term", *Computers & Mathematics with Applications*, **50** (8-9), 1311-1332 (2005).
[21] R.D. Skeel, "Thirteen ways to estimate global error", *Numer. Math*., **48,** 1-20 (1986).
[22] C.J. Roy, "Review of Discretization Error Estimators in Scientific Computing", *48-th AIAA,* 126, 1-29 (2010).
[23] Ch.J. Roy, and A. Raju, "Estimation of Discretization Errors Using the Method of Nearby Problems", *AIAA J.*, **45** (6), 1232-1243 (2007).
[24] T.S. Phillips and Ch.J. Roy, "Residual Methods for Discretization Error Estimation", *AIAA*, Paper 2011-3870, 1-18 (2011).
[25] E.J. Nielsen and W. L. Kleb, "Efficient construction of discrete adjoint operators on unstructured grids using complex variables", *AIAA J.*, **44** (4), 827–836 (2006).
[26] J.T. Oden and S. Prudhomme, "Estimation of modeling error in computational mechanics", *Journal of Computational Physics*, **182**, 496-515 (2002).
[27] A.K. Alexeev, A.E. Bondarev, "On Important Information Dynamics", *Mathematica Montisnigri*, **XXXV**, 68-89 (2016).
[28] W.S. Torgerson, "Multidimensional Scaling: Theory and Method", *Psychometrika*, **17**, 401-419, (1952).
[29] D. Burago, Yu. D. Burago, S. Ivanov, *A Course in Metric Geometry*, AMS, (2001).
[30] P.Ch. Mahalanobis, "On the generalised distance in statistics", *Proceedings of the National Institute of Sciences of India*, **2** (1), 49–55 (1936).
[31] B. Edney, "Anomalous Heat Transfer and Pressure Distributions on Blunt Bodies at Hypersonic Speeds in the Presence of an Impinging Shock", *FAA Report 115, Aeronautical Research Institute of Sweden*, (1968).
[32] R. Courant, E. Isaacson, M. Rees, "On the Solution of Nonlinear Hyperbolic Differential Equations by Finite Differences", *Comm. Pure Appl. Math.*, **5**, 243-255 (1952).
[33] A.G. Kulikovskii, N.V. Pogorelov, and A.Yu. Semenov, *Mathematical Aspects of Numerical Solution of Hyperbolic Systems*, Monographs and Surveys in Pure and Applied Mathematics, **188**, Chapman&Hall/CRC, Boca Raton, Fl, (2001).
[34] B. Van Leer, "Towards the ultimate conservative difference scheme. V. A second-order sequel to Godunov's method", *J. Comput. Phys.*, **32**, 101–136 (1979).
[35] M. Sun, K. Katayama, "An artificially upstream flux vector splitting for the Euler equations", *JCP*, **189**, 305-329 (2003).
[36] Hy Trac, Ue-Li Pen, "A Primer on Eulerian Computational Fluid Dynamics for Astrophysics", arXiv:astro-ph/0210611, **2**, 1-23 (2002).
[37] S. Osher, S. Chakravarthy, "Very high order accurate TVD schemes", *ICASE Report*, **84** (144), 229–274 (1984).
[38] C.-T. Lin et al, "High resolution finite volume scheme for the quantum hydrodynamic equations", JCP, **228** (5), (2009).
[39] S. Yamamoto, H. Daiguji, "Higher-order-accurate upwind schemes for solving the compressible Euler and Navier-Stokes equations", *Computers and Fluids*, **22**, 259-270 (1993).

Received January 15, 2017.

MOLECULAR DYNAMICS MODELING OF NANOSECOND LASER ABLATION: TRANSCRITICAL REGIME

ALEXANDER A. SAMOKHIN[1], VLADIMIR I. MAZHUKIN[2,3], ALEXANDER V. SHAPRANOV[2,3], MIKHAIL M. DEMIN[2], ALEXEY E. ZUBKO[1]

[1]A.M. Prokhorov General Physics Institute, RAS, Moscow, Russia
e-mail: asam40@mail.ru, web page: http://www.gpi.ru/eng/

[2]Keldysh Institute of Applied Mathematics, RAS, Moscow, Russia
e-mail: vim@modhef.ru, web page: http://www.keldysh.ru/

[3]National Research Nuclear University "MEPhI", Moscow, Russia
web page: https://mephi.ru/eng/

Summary. Nanosecond laser ablation regime is investigated for the case of thin liquid Al film heated with constant radiation with intensities of G = 44, 66 and 110 MW/cm^2. The film dimensions are $x\times y\times z$ = 448.7×37.3×37.3 nm^3 with periodical boundary conditions in y-z directions. For G = 44 MW/cm^2, six consequent explosions can be discerned (including one on the film back side) and at later times $t \geq 4700$ ps, the film disintegrates into multiple fragments. For higher intensities the ablation regime resembles explosive boiling process only at small times (~ 400 ps) for G = 66 MW/cm^2 while at later times the ablation process is smooth even at subcritical temperature and pressure values. For G = 110 MW/cm^2, the ablation regime is smooth for all considered times (~ 1000 ps) while temperature and pressure in the film surpass its critical values (T_C = 7630 K, P_C = 1415 bar) approximately at t = 700 ps.

1 INTRODUCTION

Explosive boiling during nanosecond laser ablation was considered in several recent papers [1-5] as well as in many other papers during about the last half a century. Some additional references can be found e.g. in [6-9]. Despite the long investigation history the explosive boiling problem is not completely clarified yet because, in particular, usual continual approach [7] is not sufficient for detailed description of liquid-vapor phase transition in highly nonequilibrium conditions when irradiated matter is in strongly superheated state.

It should be noted also that homogeneous nucleation theory used for describing explosive boiling process in many papers (see e.g. [1-5,8] and ref. therein) is not applicable for the highly nonequilibrium conditions when the arising bubbles can not be considered as independent ones. Probably for this reason in the papers [1-5,8] devoted to explosive boiling no sufficient (if any) information is given about the pressure behavior in the process. More straightforward and adequate approach to the explosive boiling problem during laser ablation can be realized in the framework of molecular dynamic calculations.

Theoretical analysis of the nanosecond laser ablation was carried out with the help of molecular modeling [10-13] for thin metal films $x\times y\times z$ = 430×6.2×6.2 nm^3 with periodically boundary conditions in y-z directions. For different ablation regimes (surface evaporation,

2010 Mathematics Subject Classification: 82D15, 82D35, 82D80.
Key words and Phrases: Evaporation, Explosive boiling, Critical Point, Molecular Dynamics.

explosive boiling, spinodal decomposition, supercritical fluid expansion) were found for constant laser intensity G = 38.5-154 MW/cm^2.

In ref. [6] similar molecular dynamic calculations was performed for G = 33 MW/cm^2 for bigger sample $x\times y\times z$ = 448.7×37.3×37.3 nm^3. It was shown that the surface evaporation regime at early times than changes to explosive boiling process at the moments t = 1740, 2655, 4545 and 4995 ps. The results qualitatively confirm previous conclusion obtained for the sample with smaller y-z periodical dimensions [10] where for G = 38.5 MW/cm2 similar explosive boiling occur at t = 1040, 1440, 1640, 2000, 2340 ps. Bigger space-dimensions and irradiated time duration considered in the present paper permit to observe more space-time inhomogeneities of the ablation process compared with the smaller sample. In the present paper, nanosecond laser ablation regime is investigated for G = 44, 66 and 110 MW/cm^2.

2 STATEMENT OF THE PROBLEM

Laser radiation propagates from right to left and is normally incident on the free surface of the film. Computational domain dimensions are 1700×37.3×37.3 nm^3 with periodical boundary conditions in y-z directions. It contains part of the film with dimensions $x\times y\times z$ = 448.7×37.3×37.3 nm^3 (17.87 millions of atoms). Part of the radiation is absorbed by the electronic components, and as a result of inelastic collisions is transferred to the ion subsystem. By using periodic boundary conditions in the directions Y, Z the problem is effectively reduced to one-dimensional approximation along the X direction (for transport processes of laser radiation and energy into electronic subsystem).

Combined TTM-MD [14] model is used to describe the processes.

Energy balance of electron subsystem is described by continuum energy equation (1) supplemented by the equation of laser radiation transfer (2):

$$\frac{\partial \varepsilon_e}{\partial t} = -\left(\frac{\partial W_e}{\partial x} + g(T_e)(T_e - T_i) + \frac{\partial G}{\partial x} \right) \tag{1}$$

$$\frac{\partial G}{\partial x} + \alpha G = 0 \tag{2}$$

Here ε_e is the volume density of electron energy, T_e, T_i are the electron and ion temperatures, $g(T_e)$ is the electron-ion coupling coefficient, G is the intensity of laser radiation in the medium, $\alpha = \alpha(T_e, n_e)$ is the coefficient of absorption of laser radiation, $W_e = -\lambda_e \dfrac{\partial T_e}{\partial x}$ is the heat flux, $\lambda_e(T_e, T_i)$ is the electron heat conductivity coefficient.

The energy balance equation of the electron subsystem (1) was solved in the condensed medium using the finite-difference method. Zero heat flux $W_e = 0$ was used as a boundary condition at the surface of the film and its fragments.

The connection between electron energy and temperature was obtained using approximation via Fermi integrals [15].

3D molecular-dynamic modeling was used to describe the ion motion:

$$\begin{cases} \dfrac{d\vec{r}_j}{dt} = \vec{\upsilon}_j \\ m_j \dfrac{d\vec{\upsilon}_j}{dt} = \vec{F}_j^{emb} + \vec{F}_j^{heat} \end{cases} \qquad (3)$$
$$j = 1 \ldots N$$

Here $m_j, \vec{r}_j, \vec{\upsilon}_j$ are the mass, radius-vector and velocity of j-th ion respectively, $\vec{F}_j^{emb} = -\dfrac{\partial U(\vec{r}_1 \ldots \vec{r}_N)}{\partial \vec{r}_j}$ is the force acting at the j-th ion from other ions, $U(\vec{r}_1 \ldots \vec{r}_N)$ is the interaction potential for which embedded atom model (EAM) potential [16] was chosen. The energy transfer from the electron subsystem to the ion is given by:

$$\vec{F}_j^{heat} = \frac{m_j(\vec{\upsilon}_j - \langle\vec{\upsilon}\rangle)}{3k_B T_i n_i} g(T_e)(T_e - T_i), \qquad (4)$$

where $\langle\vec{\upsilon}\rangle$ is the mean ion velocity in the neighborhood of the j-th ion.

At the initial time $t = 0$ the film was assumed to be heated to the temperature of 6340K, electron and ion subsystems are in thermal equilibrium.

3 RESULTS AND DISCUSSION

Increasing of radiation intensity to G = 44 MW/cm^2 does not change significantly the initial stage of film heating and vaporization, compared with G = 33 MW/cm^2. The first explosive boiling occurs at t_1 = 945 ps with recoil pressure rise up to 600 bar as compared to about 400 bar due to surface evaporation at t = 750 ps as it as seen from fig. 1,2. This maximum pressure level persists for about 150 ps with increasing to 670 bar at t = 1095 ps.

After the first explosion t = 945 ps (fig. 2) no pronounced explosive boiling occurs up to the moment t = 1860 ps (fig. 4) when the pressure reaches value P_R = 740 bar. This pressure exceeds its previous values P_R = 540 bar at t = 1515 ps, P_R = 640 bar at t = 1605 ps and P_R = 600 bar at t = 1665 ps (fig. 3). Snapshot on fig. 3 also shows several droplets formed during and after the first explosion. The vertically elongated droplet forms is due to scale differences (by factor ~5) in x and z directions.

The second explosive boiling develops in a way somewhat similar to the fourth explosive boiling for the case of smaller sample which begins at t = 1760 ps [10] and gives rise to almost simultaneous formation of two fragments (or two bubbles). No counterparts of the second and the third explosive boilings which occur in the smaller sample [10] are visible in the considered here sample.

The third explosion (t = 2805 ps) results in pressure rise up to 870 bar in interval 2565-3030 ps while the pressure minimum between the second and the third explosion is 730 bar. The pressure minimum between the third and the fourth explosion boiling is 750 bar at t = 3375 ps. During and after the fourth explosive boiling ($t \geq$ 3720 ps) the pressure is about 900 bar.

The fifth explosive boiling at t = 4050 ps is accompanied by multiply density fluctuations which develop in the region much deeper (≈ 200 nm) in the sample than in the considered before explosive boiling (≈ 50 nm). Evolution of such multiply density fluctuations similar to spinodal decomposition is presented in fig.5-8. From fig.6 it is seen also explosive boiling process on the back side of the sample with pressure rise from 370 bar to 500 bar.

It should be noted that at t = 4740 ps the back side temperature (T = 6860 K) is lower than temperature values at irradiated surface at the moments of explosive boilings at t = 945 ps (T = 6870 K), t = 1860 ps (T = 7080 K), t = 2805 ps (T = 7120 K), t = 3720 ps (T = 7180 K), t = 4050 ps (T = 7190 K). The back side temperature at t = 4740 ps is also lower than the temperature in the middle of the film where however no explosive boilings occurs probably due to pressure effect.

For G = 66 MW/cm^2 initial ablation behavior is somewhat similar to explosive boiling process with some recoil pressure jump as at is seen from fig.9-11 while at later times (fig.12) the regime with subcritical pressure and temperature values becomes more smooth.

No explosive boiling is observed for G = 110 MW/cm^2 at subcritical temperature pressure values because corresponding density fluctuations have no time to develop. As expected critical and supercritical ablation regimes also demonstrate no prominent fluctuations.

4 CONCLUSIONS

Results obtained in the present paper demonstrate evolution of nanosecond ablation regime from explosive boiling to spinodal decomposition and supercritical fluid expansion for increasing laser intensity G = 44-110 MW/cm^2. At G = 44 MW/cm^2 five explosions occur at irradiated surface in the interval from 800 ps to 4400 ps where at later times multiply fragmentation develops which corresponds to spinodal decomposition. At the same time (t = 4740 ps) the six explosive boiling is observed at the film back side though the local temperature there have the lowest value in the film. Such a behavior is probably due to effect of pressure which has the lowest value in this region.

It should be noted that many papers [1-5,8] which deal with explosive boiling investigations present no sufficient information about recoil pressure behavior during the explosion. This situation may be partially due to differences in formulations of the problem and the method of its solution.

As it was already mentioned earlier some features of explosive boiling pressure behavior investigation can give important information on critical pressure values of irradiated targets [10,11,17].

The work was supported by the RSF (project 15-11-30039).

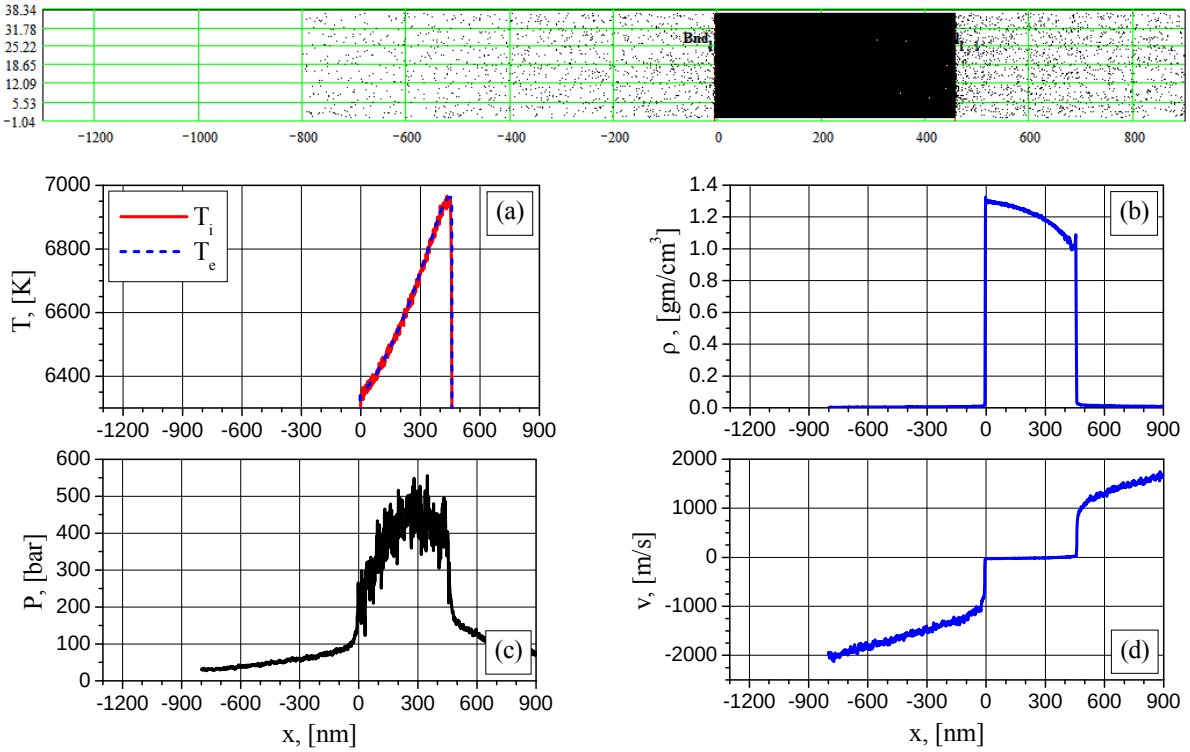

Fig. 1. 2D density particle distribution (snapshot) and 1D distributions of electron (blue) and ion (red) temperature (a), density (b), pressure (c), particle velocity (d) at the time of 750ps (G = 44 MW/cm^2).

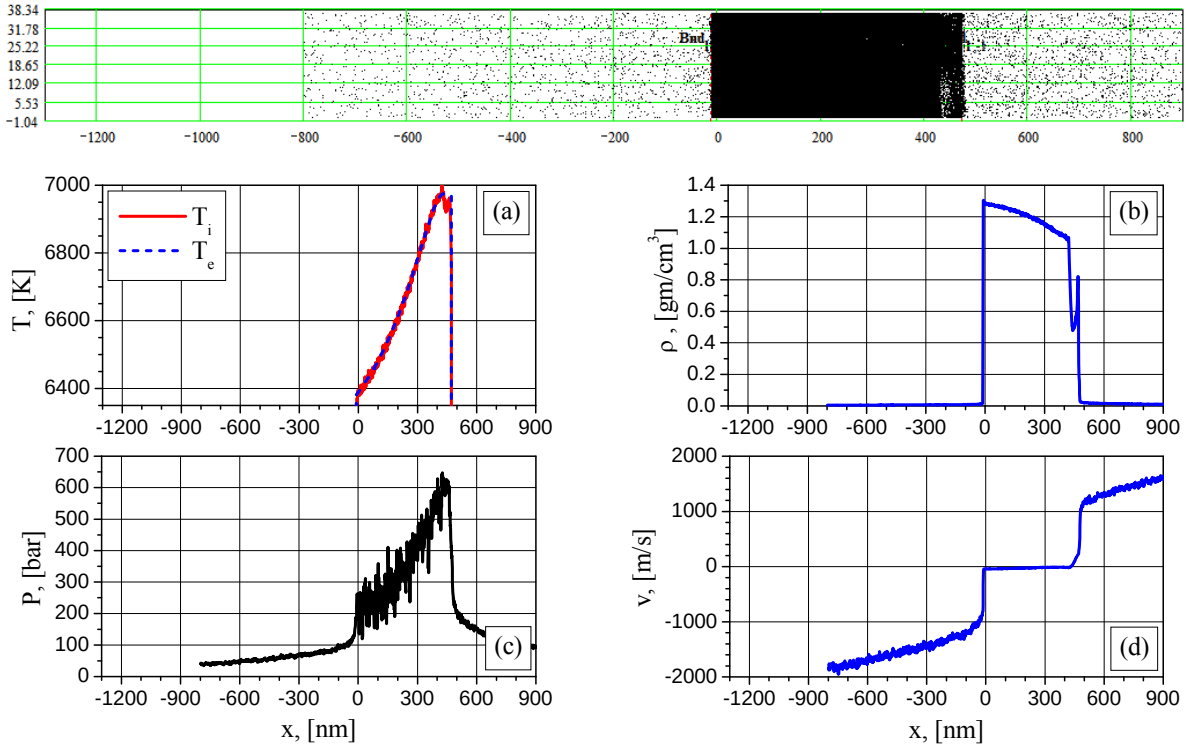

Fig. 2. 2D density particle distribution (snapshot) and 1D distributions of electron (blue) and ion (red) temperature (a), density (b), pressure (c), particle velocity (d) at the time of 945ps (G = 44 MW/cm^2).

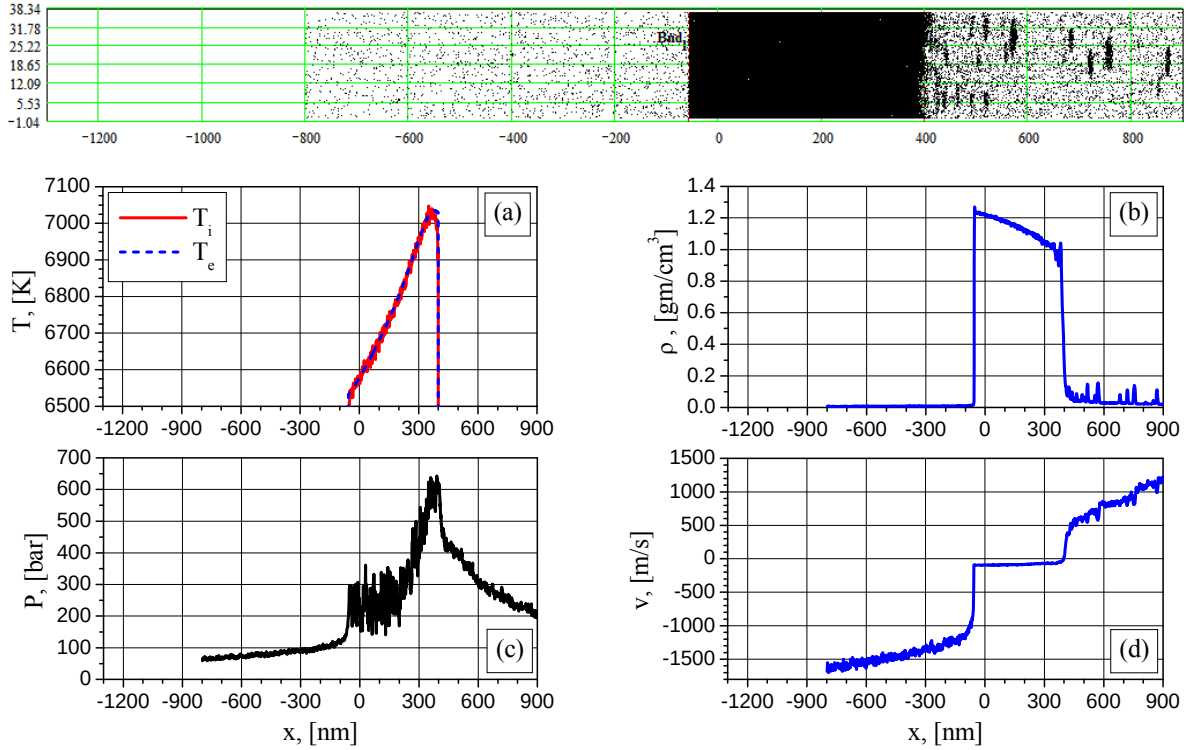

Fig. 3. 2D density particle distribution (snapshot) and 1D distributions of electron (blue) and ion (red) temperature (a), density (b), pressure (c), particle velocity (d) at the time of 1665ps (G = 44 MW/cm^2).

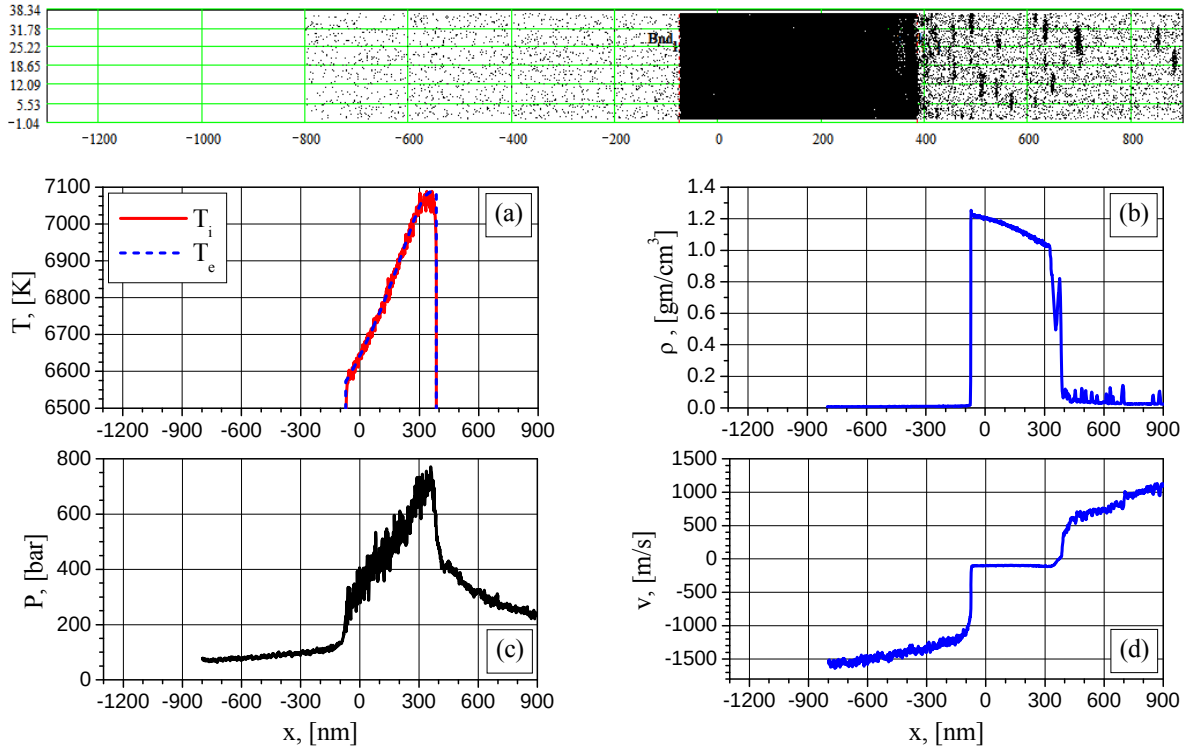

Fig. 4. 2D density particle distribution (snapshot) and 1D distributions of electron (blue) and ion (red) temperature (a), density (b), pressure (c), particle velocity (d) at the time of 1860ps (G = 44 MW/cm^2).

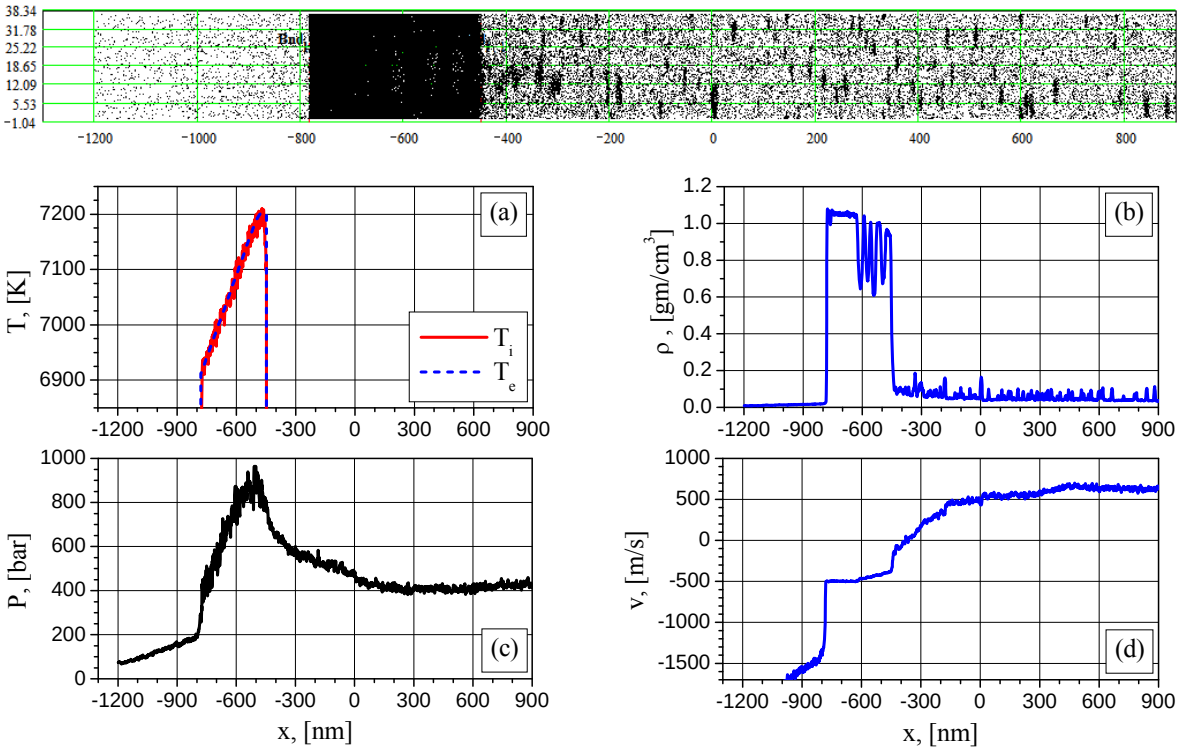

Fig. 5. 2D density particle distribution (snapshot) and 1D distributions of electron (blue) and ion (red) temperature (a), density (b), pressure (c), particle velocity (d) at the time of 4515ps (G = 44 MW/cm^2).

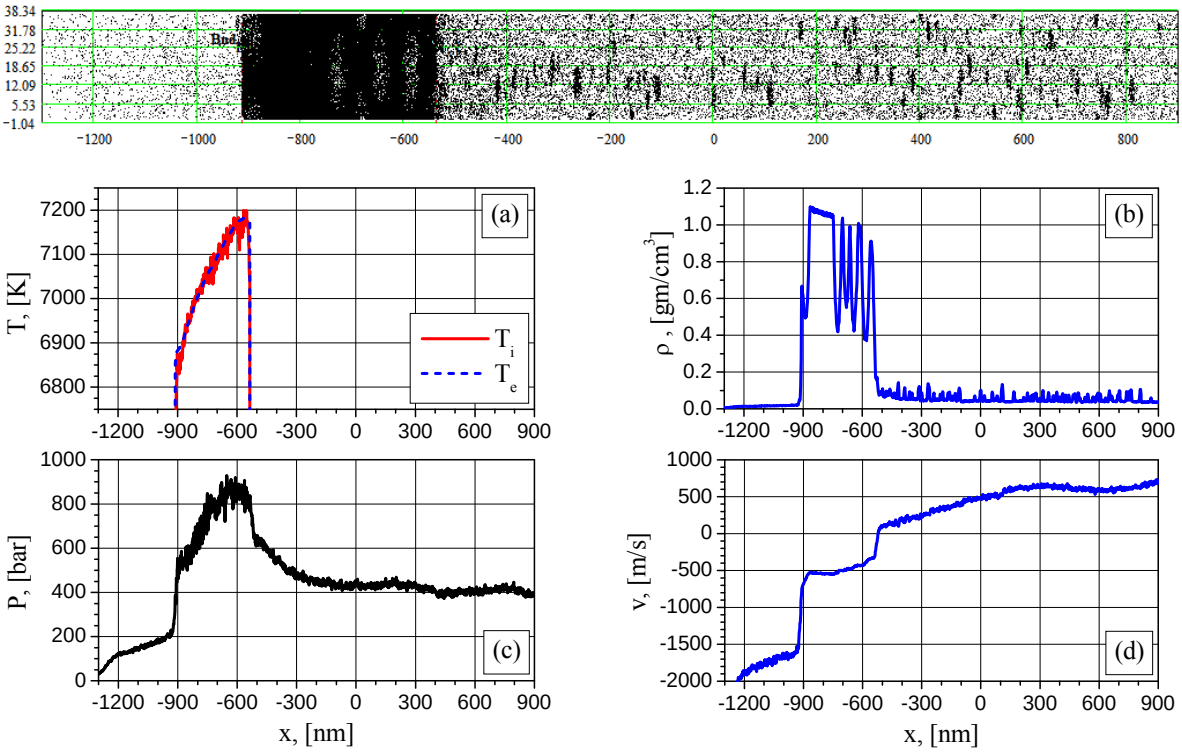

Fig. 6. 2D density particle distribution (snapshot) and 1D distributions of electron (blue) and ion (red) temperature (a), density (b), pressure (c), particle velocity (d) at the time of 4740ps (G = 44 MW/cm^2).

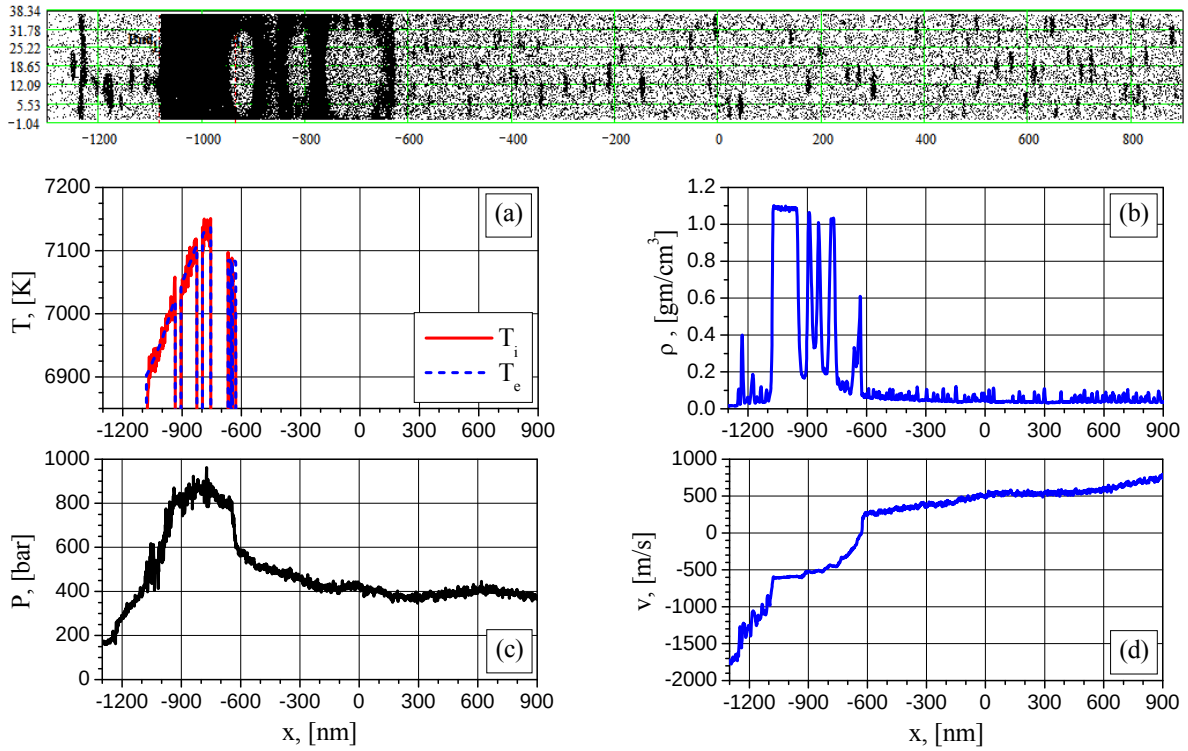

Fig. 7. 2D density particle distribution (snapshot) and 1D distributions of electron (blue) and ion (red) temperature (a), density (b), pressure (c), particle velocity (d) at the time of 5100ps (G = 44 MW/cm^2).

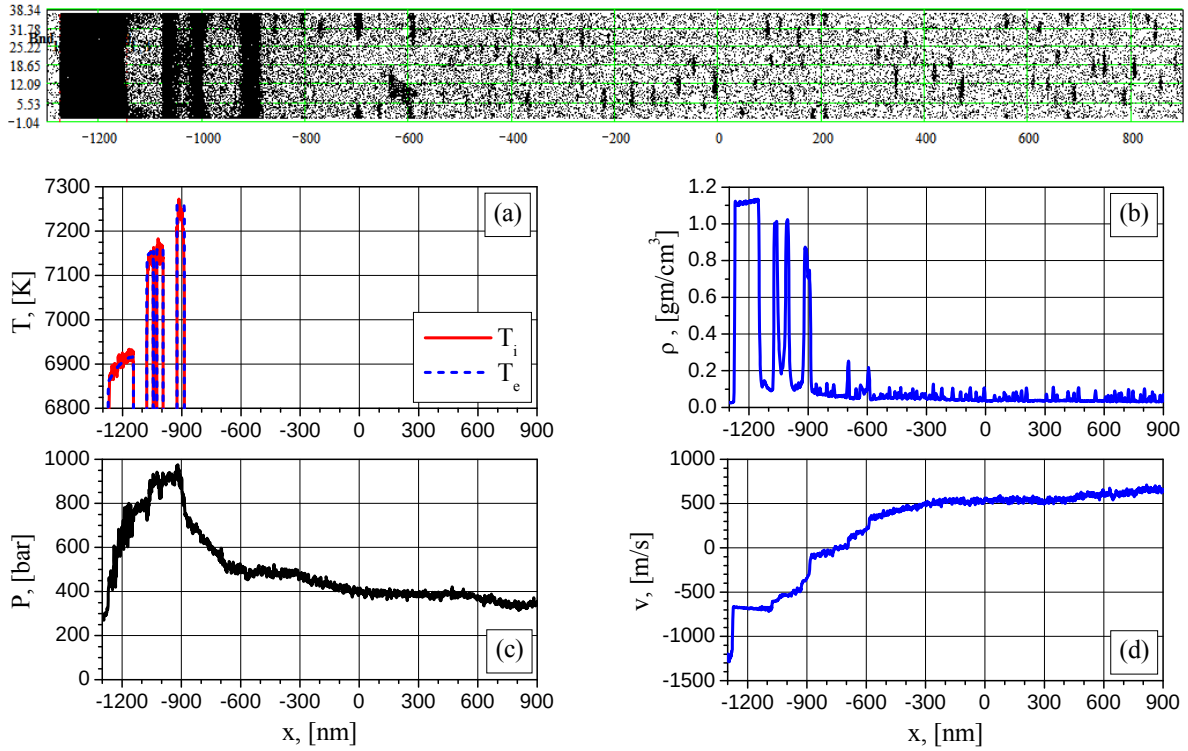

Fig. 8. 2D density particle distribution (snapshot) and 1D distributions of electron (blue) and ion (red) temperature (a), density (b), pressure (c), particle velocity (d) at the time of 5415ps (G = 44 MW/cm^2).

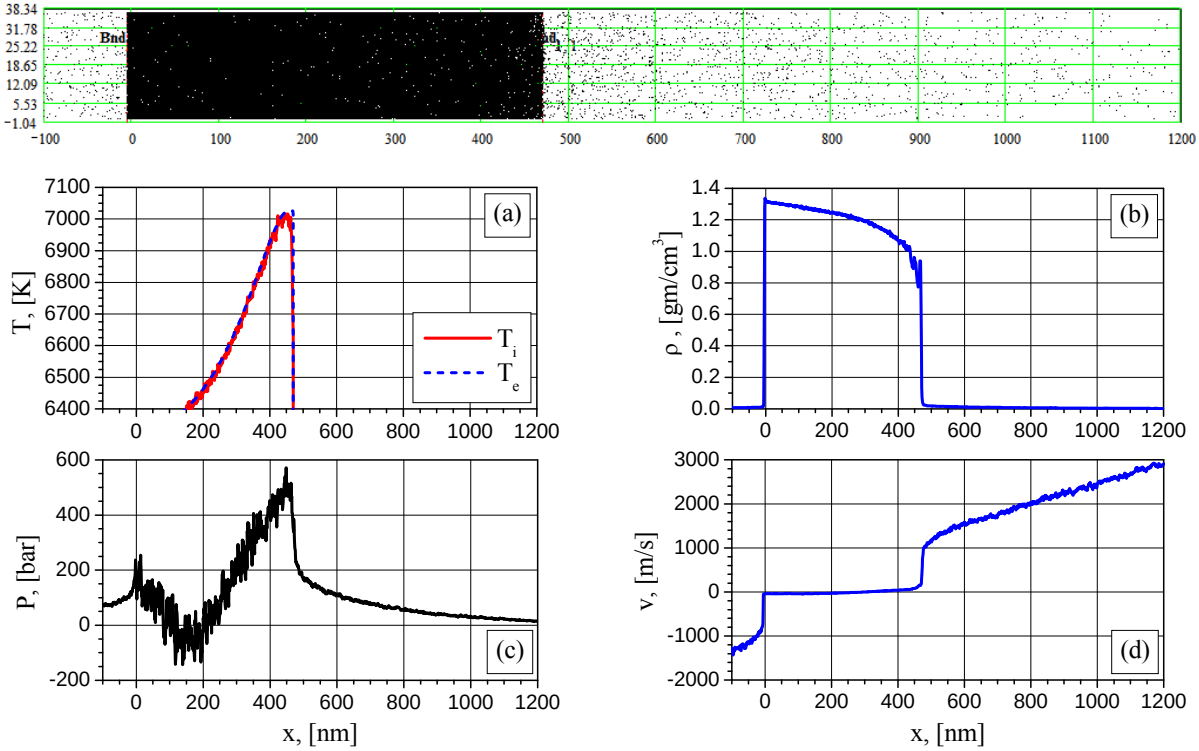

Fig. 9. 2D density particle distribution (snapshot) and 1D distributions of electron (blue) and ion (red) temperature (a), density (b), pressure (c), particle velocity (d) at the time of 375ps (G = 66 MW/cm^2).

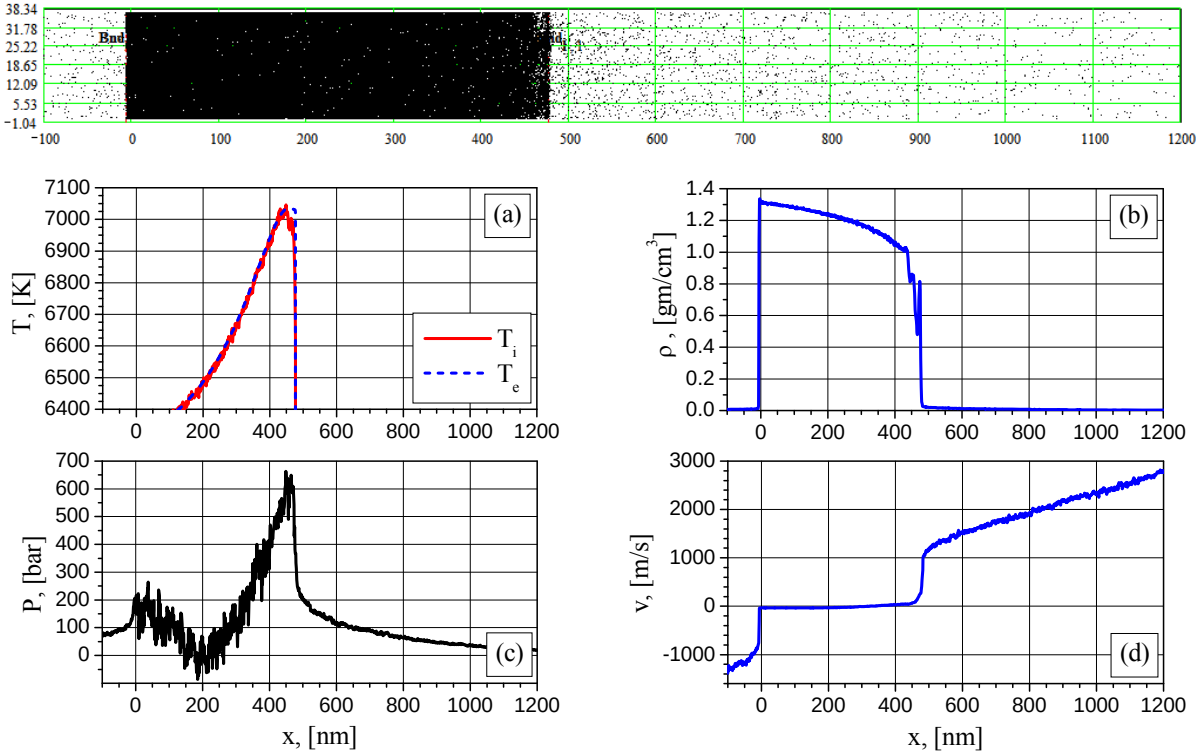

Fig. 10. 2D density particle distribution (snapshot) and 1D distributions of electron (blue) and ion (red) temperature (a), density (b), pressure (c), particle velocity (d) at the time of 415ps (G = 66 MW/cm^2).

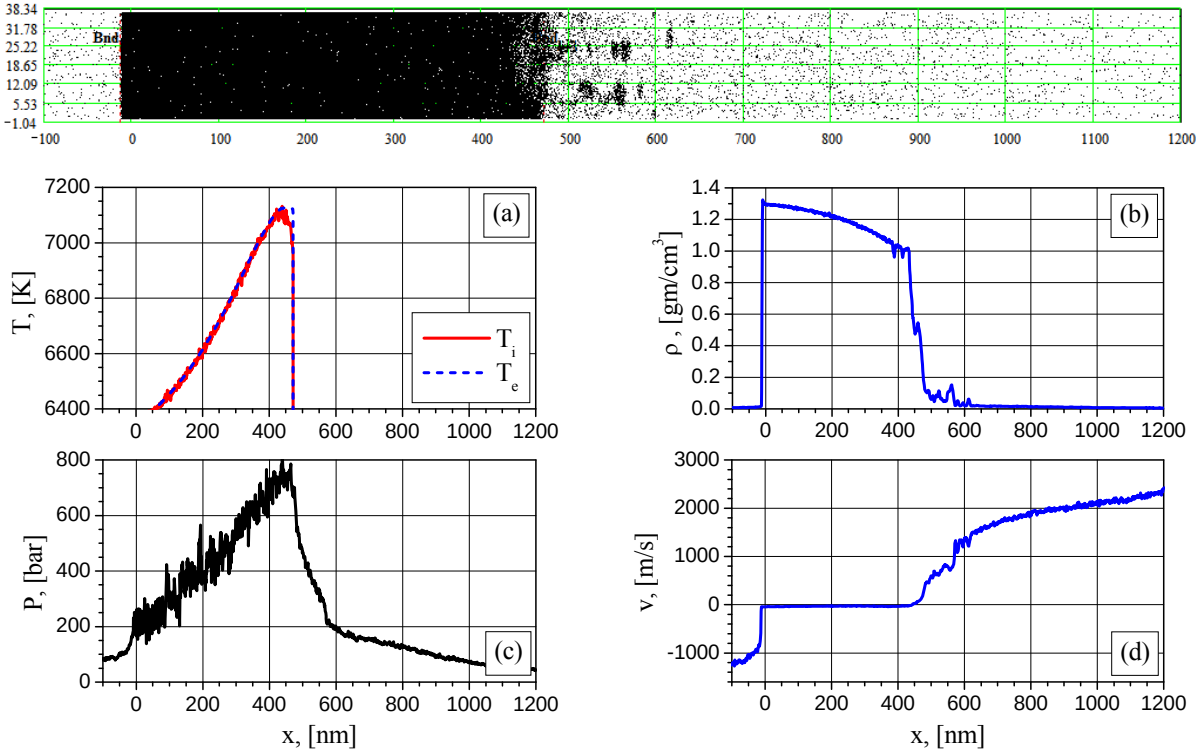

Fig. 11. 2D density particle distribution (snapshot) and 1D distributions of electron (blue) and ion (red) temperature (a), density (b), pressure (c), particle velocity (d) at the time of 595ps (G = 66 MW/cm^2).

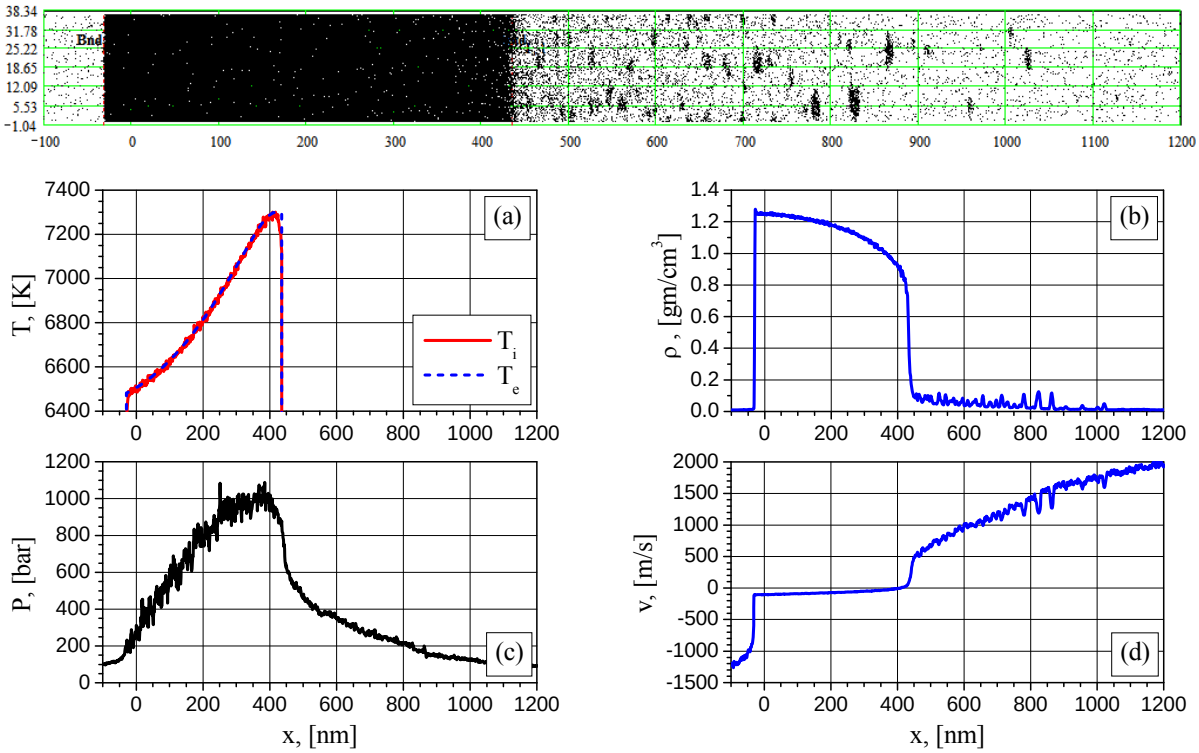

Fig. 12. 2D density particle distribution (snapshot) and 1D distributions of electron (blue) and ion (red) temperature (a), density (b), pressure (c), particle velocity (d) at the time of 900ps (G = 66 MW/cm^2).

REFERENCES

[1] A. Mazzi, A. Miotello. “Simulation of phase explosion in the nanosecond laser ablation of aluminum”, *Journal of Colloid and Interface Science* (2016), http://dx.doi.org/10.1016/j.jcis.2016.08.016

[2] A. Mazzi, F. Gorrini, A. Miotello. “Dynamics of liquid nanodroplet formation in nanosecond laser ablation of metals”, *Appl. Surf. Sci.* (2016), http://dx.doi.org/10.1016/j.apsusc.2016.09.006

[3] A. Mazzi, F. Gorrini, A. Miotello. “Liquid nanodroplet formation through phase explosion mechanism in laser-irradiated metal targets”, *Phys. Rev. E*, **92**, 031301 (2015).

[4] M.Q. Jiang, Y.P. Wei, G. Wilde, L.H. Dai. “Explosive boiling of a metallic glass superheated by nanosecond pulse laser ablation”, *Applied Physics Letters*, **106**, 021904 (2015).

[5] S. Celen. “On mechanism of explosive boiling in nanosecond regime”, *Appl. Phys. B*, **122**, 168 (2016).

[6] V.I. Mazhukin, A.V. Shapranov, M.M. Demin, A.A. Samokhin, A.E. Zubko. “Molecular dynamics modelling of nanosecond laser ablation: subcritical regime”, *Mathematica Montisnigri*, **37**, 24-42 (2016).

[7] A.A. Samokhin, S.I. Kudryashov, A.E. Zubko and A.V. Sidorin. “Modelling of nanosecond laser ablation. Continual approach”, *Mathematica Montisnigri*, **37**, 76-90 (2016).

[8] N.M. Bulgakova, A.V. Bulgakov. “Pulsed laser ablation of solids: transition from normal vaporization to phase explosion”, *Appl. Phys. A*, **73**, 199–208 (2001).

[9] S.I. Kudryashov, S. Paul, K. Lyon, S.D. Allen. “Dynamics of laser-induced surface phase explosion in silicon”, *Appl. Phys. Lett.*, **98**, 254102 (2011).

[10] V.I. Mazhukin, A.A. Samokhin, M.M. Demin, A.V. Shapranov. “Modeling of nanosecond laser vaporization and explosive boiling of metals”, *Mathematica Montisnigri*, **29**, 68-90 (2014).

[11] V.I. Mazhukin, A.A. Samokhin, M.M. Demin, A.V. Shapranov. “Explosive boiling of metals upon irradiation by a nanosecond laser pulse”, *Quantum Electronics*, **44**(4), 283-285 (2014).

[12] V.I. Mazhukin, A.A. Samokhin, A.V. Shapranov, M.M. Demin, P.A. Pivovarov. “On different regimes of condensed matter ablation depending on intensity and duration of absorbed electromagnetic pulses”, *PIERS Proceedings*, Prague, 2418-2421 (2015).

[13] V.I. Mazhukin, A.A. Samokhin, A.V. Shapranov, M.M. Demin. “Modeling of thin film explosive boiling—surface evaporation and electron thermal conductivity effect”, *Mater. Res. Express*, **2**, 016402 (2015).

[14] D.S. Ivanov and L.V. Zhigilei. “Combined atomistic-continuum modeling of short-pulse laser melting and disintegration of metal films”, *Phys. Rev. B*, **68**, 064114 (2003).

[15] V.I. Mazhukin. “Kinetics and Dynamics of Phase Transformations in Metals Under Action of Ultra-Short High-Power Laser Pulses. Chapter 8”, *In “Laser Pulses – Theory, Technology, and Applications”*, InTech., ed. by I. Peshko., 219-276 (2012).

[16] V.V. Zhakhovskii, N.A. Inogamov, Yu.V. Petrov, S.I. Ashitkov, K. Nishihara “Molecular dynamics simulation of femtosecond ablation and spallation with different interatomic potentials”, *Appl. Surf. Sci.*, **255**, 9592 (2009).

[17] A.A. Samokhin. “Some aspects of the intense evaporation of condensed media by laser radiation”, *Sov. J. Quantum Electron.*, **4**(9), 1144–1145 (1975).

Received December 20, 2016

HANDLING OF THE RADIATIVE ELECTRON EMISSION MODELING RESULTS BY USE OF THE NEURAL NETWORKS

V. EGOROVA, M. ZHUKOVSKIY

Keldysh Institute of Applied mathematics of RAS
Moscow, Russia
e-mail: eva24372@gmail.com , web page: http://www.keldysh.ru

Summary. Modeling of radiation transport often requires approximation of its results from the detector point set to another 3D point system. In particular, modeling of the radiative electromagnetic field envisages approximation of electron emission simulation results from the radiation transport detector system to a differential grid used for the solution of the Maxwell equations. The approximation of functions in the 3D geometry is a non-trivial problem. An approach based on usage of the neural networks is developed for the solution of the approximation problem in question. The multilayer perceptron is chosen for the construction of the neural network. Network training is worked out by applying the algorithm of error backpropagation. The elaborated method is applied for the approximation of the 3D data calculated by Monte Carlo modeling of electron emission generated by X-ray radiation from the boundary surfaces of irradiated object. The results of the modeling are demanded to be transferred from the given detector point system to the set of the points on the 3D grid for solution of the electromagnetic problem. The approximation is obtained as the response of the constructed neural network. The results of approximation show applicability of the neural networks for solving of the approximation problems in question.

1 INTRODUCTION

The effectiveness of the mathematical modeling of many physical phenomena has greatly increased during some years due to the rapid development of the supercomputers [1-[3] and modern paralleling technology [4]. Among the actual investigations are the interaction of laser radiation with matter; the particle fluxes transport; the radiation propagation in technical objects of complex geometry [5-[14] and others. The world known codes are developed for numerical simulation of the radiation transport processes (MCNP [15], Geant-4 [16], PENELOPE [17], EGSnrc [18] etc.).

The statistical simulation by the use of Monte Carlo method is applied in various fields of the computational physics [5,[7-[11]. The method is convenient and usable for solving the complex boundary problems and allows the high-performance calculation by the use of supercomputers with heterogeneous architecture [7,[8, [11]. The effectiveness of parallelization of the Monte Carlo calculations can reach 100% and its scalability is infinite.

The mathematical modeling often requires to solve the approximation tasks as a part of numerical simulation [6, [10, [19,[20]. For instance, the problem of appropriate treatment of the modeling results occurs during simulation of the radiation transport.

Let us consider the radiative electron emission problem [7,[8]. The photon propagation through matter produces fast electron fluxes. These electrons can leave an object being under photon radiation. Thus, the electron fluxes appear outside and in interior cavities of the

2010 Mathematics Subject Classification: 97M50, 93A30.
Key words and Phrases: Radiative Electron Emission, Statistical Modeling, Neural Network, 3D-approximation

investigated object. The scheme of the emission process is presented in fig. 1.

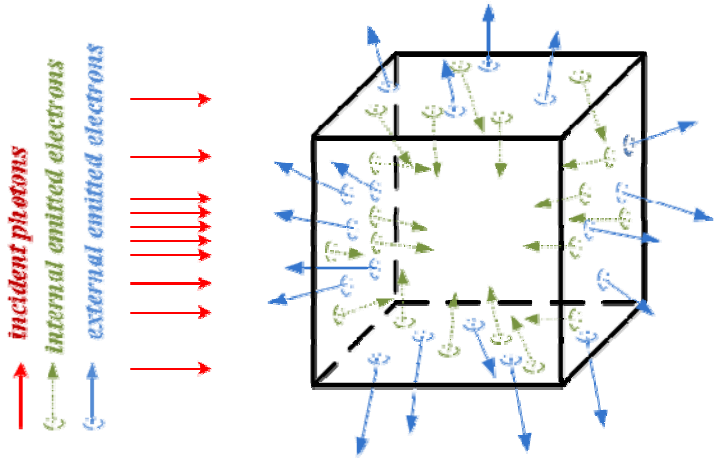

Figure 1: Radiative electron emission process

Modeling of the electron emission processes requires solving the complex boundary-value problems of the photon-electron cascade transport in 3D geometry.

Modeling of radiative electron emission includes the following stages:

− simulating the photon transport in the objects of complex inner structure with accounting of the processes of elastic and inelastic interaction between X-rays and matter;

− modeling of generation of fast electron fluxes produced due to photo absorption and Compton scattering of X-rays in the object;

− simulating of the electron transport in matter with taking into account the various collision processes up to leaving the electron from the object or up to the fast electron thermalization;

− modeling of emitted electrons registration by detecting system.

The algorithms of statistical simulation of electron emission processes are created by developing the weight versions of the Monte Carlo method. The discrete detector system is used for modeling of the registration of the generated electron fluxes.

The results of electron fluxes computing can play the role of initial data for the modeling of the radiative electromagnetic field, for instance. The electromagnetic field is described by the Maxwell equations. The approximation of the computed electron flux data from the mentioned detector system to the differential grid being used for the solution of the Maxwell equations is a non-trivial problem.

The technology of neural networks [21,[22] is used for the solution of the approximation task in question. The multilayer perceptron is chosen for the neural network construction. The network training is worked out by using the algorithm of error backpropagation [22]. The approximation is obtained as the response of constructed neural network.

2 THE PROBLEM STATEMENT

The modeling of the radiation electron emission consists of two stages:

- the statistical simulation of photon-electron transport in an object;
- the evaluation of the flux density of electrons leaving the boundaries of irradiated object.

The surface oriented description of objects is used for modeling of radiation transport [9]. The discrete description of the boundary surfaces of irradiated object is implemented by the triangulation (fig. 2).

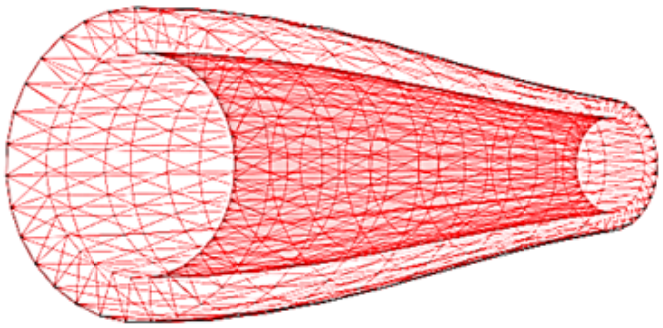

Figure 2: Triangulation of the boundary surfaces

The model of the detector system is worked out for evaluation of the flux density of electrons leaving the boundary surfaces of irradiated object. An example of the model is depicted in fig. 3.

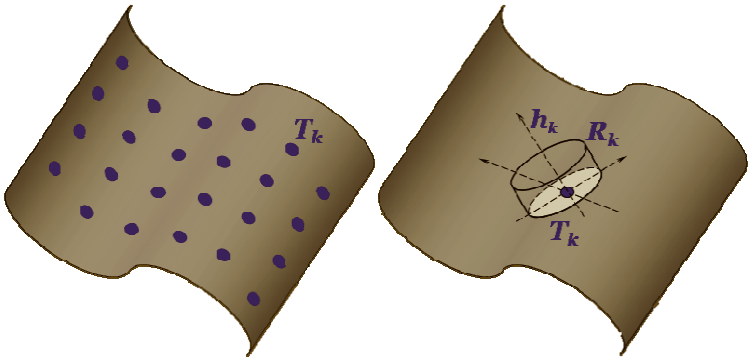

Figure 3: An example of the detector system

A set $\{T_k\}_{k=1}^{K}$ of detectors T_k consists of K different (generally speaking) detectors. Every disk detector (T_k) has a radius (R_k) and a height (h_k) [7]. Every detector of the system belongs to some triangle of corresponding surface after its triangulation.

Thus, statistical evaluation of the electron fluxes is carried out by the use of described discrete detector system.

The results of some physical process computing play often the role of initial data for another phenomenon. Let us consider the generation of the radiative electromagnetic field (REMF) inside and outside the irradiated object [10].

Self-consistent REMF is described by the Maxwell equations. Numerical solution of these equations requires creation of the differential grid constructed by the use of a rectangular grid in Cartesian coordinate system [10]. An example of the grid is presented in fig. 4.

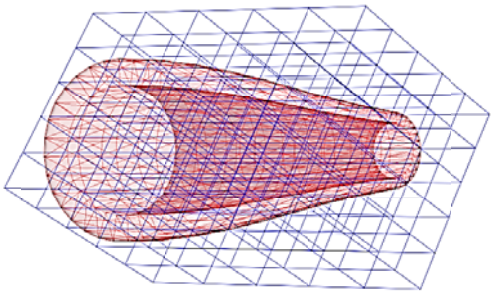

The problem of approximation of electrical current density computed in the points of the set $\{T_k\}_{k=1}^{K}$ to the cells of rectangular electrodynamical grid is actual in that case.

This problem can be formulated as followed.

Let region $\Omega \in \mathbb{R}^3$ be the domain of the function $f(\mathbf{r}) = f(x,y,z), \mathbf{r} \in \Omega$ and sets $Q_N = \{\mathbf{r}_n\}_{n=1}^{N} \in \Omega, Q_M = \{\mathbf{r}_m\}_{m=1}^{M} \in \Omega$ are known. Let $f(Q_N)$ be known. It is required to find $f(Q_M)$ by approximating the $f(Q_N)$ from the set Q_N to the set Q_M.

The neural network technique is applied for solving this problem.

It should be noted that Q_N is called training set (TS), and Q_M is called destination set (DT).

3 THE APPROXIMATION ALGORITHM

A neural network consists of a set of formal neurons. Neurons are connected to each other by some method. Network has layers and every layer has a few neurons. There are input layer and output one. The rest of layers are hidden. An example of neural network topology is presented in fig. 5.

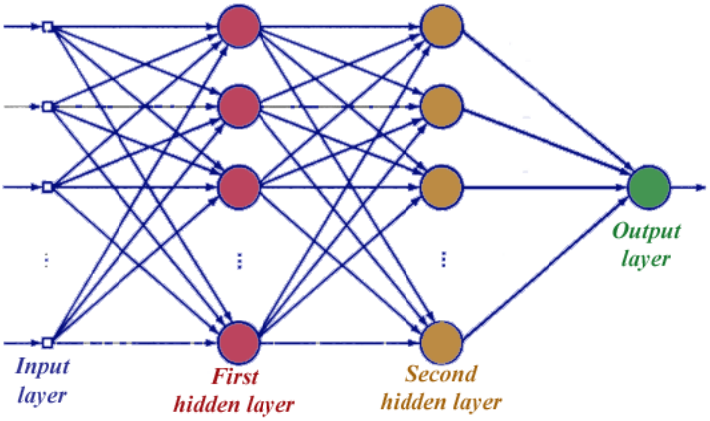

Figure 5: Neural network with two hidden layers

Input information is applied for the entrance of the input layer neurons. Output information is created by neurons of the output layer (the network response). Every neuron of previous layer gives a signal to every neuron of the next layer.

An operation scheme of formal neuron is depicted in fig. 6.

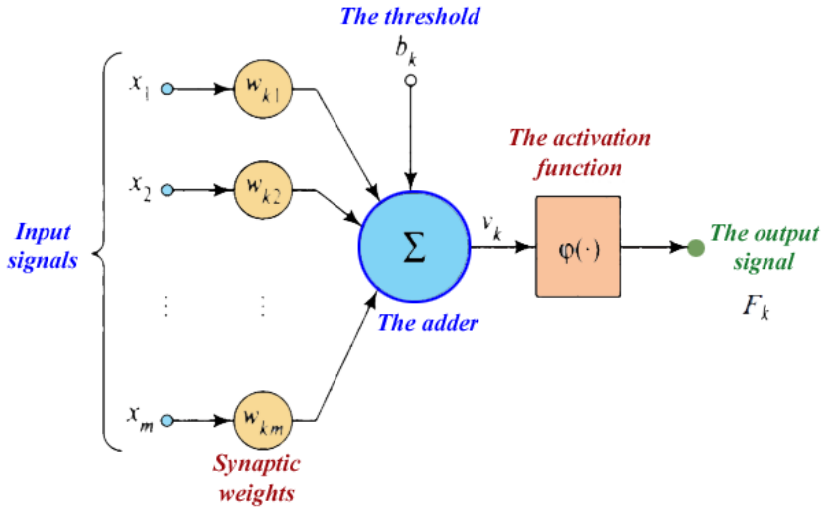

Figure 6: Operating model of some neuron of the layer number k

The function $\varphi(t)=\dfrac{1}{1+e^{-t}}$ is chosen as an activation function. The output signal of k^{th} layer is $F_k=\varphi\left(\sum_{i=1}^{m} w_{ki}x_i+b_k\right)$, where w_{ki} are synaptic weights and b_k are thresholds [21].

Let $F(\mathbf{r})$ be an approximation function having to be constructed by use of a neural network as continuous mapping $F:\Omega\in\mathbb{R}^3\Rightarrow\mathbb{R}^1$ (see section 2).

The general approach of discussed method is presented in fig. 7.

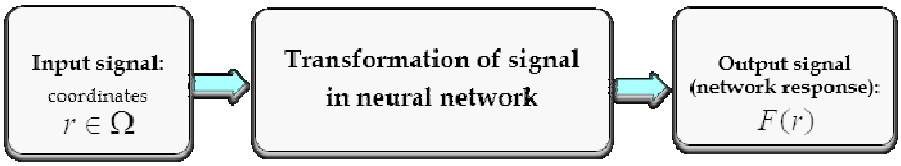

Figure 7: The general scheme of the method

The training set Q_N and $f(Q_N)$ are employed for creating the neural network by applying the algorithm of error backpropagation [21, 22].

The goal of the algorithm is to minimize the mean-square error E

$$E=\frac{1}{2N}\sum_{i=1}^{N}\left[f(r_i)-F(r_i)\right]^2, r_i\in Q_N$$

The minimizing process is carried out by the gradient descent method.

The network response and the error E are calculated in the forward direction. The correction of the synaptic weights (w_{ki}) is carried out in back direction:

$\Delta w_{ij}=-\eta\dfrac{\partial E}{\partial w_{ij}};\Delta b_i=-\eta\dfrac{\partial E}{\partial b_i}$, $\eta\in(0,1)$ is called the rate of network training [21].

4 THE EXAMPLE OF SOLVING THE APPROXIMATION PROBLEM

Let us consider an object having the form of a truncated cone with aluminum wall 5 mm of thickness. The object is irradiated by X-ray plane flux of 100 keV energy. The flux density $f(Q_N)$ of emitted electrons in the points of the detector set Q_N (fig. 8) is the result of the statistical modeling of the process in question.

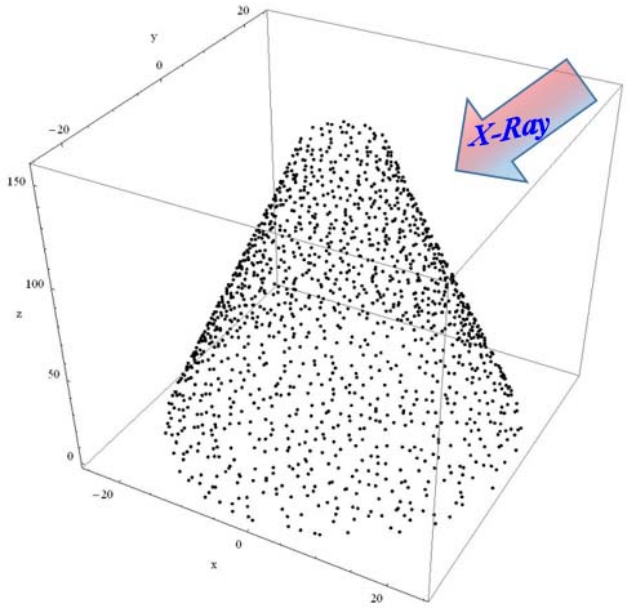

Figure 8: The set of the detector points

The process of network construction is described below.

One hidden layer having 5 neurons is chosen as an initial network topology. Then the mean-square error E is calculated on the training set Q_N. Neurons and layers are added untill the error reaches specified level (the chosen level of the error is 2%).

Firstly the neurons are added to the first hidden layer. The second layer is added when the network error is still more than specified value and is not decreasing by rising of neurons of the first layer (fig. 9).

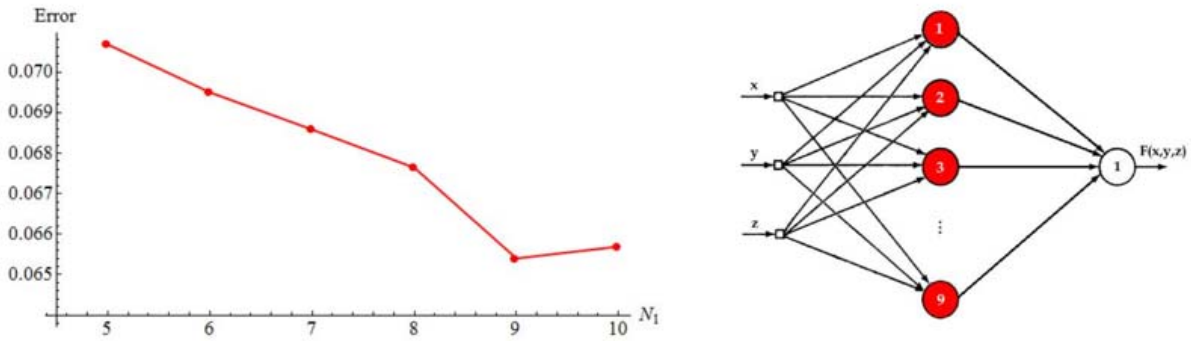

Figure 9: The process of configuration of the first hidden layer

Then the other layers are configurated (fig. 10, 11).

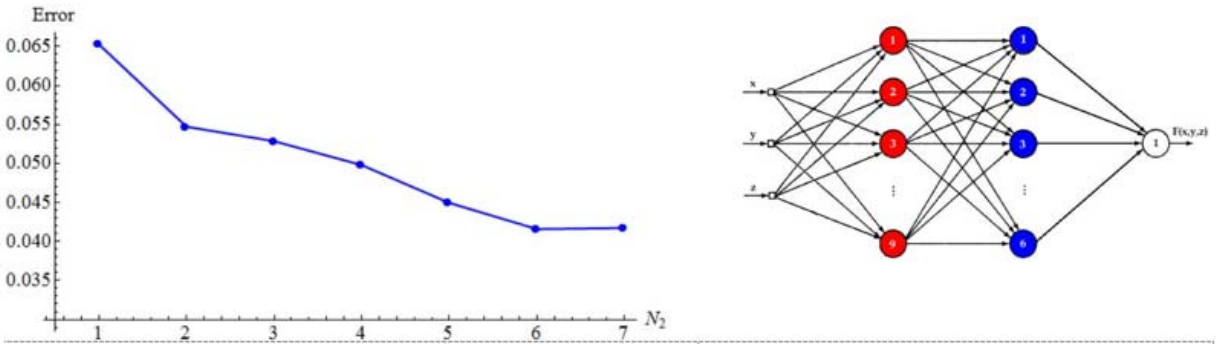

Figure 10: The process of configuration of the second hidden layer

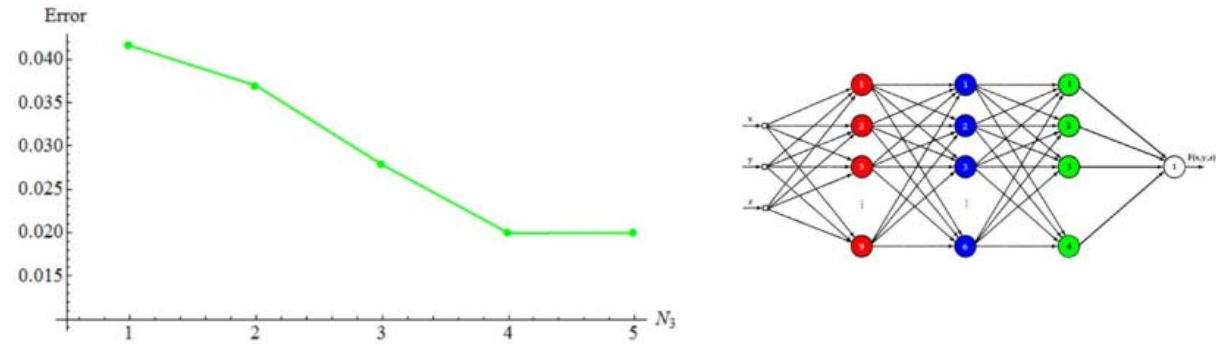

Figure 11: The process of configuration of the third hidden layer

Total process of the network configuration is presented in fig. 12.

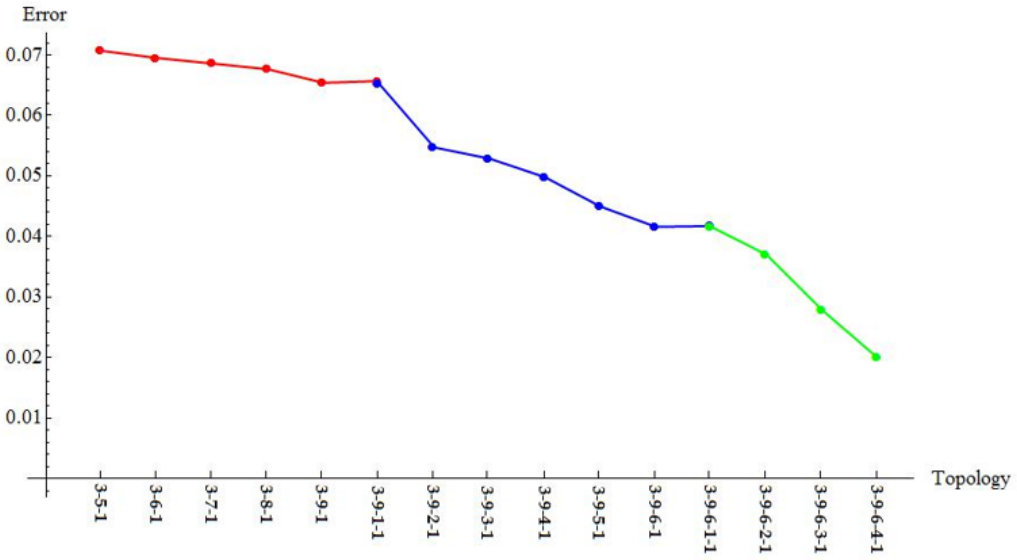

Figure 12: The total process of the network configuration

Thus, the resulting neural network has three hidden layers having 9, 6 and 4 neurons accordingly. The network is depicted in fig. 13.

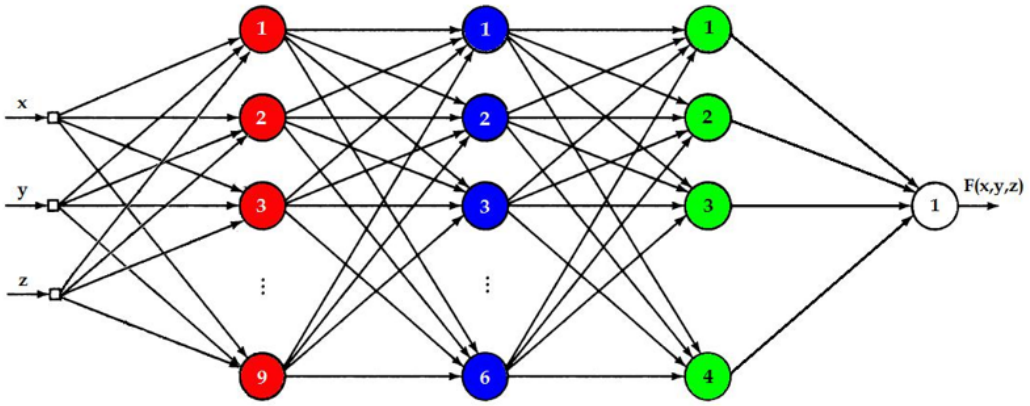

Figure 13: Final configuration of the network

Then the approximation (network response) $F(\mathbf{r}), \mathbf{r} \in Q_M$, is obtained by application of constructed network (fig. 13). The destination set Q_M is the set of points in edges of electrodynamic differential grid (fig. 4). The training set and destination one are presented in fig. 14.

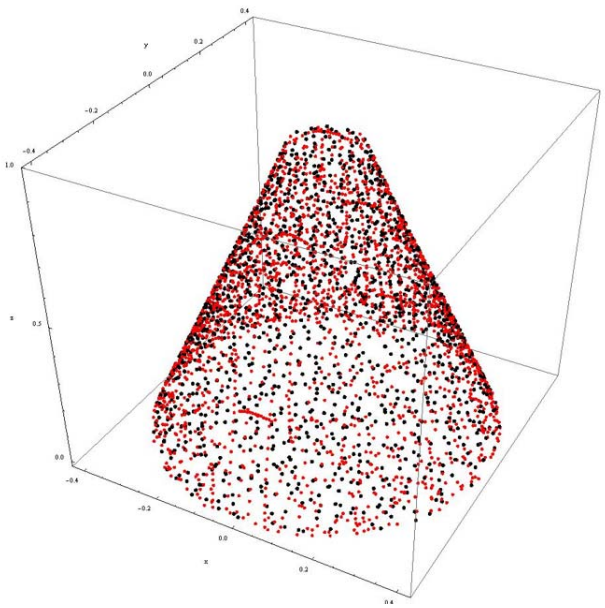

Figure 14: Training set (black points) and destination set (red points)

A visual evaluating of approximation quality is carried out using the following approach. A random point r_0 is chosen from the training set (reference point).

The distance R from r_0 to the axis OZ is calculated. A circle of radius R is constructed in a plane perpendicular to the axis OZ. A uniform angle grid $\{\theta_j\}_{j=1}^{J} = \left\{\theta_1 = \frac{2\pi}{J}, ..., \theta_J = 2\pi\right\}$ is created on the circle.

Two points nearest to every point of the grid $\{\theta_j\}_{j=1}^{J}$ are found. One point belongs to the training set and second one belongs to the destination set. Thus, we have two arrays $A_J \in Q_N$, $B_J \in Q_M$ and two arrays $f(A_J)$, $F(B_J)$ accordingly.

Then the symmetrization of the arrays $f(A_J)$ and $F(B_J)$ is carried out because the approximated function is symmetrical with respect to the axis XOZ a priori:

$$f_s = (f + flip(f))/2; \quad F_s = (F + flip(F))/2.$$

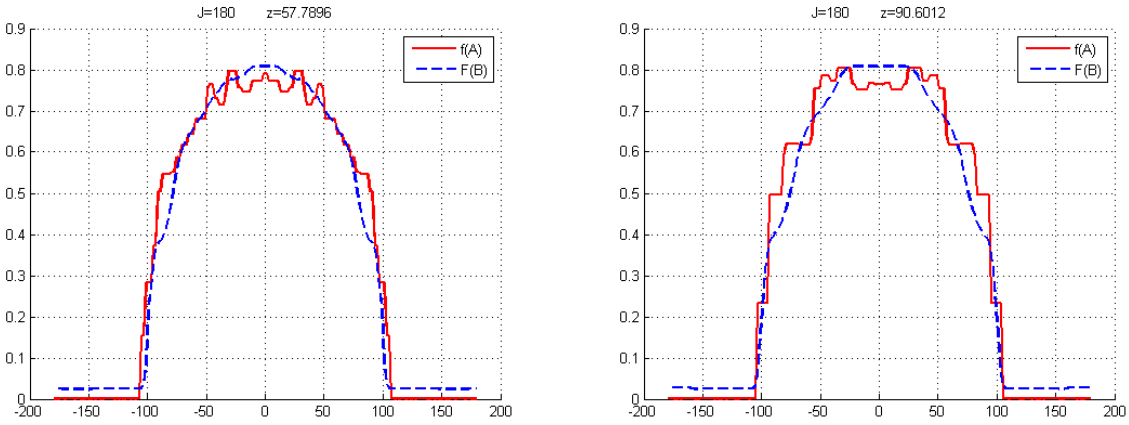

Figure 15: Left picture – $z(r_0)$~58, right picture - $z(r_0)$~91

Some results of visualization are presented in fig. 15 for various r_0. Presented results demonstrated satisfactory quality of required approximation. In addition, smoothing properties of the developed method are shown in the fig. 15. It is significant for the statistical modeling because of existing the non-physical fluctuations.

5 CONCLUSION

Results obtained in the present paper show applicability of the neural network technology for the solution of the problem of processing of the radiation transport modeling results by means of the developed approach to 3D function approximation. The presented method gives the opportunity to use the results of numerical solution of the transport problems in EMF tasks as a current source. Moreover, the elaborated technique allows smoothing the simulation results fluctuations generated by Monte Carlo application.

Further development of the developed approach is planned for solving the vector-function approximation problems in 6D space (space of coordinates and pulses). The input layer will have 6 neurons and output one will have 3 neurons in this case. It is actual, for instance, in

numerical modeling of radiation particle velocities. The results of the method development will be presented later.

The work was partially supported by RFBR grant **№ 15-01-03027**.

REFERENCES

[1] Top500 Supercomputers, URL: http://top500.org/.
[2] Yang Xue-Jun et al. "The TianHe-1A Supercomputer: Its Hardware and Software", *Journal of computer science and technology*, **26**(3), 344-351 (2011).
[3] http://www.intel.ru/content/www/ru/ru/processors/xeon/xeon-phi-detail.html.
[4] http://www.nvidia.ru/object/cuda-parallel-computing-ru.html.
[5] G.Z. Lotova, M.A. Marchenko, G.A. Mikhailov, S.V. Rogazinskii, S.V. Ukhinov, V.A. Shklyaev, "Numerical statistical modelling algorithms for electron avalanches in gases", *Russian Journal of Numerical Analysis and Mathematical Modelling*, **29** (4) 251–263 (2014).
[6] I.P. Tsygvintsev, V.A. Gasilov, A.YU. Krukovskiy, V.G. Novikov, I.V. Popov. "Three-dimensional modeling of the laser radiation absorption", *Mathematica Montisnigri*, **XXVII**, 135-152 (2013).
[7] M.E. Zhukovskiy, M.B. Markov, S.V. Podoliako and R.V. Uskov, "Hybrid Parallelization of Computing the Electron Fluxes produced by Photon Radiation", *Mathematica Montisnigri*, **XXXI**, 43-53 (2014).
[8] M. E. Zhukovskiy and R. V. Uskov, "Hybrid Parallelization of the Algorithms of Radiation Cascade Transport Modeling", *Mathematical Models and Computer Simulations*, **7** (6), 601–610 (2015).
[9] M. Zhukovskiy, S. Podoliako, G.-R. Jaenisch, C. Bellon, "Monte-Carlo-Simulation und CAD - Strahlungsausbreitung an realen Bauteilgeometrien", *Materialpruefung*, 47(4), 210-218 (2005)
[10] M.E. Zhukovskiy, M.B. Markov, "Modeling the radiative electromagnetic field", *International Journal of Computing Science and Mathematics*, **2** (1), 46-59 (2008).
[11] A. V. Berezin, A. S. Vorontsov, M. E. Zhukovskiy, M. B. Markov, and S. V. Parot'kin, "Particle Method for Electrons in a Scattering Medium", *Computational Mathematics and Mathematical Physics*, **55** (9), 1534–1546 (2015).
[12] V.I. Mazhukin, A.V. Shapranov, A. A. Samokhin, A.Y. Ivochkin, "Mathematical modeling of non-equilibrium phase transition in rapidly heated thin liquid film", *Mathematica Montisnigri*, **XXVII**, 65-90 (2013).
[13] V.I. Mazhukin, A.A. Samokhin, M.M. Demin, A.V. Shapranov, "Modeling of nanosecond laser vaporization and explosive boiling of metals", *Mathematica Montisnigri*, **XXIX**, 68-90 (2014).
[14] V.I. Mazhukin, A.V. Shapranov, A.V. Mazhukin, O.N. Koroleva, "Mathematical formulation of a kinetic version of Stefan problem for heterogeneous melting/crystallization of metals", *Mathematica Montisnigri*, **XXXVI**, 58-77 (2016).
[15] D. B. Pelowitz, ed., "MCNPX User's Manual, Version 2.6.0", *Los Alamos National Laboratory report LA-CP-07-1473*, (2008).
[16] S. Agostinelli et al, "GEANT4—a simulation toolkit", *Nucl. Instr. Meth. Phys. Res.*, **A506** (3), 250–303 (2003).
[17] Salvat, J.M. Fernández-Varea and J. Sempau, *PENELOPE-2011: A Code System for Monte Carlo Simulation of Electron and Photon Transport*, OECD NEA Data Bank/NSC DOC (2011)/5 (OECD Nuclear Energy Agency, Issy-les-Moulineaux), (2011).
[18] I. Kawrakow, E. Mainegra-Hing, D.W.O. Rogers, F. Tessier, B.R.B. Walters, "The EGSnrc Code System: Monte Carlo Simulation of Electron and Photon Transport", *NRCC Report PIPS-701,* (2009).

[19] O.N. Koroleva, A.V. Mazhukin , V.I. Mazhukin, P.V. Breslavskiy, “Approximation of Fermi-Dirac integrals of different orders used to determine the thermal properties of metals and semiconductors”, *Mathematica Montisnigri*, **XXXV**, 37-54 (2016).
[20] O.B. Feodoritova, N.D. Novikova, V.T. Zhukov, “Multigrid method for diffusion equations based on adaptive smoothing”, *Mathematica Montisnigri*, **XXXVI**, 14-25 (2016).
[21] Simon Haykin, “Neural Networks - A Comprehensive Foundation, Second Edition”, *Pearson Education, Inc., Reprint*, (2005).
[22] S. Saarinen, R.B. Bramely and G. Cybenko, “Neural NetWorks, backpropagation and automatic differentiation in Automatic Differentiation of Algorithms: Theory, Implementation and Application”, *A. Griewank and G.F. Corliss, eds., Philadelphia: SIAM*, 31-42 (1992).

Received December 15, 2016